Moiré Interferometry at High Temperatures

by

Jau-Je Wu

Dissertation submitted to the Faculty of the
Virginia Polytechnic Institute and State University
in partial fulfillment of the requirements for the degree of

DOCTOR OF PHILOSOPHY
in
Engineering Mechanics

APPROVED:

R. Czarnek, Chairman

C.W. Smith

J. Morton

R.H. Plaut

R.O. Claus

September, 1992
Blacksburg, Virginia

Moiré Interferometry at High Temperatures

by

Jau-Je Wu

Committee Chairman : Robert Czarnek

Engineering Mechanics

(ABSTRACT)

The objective of this study was to provide an optical technique allowing full-field in-plane deformation measurements at high temperature by using high-sensitivity moiré interferometry.

This was achieved by a new approach of performing deformation measurements at high temperatures in a vacuum oven using an achromatic interferometer. The moiré system setup was designed with particular consideration for the stability, compactness, flexibility, and ease of control. A vacuum testing environment was provided to minimize the instability of the patterns by protecting the optical instruments from the thermal convection currents.

Also, a preparation procedure for the high-temperature specimen grating was developed with the use of the plasma-etched

technique. Gold was used as a metallic layer in this procedure. This method was demonstrated on a ceramic block, metal/matrix composite, and quartz.

Thermal deformation of a quartz specimen was successfully measured in vacuum at 980 degrees Celsius, with the sensitivity of 417 nm per fringe. The stable and well-defined interference patterns confirmed the feasibility of the developments, including the high-temperature moiré system and high-temperature specimen grating. The moiré system was demonstrated to be vibration-insensitive. Also, the contrast of interference fringes at high temperature was enhanced by means of a spatial filter and a narrow band interference filter to minimize the background noise from the glow of the specimen and heater.

The system was verified by a free thermal expansion test of an aluminum block. Good agreement demonstrated the validity of the optical design. The measurements of thermal deformation mismatch were performed on a graphite/epoxy composite, a metal/matrix composite equipped with an optical fiber, and a cutting tool bit. A high-resolution data-reduction technique was used to measure the strain distribution of the cutting tool bit.

ACKNOWLEDGMENTS

The author wishes to express his sincere appreciation to Dr. Czarnek, the chairman of the committee, for his assistance and guidance during this research. Dr. Czarnek has shared with the author his intelligent ideas and valuable experiences on the technical issues of this work. Also his deep concerns on author's non-technical matters are greatly appreciated.

In addition, the author wishes to thank

- his committee members for their participation and guidance,
- Dr. Joosik Lee and Dr. Shih-Yung Lin for their help in experimental techniques and friendship, and other colleagues, Tom Rantis, Che-Way Chang, Ray Boeman, Bongtae Han, Peter Ifju, Lei Wang, J. Andre Lavoie, and Kuen Tat Teh for their cooperation and friendship,
- Vicky Czarnek for her constant concern and friendship,
- his family whose support were indispensable for the author to accomplish his work,
- National Science Foundation — Science and Technology Center, duPont, Center for Innovative Technology, and NASA Langley Research Center for their financial supports.

TABLE OF CONTENTS

Page

LIST OF TABLES

LIST OF FIGURES

Page

Page

Page

1 INTRODUCTION

1.1 Motivation

The purpose of this study was to extend the capability of moiré interferometry to measurement of displacement at high temperatures.

For many years, significant attention has been concentrated on the developments and applications of experimental techniques capable of performing displacement or strain measurements on structural materials at high temperatures. The displacement or strain information can be used to study mechanical behavior, thus providing the safety evaluation of a structure, or the criterion of a design. Recently, the increasing developments in composite materials have included the high-temperature and high-performance materials, such as ceramic composites and metal/matrix composites. Due to their light weight and improved high-temperature performance, some applications of these materials include using them as components of the internal combustion engine, parts on high-speed aircraft, and spacecraft structures. Therefore, a technique providing precise deformation measurement and analysis is critical to the design of these structures.

Moiré interferometry is one of the sophisticated techniques, in comparison with mechanical and optical methods. It is an optical technique which provides high-sensitivity, high-spatial-resolution, full-field, and in-plane deformation measurement on the surface of solid bodies. The easy-to-interpret interferogram of a very high contrast is of great advantage. Through data processing, the full-field strain distribution can be extracted from the displacement contours by differentiation using displacement-strain equations. The full-field stress distribution can be obtained easily when the material properties are known.

In 1956, Guild [1] introduced high-sensitivity moiré interferometry which extended the sensitivity of traditional moiré interferometry by two orders of magnitude. Since then, a wide range of applications has been pursued [2,3,4,5], ranging from simple isotropic materials to anisotropic composite materials. In particular, moiré interferometry is a unique tool for the analysis of composite materials. Though this method has found widespread applications in solid mechanics, almost all measurements have been performed at room temperature so far.

Attempts at high-temperature measurements have been made in the past, but the instability, complexity, and high cost of the moiré system setup, as well as the survivability of the specimen grating prevented the achievement in extending this experimental technique to the high-temperature regime. Furthermore, as the

temperature of the specimen increases, background noise degrades the contrast of fringe pattern, making recording difficult. Meanwhile, the convection currents change the refractive index of the air along the optical path of laser beam, causing an instable fringe pattern.

The primary motivation was to overcome these existing difficulties and to promote this experimental method into the high-temperature regime, thus providing a valuable and practical research tool for the evaluation of a structural component subjected to thermal loading.

1.2 Literature Review

Earlier work on deformation or strain measurement at high temperature is reviewed. The overview then focuses on the use of moiré interferometry in the past and on some of the difficulties experienced during its application to high-temperature testing. Finally, current developments of this method are discussed.

1.2.1 Electro-Mechanical Methods for Strain Measurement at High Temperatures

Significant work [6,7,8] has been devoted to improving the techniques of performing displacement or strain measurements at

high temperatures or in hostile environments. Of all available techniques, electro-mechanical and optical methods appear to be the two categories covering most achievements. The capacitance strain gage and electrical resistance strain gage fit into the first category. Their advantages are low cost and easy installation, and they are particularly attractive for room temperature tests. However, because these gages must have mechanical contact with the specimen, the durability of the adhesive bond becomes a problem as the temperature is increased for high-temperature tests. In many instances, electromagnetic interference from power sources could affect the data reading. In fact, it is the resistance of adhesive and gage materials to heat that limits the peak operating temperature of these strain gages. Temperature-compensated electrical resistance strain gages can be used up to 800°C [9]. Some extensometers were designed for axial and torsional strain measurement at temperatures up to 1200°C [10]. Even though they can be utilized for high-temperature measurements, they can only provide information at a single point.

1.2.2 Optical Methods for Strain Measurement at High Temperatures

Many researchers prefer optical techniques [11,12], which can be performed away from the heating area without mechanical contact with the specimen, thereby eliminating the need for special

gages, able to work and survive in hostile environments. Interest in these techniques grew rapidly once lasers became available. For example, the diffractographic strain gage [13] and the interferometric strain gage [14,15,16] could be used for measurements at high temperatures. In order to use the optical phenomenon of diffraction, Pryor et al. [13] attached two strips to the specimen to form an aperture. The diffractograms, obtained due to the changes in aperture dimension at various loads, could be used to measure the relative displacement, or average strain, between these two strips. Using the same phenomenon, Pih et al. [17] introduced a video/image processing system, in which a photodetector was used to measure the spacing of diffracted interference fringes, thus enabling real time measurements. In this method, errors can arise during interpolation for fractional fringes.

By using the interference of reflected beams from two small surfaces cut at a specified angle on the specimen, Sharpe [14,15] designed the interference strain/displacement gage which could measure the relative displacement between the two cuts. Recently, two small attachable interferometric strain gages were developed by Sharpe et al. [16]. One was for measurement at high temperatures or corrosive environments, and the other could be used with nonreflective materials.

Marion [18] used a digital line scan camera to track two optically small ceramic-cement targets placed on the specimen. A

strain measurement up to 3000°K was presented. In addition, Tompkins et al. [19] proposed a Fizeau-type laser-interferometric dilatometer to measure the thermal expansion of composites.

With the non-contacting capability, the above mentioned methods provide only point-by-point information about average strain useful for isotropic materials. However, for advanced composite materials, these techniques cannot provide enough data needed in the study of complicated behaviors, such as mechanical properties near the interface of two materials. In addition, the data errors could arise due to a material's nonuniformity because these methods lack the full-field measurement capability. This capability is important in many cases, because the locations of defects or weak points are not usually known in advance.

1.2.3 Speckle Pattern And Holography Interferometry

With the full-field capability, the laser-speckle method is greatly explored on high temperature works these days [20,21,22,23,24]. This technique could also be used for vibration analysis in high-temperature environments. The other advantage of this technique is that no surface preparation of the specimen is necessary. However, because the method is based on the interference of beams of light scattered from the specimen surface, the information beams mix with optical noise, which results in low

and varying contrast of the original specklegram. In order to correlate the deformation or strain, one cannot avoid superposing two specklegrams or employing image processing. This necessity complicates the process of analysis and makes the method user-unfriendly.

Theoretically, both moiré interferometry and speckle interferometry can provide high-sensitivity and full-field measurement capabilities and could use the carrier fringes of rotation or extension to enhance the accuracy of data extraction. However, in practice, as far as the full-field capability is concerned, because the strain range of the speckle interferometry is limited compared to that of moiré technique, the distance between two speckles cannot be too large. This characteristic limits its application. In addition, the method is sensitive to rigid body translation during the test because this makes the specklegram uncorrelated.

When the temperature increases, thermal convection currents around the hot specimen produce noise and make data correlation more difficult. Also, oxidation of the specimen surface is another source of noise. It is more severe in atmospheric testing environments than in the vacuum environment. Since the original specklegram already contains noise, speckle technique is more susceptible to thermal noise than moiré technique. Recently, pulsed

lasers have been used in speckle measurements to minimize the effect from thermal current by reducing the exposure time.

Based on the holographic interferometry, and made possible by introduction of the sensor equipment, digital computer and image processing system, ESPI (Electronic Speckle Pattern Interferometry) and DSPI (Digital Speckle Interferometry) have been widely studied in some high-temperature investigations [25,26,27,28]. These techniques will shorten the processing time; however, the memory requirements for speckle patterns of each successive stage are enormous, and the use of video camera results in sacrificing spatial resolution. In summary, this technique is usable at temperatures below 900°C [12]. In practice, no single technique is suitable for all applications at the present time, but the low contrast of the specklegram, limited range of full-field capabilities, and highly time-consuming data processing do make this technique less attractive and user-unfriendly.

1.2.4 Moiré Interferometry

While considering the attractive features of moiré interferometry, some researchers have tried to use this technique as a tool for high-temperature displacement measurements. For example, Bowles et al. [29] used high-sensitivity moiré interferometry to measure the coefficients of thermal expansion of

composite materials. The test temperature was reported to be up to 300°F. In their design, a real reference grating was positioned in front of the specimen grating as part of an interferometer. The setup was then placed in an oven. Due to the thermal expansion of the real grating, the frequency of the reference grating changed, and the information beams were distorted. A correction was necessary to obtain the true thermal strain. Through two-step calibrations performed on the real reference grating, a correction factor was obtained. Even though the experimental data were calibrated, it was not a convenient approach, and it contained uncertain error from the expansion of the real reference grating.

Another approach was adopted by Kang et al. [30], who used a standard moiré system outside an oven, with windows on the front face of the oven to pass the beams of light. Similarly, the windows made of wedges were heated, and the information beam was distorted.

Convection ovens were widely used to heat the specimen, which offered the advantages of easy heating and simplified design of the load mechanism. But, as the temperature increased, thermal convection currents would change the refractive index along the path of the beam, making the fringes unstable. Arranging the interferometer to reduce the optical path length would minimize the effect of thermal convection currents [29,30]. A high-power laser was also considered to reduce the photographic exposure time and

minimize this effect. In addition, Sciammarella [31] proposed a technique of displacement averaging which utilized the sensor system to grab forty patterns, computed the phase of each pattern, and then averaged the phases to generate the final fringe pattern for each temperature step. As the thermal currents increased, an additional sensor became necessary to record the fast-changing patterns.

1.2.5 Achromatic Interferometer

The three-mirror four-beam moiré system [32,33] arranged on a vibration isolated table is a convenient design for measuring the in-plane displacement on both horizontal and vertical fields. Typical moiré systems have strict requirements on laser coherence and vibration. However, when vibration sources, such as testing machines or outdoor environments, are unavoidable, the achromatic interferometer developed by Czarnek [34] is a good choice. Unlike traditional moiré systems, this interferometer is vibration-insensitive, and does not require a monochromatic source of light. Measurement of the thermal deformation of a composite [35] during heating up to 180°C and cooling in atmosphere has been demonstrated by using this interferometer.

1.2.6 High-Temperature Specimen Gratings

For room temperature tests, several techniques of preparing the specimen grating have been explored, such as a ruled grating, etched grating, and holographic grating made of a high-resolution holographic plate or a photoresist coated plate. The fundamental requirement in high-temperature moiré is to have a specimen grating that will both survive at high temperatures and yield a photographable fringe pattern.

The techniques of ruled grating have been widely discussed [36,37]. Today, this grating can be machined directly on the specimen to a very high frequency (1200 lines/mm). This grating can work at high temperatures, as long as the material itself survives. However, the high machining cost does limit the applicability of this grating as a specimen grating.

The standard procedure for specimen grating preparation is to replicate the grating from a mold, on which a metallic layer has been deposited by evaporation, onto the specimen by using the epoxy adhesive [38]. Such a specimen grating's peak operating temperature is about 220°C because the epoxy adhesive begins to deteriorate. In general, this temperature limitation is high enough for the applications to most polymer matrix composites.

Work on higher temperature survivability of the grating is in progress. Silicone rubber was used [30] instead of epoxy to transfer

the grating directly from the mold. However, for high-temperature and high-performance composites, like ceramic composites or metal-matrix composites, the peak temperature reached is still too low. Another technique, called the etched grating, which evolved from the photoresist grating, was chosen. The idea was to apply photoresist to the polished specimen surface, then expose it to a source of light, either with grid mask [39] or in an interferometry system with two-beam interference [35,40]. After developing, a bar and space photoresist grating was created. An etched grating was then obtained either by using a chemical [39] or a plasma etching process [35,40]. A preliminary study performed by Czarnek et al. [35] demonstrated that it was promising to use a plasma-etched gold grating for higher-temperature applications.

Furthermore, several different approaches were tried for making a high-temperature specimen grating. For example, Forno [41] used a nickel mesh with a frequency of 40 lines/mm on the specimen. A chemical etching process was then utilized to obtain the specimen grating. Cloud [42] sprayed refractory paint on top of the specimen with photoresist grating to enhance high-temperature resistance. A serious problem was that the refractory paint was easy to corrugate and could not adhere well enough at high temperatures. Instead of using a refractory paint, another approach was to vacuum-deposit a metallic layer on top of the photoresist grating as a coating. The grating was hardly visible, as the photoresist disappeared at elevated temperatures. Recently, a new

technique developed by Cloud et al. [43] was to spray a layer of ceramic refractory paint on top of the specimen, and then press a nickel mesh immediately over it. After curing, a ceramic grating with embedded mesh was obtained. The interference pattern was demonstrated at the temperature up to 1370°C. However, the complexity of preparation and low sensitivity (with a frequency of 40 lines/mm) of the specimen grating limit its application.

1.2.7 Current Status of Moiré Interferometry

Moiré interferometry can provide the capabilities of the high sensitivity of 417 nm, and high resolution of about 100 nm. These capabilities are a good compromise between the efficiency of light and the compactness of a moiré system, and are sufficient for most applications. However, for micromechanics studies a higher sensitivity is necessary. A super high sensitivity interferometer was developed [44] by using the method of holographic wavefront multiplication. This enhanced the sensitivity by an order of magnitude to around 50 nm per fringe order.

In the case of low-density patterns, such as those encountered in residual strain analysis, and when small regions of interest are investigated, a higher-resolution measurement is desired. A high-resolution data-reduction technique was developed by Czarnek and Lee [45,46], and recently modified by Czarnek and Lin [47,48] by

introducing a data-smoothing concept. By digitizing a slightly overexposed moiré pattern with carrier fringes along their central lines, and using FEM (Finite Element Method) analysis, the resolution was increased to 20 nm.

1.3 Summary of Literature Review And Objectives

Great efforts have been concentrated on the high-temperature displacement and strain measurements using optical methods. Each technique features suitable for particular applications. No matter what limitations and difficulties existed in every technique, improvements will make these techniques more practical and strengthen their capabilities.

Moiré interferometry is a powerful measuring tool with significant advantages over other techniques. The main objective of this study was to develop an experimental method allowing full-field in-plane deformation measurements using high-sensitivity moiré interferometry. The temperature objective was close to 1000°C, which is a landmark suitable for most applications at high-temperature environment.

The work consisted of the development of mechanical and optical configurations in which the existing difficulties would be circumvented, and compactness, flexibility and ease of control of the design should be reached optimally.

The objective also included the development of a specimen grating which could survive at high temperatures and would provide photographable interference fringes.

Several measurements would be performed at intermediate temperatures in this newly developed system to demonstrate its appropriateness for practical applications. Also, the high-resolution data-reduction technique [47,48] would be used in the strain analysis of a cutting tool bit subjected to thermal loading.

2 MOIRÉ INTERFEROMETRY

Moiré interferometry is an optical measuring technique based on the interference of two mutually coherent, collimated beams of light. It can provide high-sensitivity, high-resolution, and full-field deformation measurement on the surface of a specimen. This method can be classified as a combination of holography and the traditional geometric moiré method. It maintains all the sensitivity of holography, and at the same time offers easy-to-interpret interferograms. The contrast of the interferogram is usually better than the one obtained in either of the parent techniques. With the standard configuration, the sensitivity of the measurements is equal to 417 nm per fringe order. In practice, the laser is widely used as the source of illumination because of its longer coherent length.

2.1 Formation and Analysis of the Interferogram

Diffraction and interference of light are the two basic physical phenomena in moiré interferometry. The optical interference is produced by the superposition of two or more coherent beams of light. In order to have interference fringes, polarization, collimation and coherence of the light source should be satisfied. A basic two-beam interferometer, illustrated in Figure 2.1, shows how a moiré interferometer works. Two collimated and mutually coherent beams of light, A and B, are symmetrical with

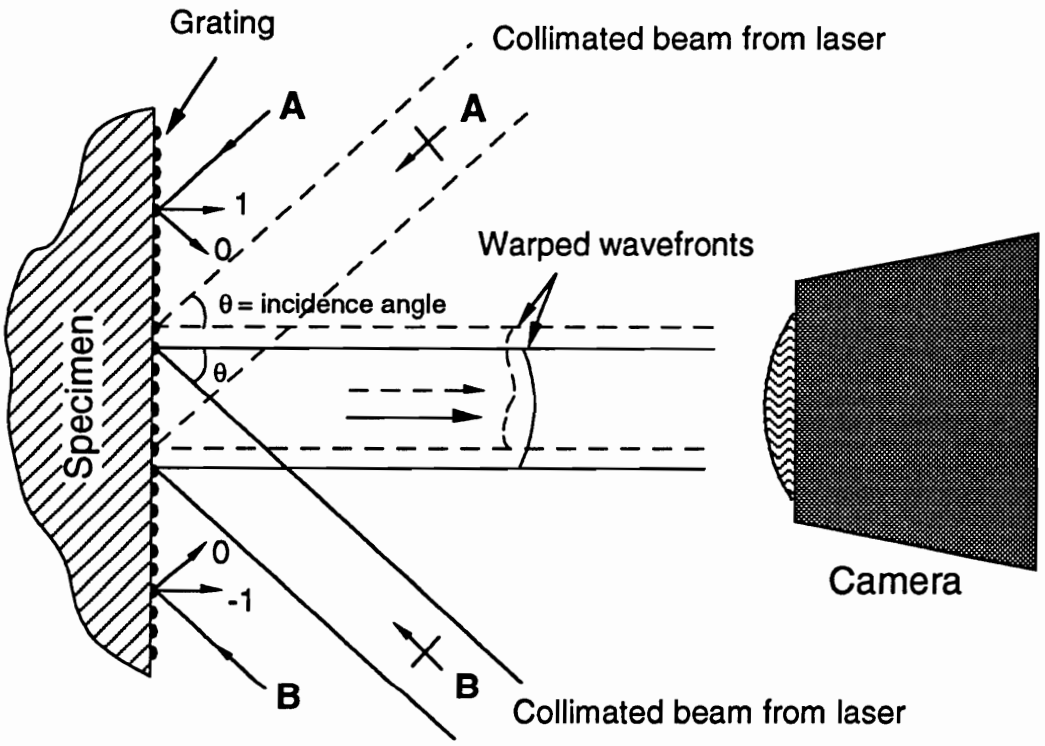

Figure 2.1 Basic two-beam moiré interferometer for one-dimensional measurements.

respect to the normal to the specimen surface. When the two beams illuminate the diffraction grating produced on a flat surface of the specimen, the diffraction phenomenon produced is governed by the fundamental diffraction equation:

$$\sin\alpha = m\lambda f + \sin\rho, \qquad (2.1)$$

where ρ is the angle of incidence, α is the angle of diffraction, m is a diffraction order, λ is the wavelength, and f is the frequency of the grating.

A', the first diffraction order of illuminating beam A, and B', the minus-first diffraction order of the second illuminating beam, interfere, producing an interference fringe pattern (also known as interferogram) recorded on the camera back. Initially, the interferometer is tuned so that the two diffracted beams will emerge together along the normal to the specimen surface. The pattern produced is a field of uniform intensity called a null field. When a load is applied, the specimen grating deforms with the specimen surface; its frequency is changed, modulating the shape of the wavefronts of the diffracted beams. The interference pattern created represents a contour map of in-plane displacement in the direction perpendicular to the grating lines. The fringes are assigned numbers called fringe orders, defined by Equation (2.2):

$$N = \frac{S}{\lambda} + C, \qquad (2.2)$$

where N is the fringe order,

S is the phase difference in terms of the distance between the wavefronts,

λ is the wavelength of light,

C is a constant corresponding to rigid body motion.

In this example, the first diffraction order of illuminating beam is used. In practice, the second or higher diffraction orders of the illuminating beam can also be used in moiré interferometry, depending on the selection of the frequency of specimen grating and the angle of incidence.

2.2 In-plane Measurement

By extending the concept of the two-beam interferometer to two-dimensional measurement, i.e. in the x-y plane, a cross grating is replicated on the specimen and illuminated in both horizontal and vertical directions to give the in-plane surface deformation. A three-mirror four-beam interferometer depicted in Figure 2.2 is a convenient arrangement for this purpose. The relationships between the fringe orders and the displacements are expressed in Equation (2.3):

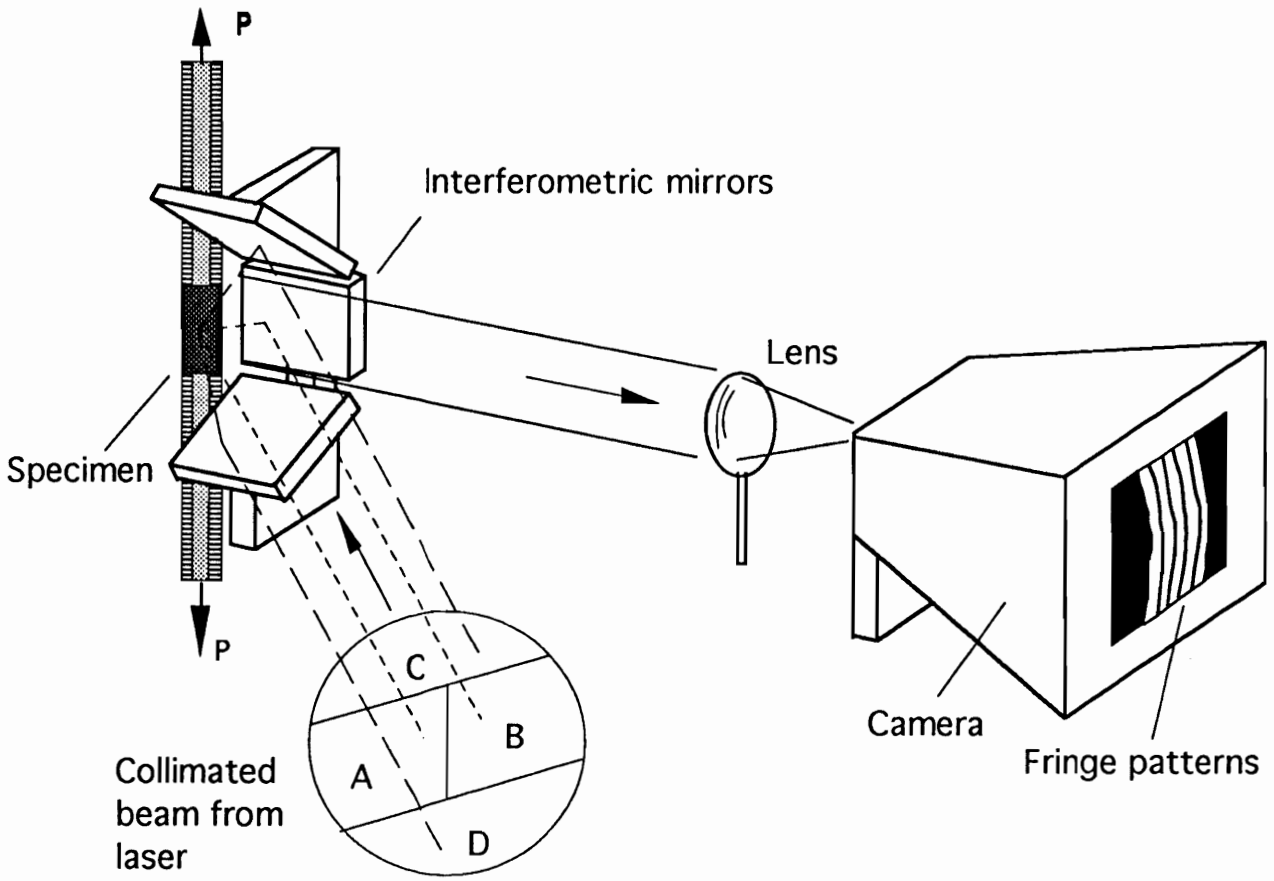

Figure 2.2 Three-mirror four-beam moiré interferometer.

$$U(x,y) = \frac{\lambda}{2\ \sin\theta} N_x(x,y); \tag{2.3a}$$

$$V(x,y) = \frac{\lambda}{2\ \sin\theta} N_y(x,y), \tag{2.3b}$$

where $N_x(x,y)$ and $N_y(x,y)$ are the fringe orders at each point in the moiré pattern for the U and V fields, respectively.

Two-dimensional strain components, including the normal strains (ε_x, ε_y) and engineering shear strain (γ_{xy}), can be obtained from the strain-displacement relation shown in Equation (2.4) when the displacement gradient is small:

$$\varepsilon_x = \frac{\partial U}{\partial x} = \frac{\lambda}{2\ \sin\theta} \frac{\partial N_x}{\partial x}; \tag{2.4a}$$

$$\varepsilon_y = \frac{\partial V}{\partial y} = \frac{\lambda}{2\ \sin\theta} \frac{\partial N_y}{\partial y}; \tag{2.4b}$$

$$\gamma_{xy} = \frac{\partial U}{\partial x} + \frac{\partial V}{\partial y} = \frac{\lambda}{2\ \sin\theta} \left[\frac{\partial U}{\partial x} + \frac{\partial V}{\partial y}\right]. \tag{2.4c}$$

2.3 Contrast of the Interferogram

Because of the loss of contrast in moiré interferometry at high temperatures, a discussion of some factors affecting contrast loss of the interferogram is discussed in this section. The resultant intensity of two emergent beams is defined in Equation (2.5):

$$I = I_1+I_2 \pm 2\sqrt{I_1 I_2}\ \cos(2\pi\frac{S}{\lambda}), \qquad (2.5)$$

where I_1 and I_2 are the intensities of two diffracted beams of light, and S is the phase difference. The maximum (I_{max}) and minimum (I_{min}) resultant intensities can be represented in Equations (2.6):

$$I_{max} = I_1+I_2 + 2\sqrt{I_1 I_2}; \qquad (2.6a)$$

$$I_{min} = I_1+I_2 - 2\sqrt{I_1 I_2}. \qquad (2.6b)$$

The contrast of the interferogram is defined in Equation (2.7):

$$\text{percent of contrast} = \frac{I_{max} - I_{min}}{I_{max}} \times 100\%. \qquad (2.7)$$

The contrast is insensitive to the impurity of interference [4]. In practice, the intensities of two diffracted beams are equal in the setup of the typical moiré system; for this reason, the contrast loss due to the impurity of interference is neglected.

In high-temperature moiré interferometry, the glow from the specimen and heater tends to wash out the initially good contrast of the fringe pattern. The optical noise can be categorized into noise coming from spatially incoherent and temporarily incoherent noise sources. The first type noise cannot be converged to a point; thus,

its removal can be implemented with a lens and an aperture located at the focal point. The purpose of the lens is to converge the information beams to a point, where they pass through the aperture. For the temporarily incoherent noise, a narrow band interference filter can be used. By using the described arrangements, the light intensity will be reduced, and the exposure time increased. For this reason, the design of the system to be light-efficient is more important than the design of the moiré system for measurements at room temperature. The arrangement of the filter system for high-temperature measurement is demonstrated in Chapter 5.

The contrast loss due to the effect of the background noise can be explained as follows. The resultant intensity distribution I' can be expressed as

$$I' = I_b + I, \tag{2.8}$$

where I_b is a random background term and I is the resultant intensity on the interferogram as expressed in Equation (2.5). In fact, the values of these two terms are a function of the location on the interferogram. For simplicity, in this discussion, they are assumed to be uniform across the interferogram. In the case of two beams with the equal intensity, I_{min} is equal to zero as observed in Equation (2.6b). Thus, the maximum (I'_{max}) and minimum (I'_{min}) intensities can be expressed in Equations (2.9) as

$$I'_{max} = I_b + I_{max}, \tag{2.9a}$$

$$I'_{min} = I_b, \tag{2.9b}$$

where the background noise raises the resultant intensity level of I'_{max} and I'_{min}. The relation between the contrast loss and the intensity ratio of background noise to illuminating beam can be expressed in Table 2.1. It shows that the higher the intensity ratio of noise to illuminating beam intensity (I_b/I_{max}), the lower the contrast.

As the test temperature increases, the specimen surface begins to glow red. The intensity of background noise (I_b) from the specimen and heater increases, thereby degrading the contrast of the interferogram; therefore, the ratio of I_b/I_{max} increases. This explains why it is difficult to photograph fringe patterns in high-temperature measurements. In other words, the lower the value of the ratio of I_b/I_{max}, the higher the contrast. For this reason, a higher power laser can provide a means to reduce the contrast loss at high temperature, since the ratio of I_b/I_{max} is reduced. However, safety becomes an issue when a high-power laser is used, thus increasing the expense.

Table 2.1 Loss of contrast due to background noise.

I_b/I_{max}	I'_{max}/I_{max} Eq. (2.9a)	I'_{min}/I_{max} Eq. (2.9b)	Contrast Eq. (2.7)
1 %	1.01	0.01	99 %
5 %	1.05	0.05	95.2 %
10 %	1.1	0.1	90.9 %
20 %	1.2	0.2	83.3 %
50 %	1.5	0.5	66.7 %
100 %	2	1	50 %
200%	3	2	33.3%

Notes

I_b : Intensity of backgroud noise

I'_{max} : Maximum resultant intensity

I'_{min} : Minimum resultant intensity

2.4 Achromatic Interferometer [35]

The moiré interferometer used in this study is an achromatic interferometer. Figure 2.3 depicts the configuration of this interferometer. A typical moiré interferometer is so sensitive to vibration that most tests must be confined to the holographic table with vibration isolation. When the test environment has some slight and unavoidable vibration, the achromatic interferometer is a better choice. There are many features in its design different from those of the typical moiré interferometer. First of all, a compensation grating is introduced and illuminated by a collimated beam at normal incidence. For normal incidence of the beam, ρ is zero. Equation (2.1) becomes

$$\sin\alpha = m\lambda f_C, \qquad (2.10)$$

where f_c represents the frequency of the compensator grating and α is the diffraction angle. In this design, the diffraction beams with the order values +1 and -1 are reflected by the mirrors and illuminate the specimen grating with an intersection angle of 2θ. Then the interference pattern is generated by the diffracted beams of light. Note that the incidence angle θ is the same as the diffraction angle α. The sensitivity of this measurement is thus defined in Equation (2.11):

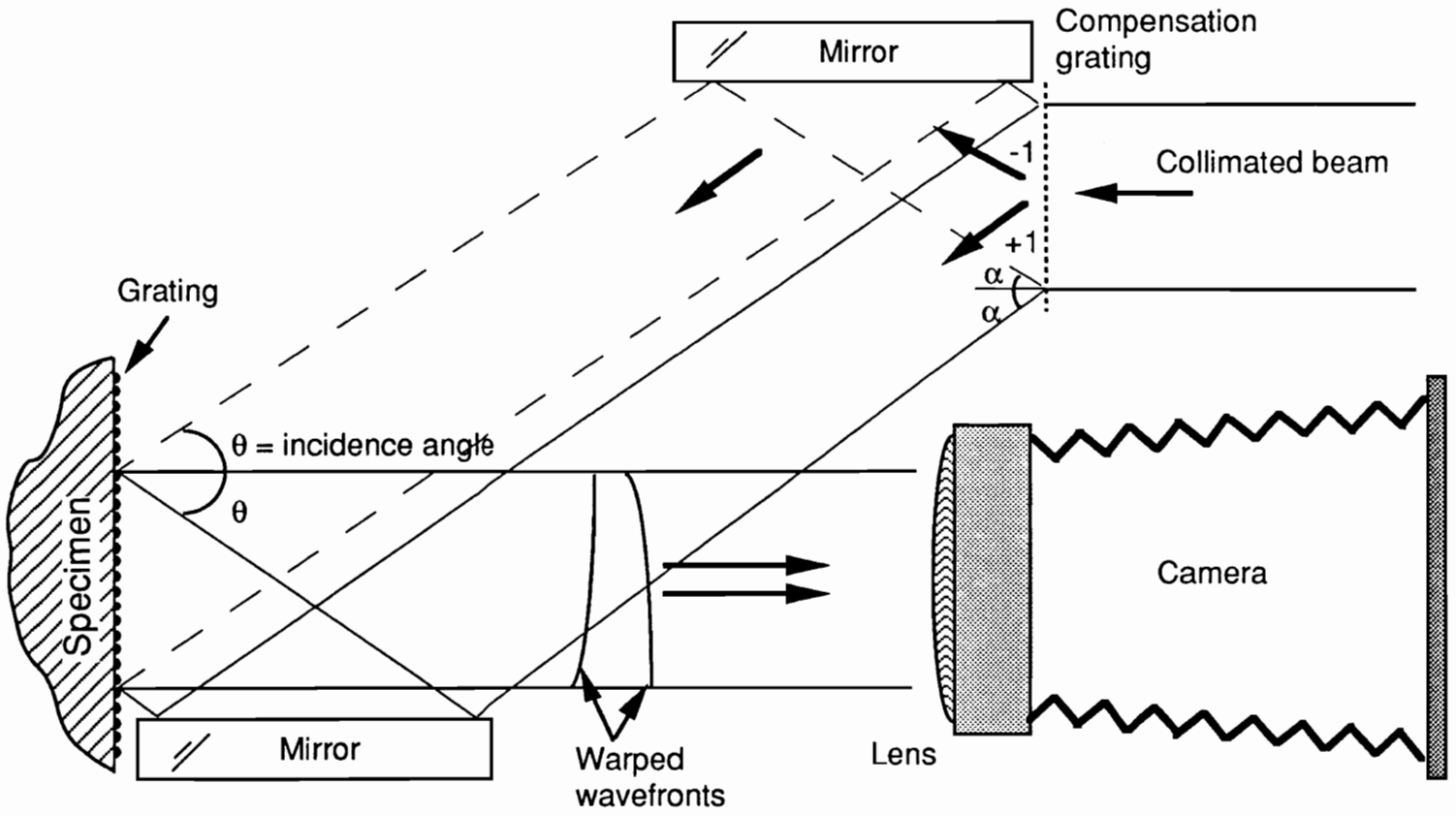

Figure 2.3 Achromatic moiré interferometer.

$$\text{sensitivity} = \frac{\lambda}{2 \sin\alpha}. \qquad (2.11)$$

Since the diffraction order (m) equals 1 in this arrangement, Equation (2.10) can be expressed as

$$f_c = \frac{\sin\alpha}{\lambda}. \qquad (2.12)$$

By comparing Equation (2.11) and Equation (2.12), the sensitivity can be obtained, which equals $1/(2f_c)$.

The above derivation shows that the sensitivity of the system depends on the frequency of the compensation grating only, instead of being dependent of the wavelength of the illuminating light. This feature allows us to use noncoherent (or polychromatic) sources of light. Instead of using a monochromatic source such as a laser, it is possible to reduce the expense, size and weight of the light source by using a laser diode.

The small angular deviation of the illuminating beam does not change the sensitivity of measurement. This was proved in [35]. Thus, the effect of vibration due to the relative motion between the illuminating source and the interferometer is minimized. This feature allows us to separate the illuminating source from the interferometer, thereby increasing the compactness of this system.

Also, the small angular rotation of the illuminating beam will move the illuminated area back and forth, or left and right, without changing its size. This feature allows us to select the location of the area of interest by simply shifting the illuminating beam.

As far as vibration is concerned, the optics are rigidly mounted on a common frame to minimize relative motion between the optics. If the whole interferometer is attached to the testing machine during the test, then the compensator and mirror system can move synchronously with the specimen so that it is relatively insensitive to the vibration from the testing machine. For this reason, the system is insensitive to rigid body motion. This feature provides the means to minimize the influence of rigid body motion during the test.

2.5 Specimen Grating Preparation

A specific characteristic of moiré interferometry is that a grating is prepared on the specimen surface. The replication procedure is shown in Figure 2.4. The mold grating can be a ruled grating, or a holographic grating made of a high-resolution plate or a photoresist coated plate. Even though the efficiency of the holographic grating made of a high-resolution plate is lower than the efficiencies of the other two, this type of grating has the advantage of low cost and easy fabrication process. Therefore, a

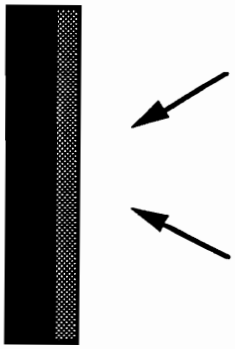

Exposure of a holographic plate to two interfering beams of light

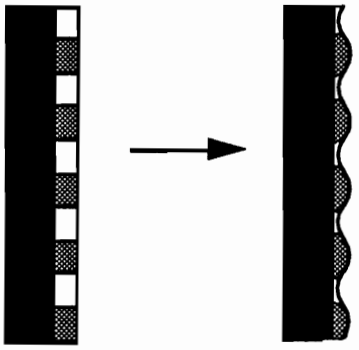

Development of the plate; unexposed emulsion shrinks creating a phase diffraction grating

Thin layer of metal is vacuum deposited on the grating surface treated with a parting agent. The mold is ready to be used.

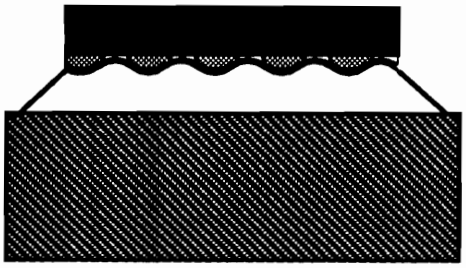

The mold is cemented to the specimen surface.

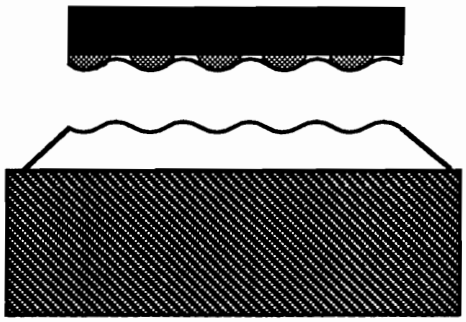

The mold is separated from the specimen. A reflective phase diffraction grating is replicated on the specimen surface.

Figure 2.4 Specimen grating replication procedure.

holographic plate is chosen in our routine applications because of its ease of use.

The mold is made of a high-resolution holographic plate exposed in an interferometry system to the interference of two collimated beams of light. Then, the unexposed emulsion will shrink and create a linear diffraction grating after the development process. It is a phase grating with a sinusoidal shape. A release agent is applied in order to obtain easy separation. After the grating mold is dry, it is vacuum coated with a thin metallic layer such as aluminum for its high reflection efficiency. Sometimes an extra layer of aluminum is applied as a release agent.

In order to transfer the grating from the mold to the specimen, the mold is then cemented to the specimen surface. A two-component epoxy adhesive is used and weight is applied between the specimen and mold to control the thickness of the epoxy. After curing and separating, a specimen with a reflective phase grating is created.

Similarly, silicone rubber can also be used as a cement for making a replicated grating. However, in order to prepare high-temperature specimen grating to reach our objective close to the temperature of 1000°C, a new approach must be used. It is discussed in Chapter 4.

3 HIGH-TEMPERATURE MOIRÉ INTERFEROMETER

The existing difficulties for extending the moiré technique into high-temperature regime consisted mainly of the instability of moiré system and the survivability of the specimen grating. To achieve our objectives, a new approach was used. The approach included the design of a high-temperature vacuum oven and a moiré interferometer. Measurements were made in a vacuum oven using an achromatic interferometer. Vibration and thermal convection currents were intended to be minimized. The concepts and features of the design are discussed in detail in this chapter. Furthermore, a preparation procedure for a high-temperature specimen grating is described in the next chapter. The objective of the work was to establish whether the uses of the vacuum interferometer and plasma-etched grating were feasible for high-temperature measurements.

3.1 High-temperature Vacuum Oven

The design criterion of the whole system setup is based on compactness, flexibility, cost, and ease of control. The measurement is intended to be performed away from a holographic table to increase the flexibility of operation. Thus, the vibration isolation of the system should be considered carefully. Also, one of the important features of this design is that it provides a vacuum

testing environment. In order to apply vacuum, the design of the whole system is intended to be as compact as possible, to minimize the evacuated space.

The outer configuration of the whole system setup is shown in Figure 3.1. The vacuum oven is constructed from two large-diameter (450 mm) steel pipes welded together to form a T. One is used as the specimen compartment which is 750 mm high. Both ends are closed by removable plates that allow easy access to the specimen and fixtures. One small opening (25 mm diameter) on the bottom plate serves as the vacuum port. The other compartment houses the optical components. This vacuum oven minimizes the volume of space that must be handled by the vacuum pump and at the same time provides a relatively large useful space for the specimen and the loading frame.

A mechanical pump provides vacuum to the oven. Typically, this pump is able to maintain pressure inside the oven down to two torrs after about ten minutes of pumping. The vacuum greatly reduces the thermal deformation of the optical components and the instability of the interference fringes produced by convection currents during heating, especially at high temperature.

The use of a mechanical pump produces considerable vibration. In order to minimize the vibration, the whole apparatus was mounted on a steel frame suspended on four air mounts and stabilized by precision leveling valves. A six-foot hose was installed, connecting

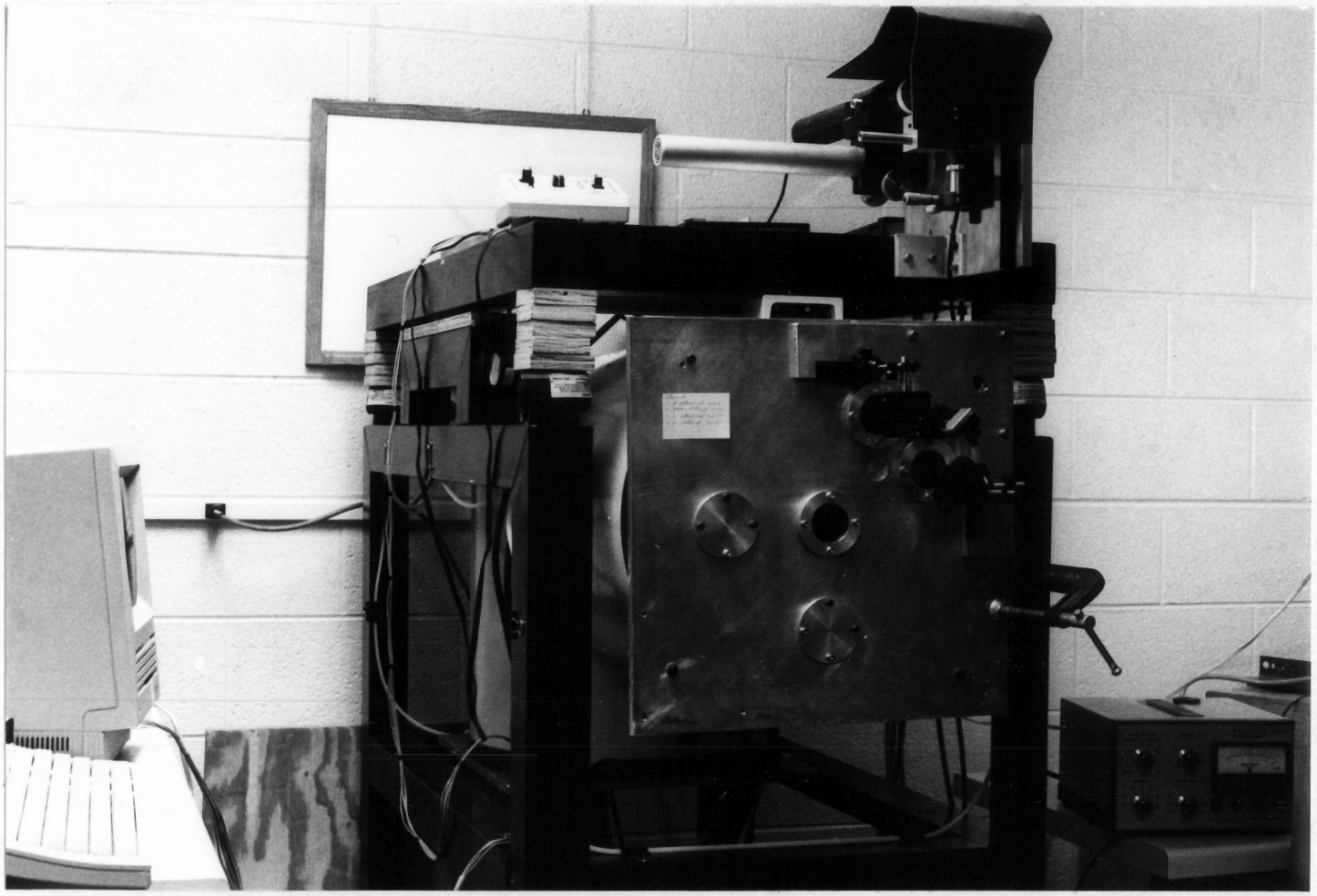

Figure 3.1 High-temperature moiré system setup.

the mechanical pump and the oven. Also, the mechanical pump, placed away from the oven, and part of the hose were placed on a vibration isolation pad and clamped at several locations to reduce the transfer of vibration. A vibration-insensitive interferometer was chosen. With this setup, the fringes of moiré pattern were stable, thus increasing the reliability of data recording during the experiment.

3.2 The Moiré Interferometer

The achromatic interferometer developed for use in a materials-testing environment was less sensitive to vibrations than the traditional moiré interferometers and, for this reason, was chosen for the high-temperature work. However, as shown in Figure 2.3, the location of one optical component is very close to the specimen. This design is useful for room-temperature measurements, since the interferometer can be attached to a testing machine to synchronize the motion with the specimen. In high-temperature measurements, this optical component would be strongly affected by heat, deforming and affecting the experimental results. The interferometer was modified to maximize the distance (150 mm) between the specimen and the nearest optics but to preserve the compactness of the configuration.

This new design of the achromatic interferometer is schematically illustrated in Figure 3.2. A collimated beam illuminates a diffraction grating at normal incidence. This grating, used as a compensator, has a frequency of 1200 lines per mm. The first and minus-first diffraction orders are directed by a system of four mirrors to illuminate the specimen grating at precisely defined angles. The interference pattern is captured by the camera back through two lenses. To accommodate different wavelengths of the light sources, the adjustability of mirrors is provided. The sensitivity of the system is 417 nm, and the intersection angle is 49.4°, which corresponds to the wavelength of 632.8 nm by using a He-Ne laser. If higher power is necessary, the geometry of the vacuum interferometer also preserves the possibility of using an Argon laser, which requires an intersection angle of 38.08° because of its shorter wavelength of 514 nm. The argon laser could be used to increase the power by two orders of magnitude, and therefore minimize the exposure time.

Remote control is provided in this interferometer. One of the mirrors, mirror D in the diagram, can be adjusted, allowing the instrument to be fine tuned. High-precision electric actuators are used to provide a way for remote control when the interferometer is positioned in the vacuum oven. More features of this design are shown in the following sections.

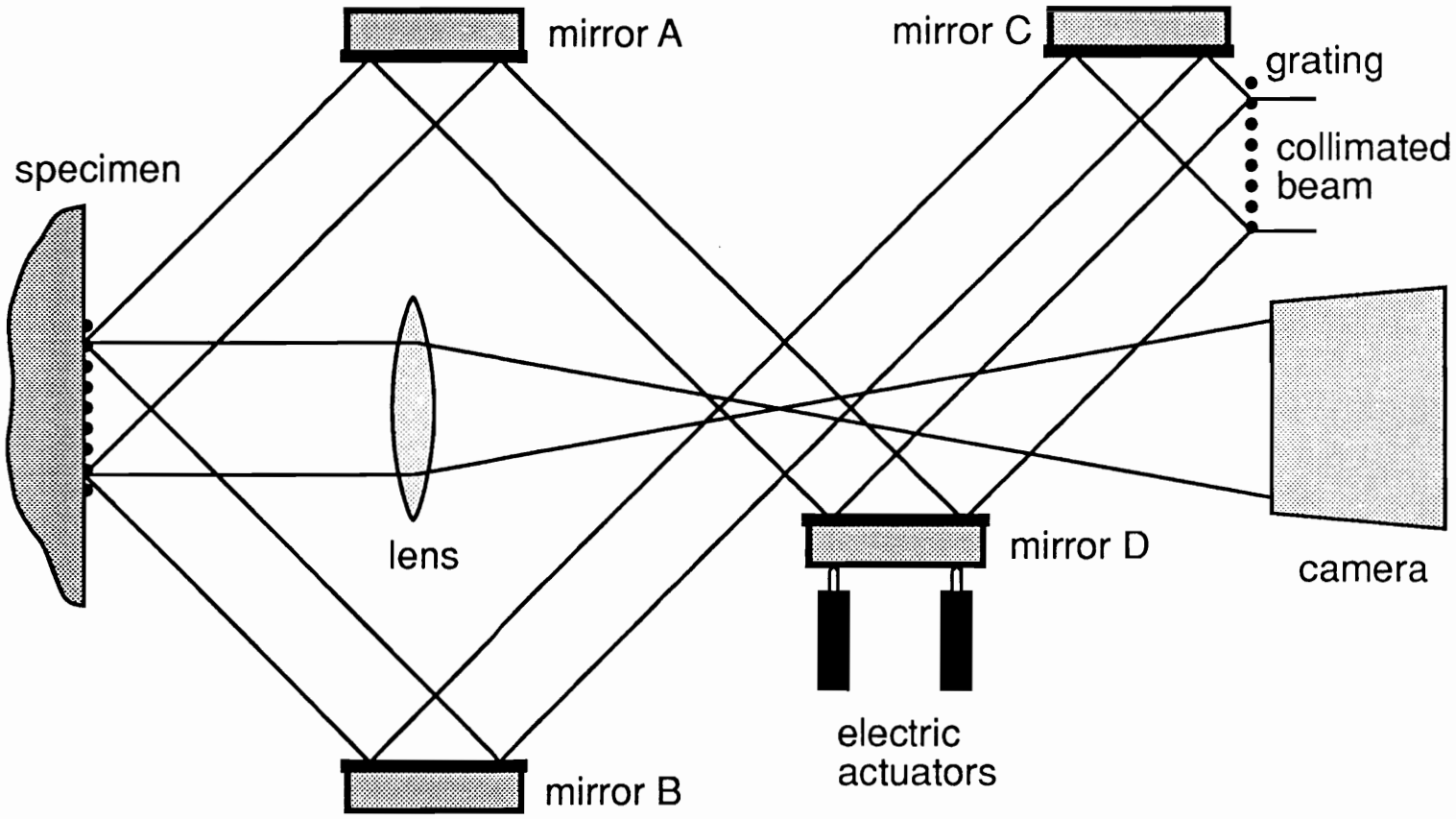

Figure 3.2 Moiré interferometer for high-temperature measurements.

To obtain all three components of the in-plane strain tensor, it is necessary to measure two orthogonal components of the in-plane displacement field. To achieve this goal, two systems were built on a common frame, creating a stable and compact instrument. Figure 3.3 depicts the configuration of the interferometer for two-dimensional applications. A total of four remotely controlled actuators were used to control the system in two-dimensional measurements. This design allows not only fine tuning of the interferometer to eliminate the initial field, but also a rigid-body rotation of the whole instrument with respect to the specimen. This is useful in introducing a carrier pattern of rotation, which can be used in a high-resolution analysis of deformation of the specimen [44].

3.3 Features of the Whole System

The interferometer is positioned in the vacuum oven that was designed and built specifically for this purpose. Due to the use of the achromatic interferometer, the sensitivity of this system does not change from small angular deviations of illuminating beam. For this reason, the laser, the collimating optics, and the camera back can be positioned outside of the vacuum oven, as illustrated in Figure 3.4, thereby reducing the requirements for the size of the interferometer and oven. Thus the volume to be evacuated is reduced.

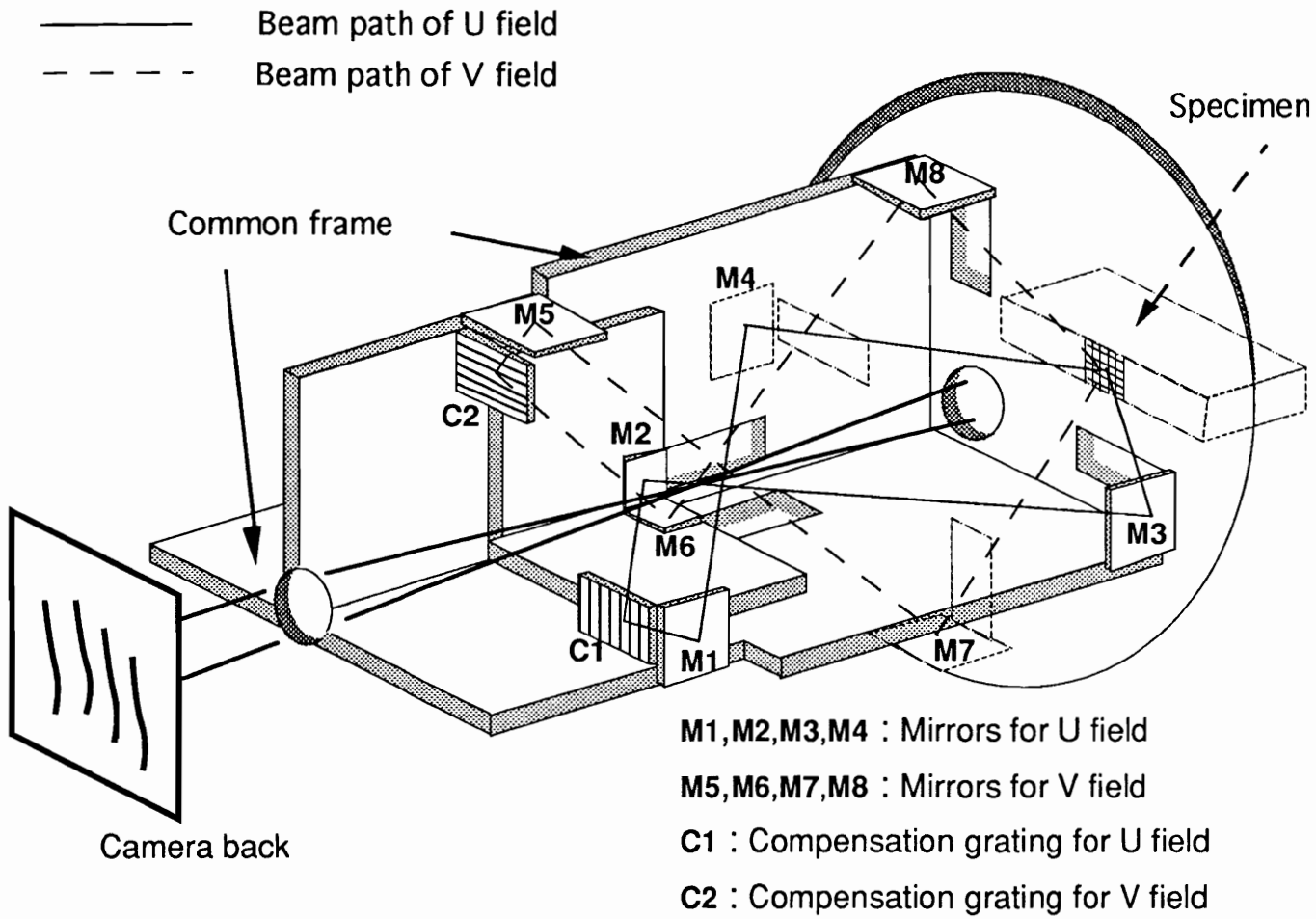

Figure 3.3 High-temperature moiré interferometer for two-dimensional measurements.

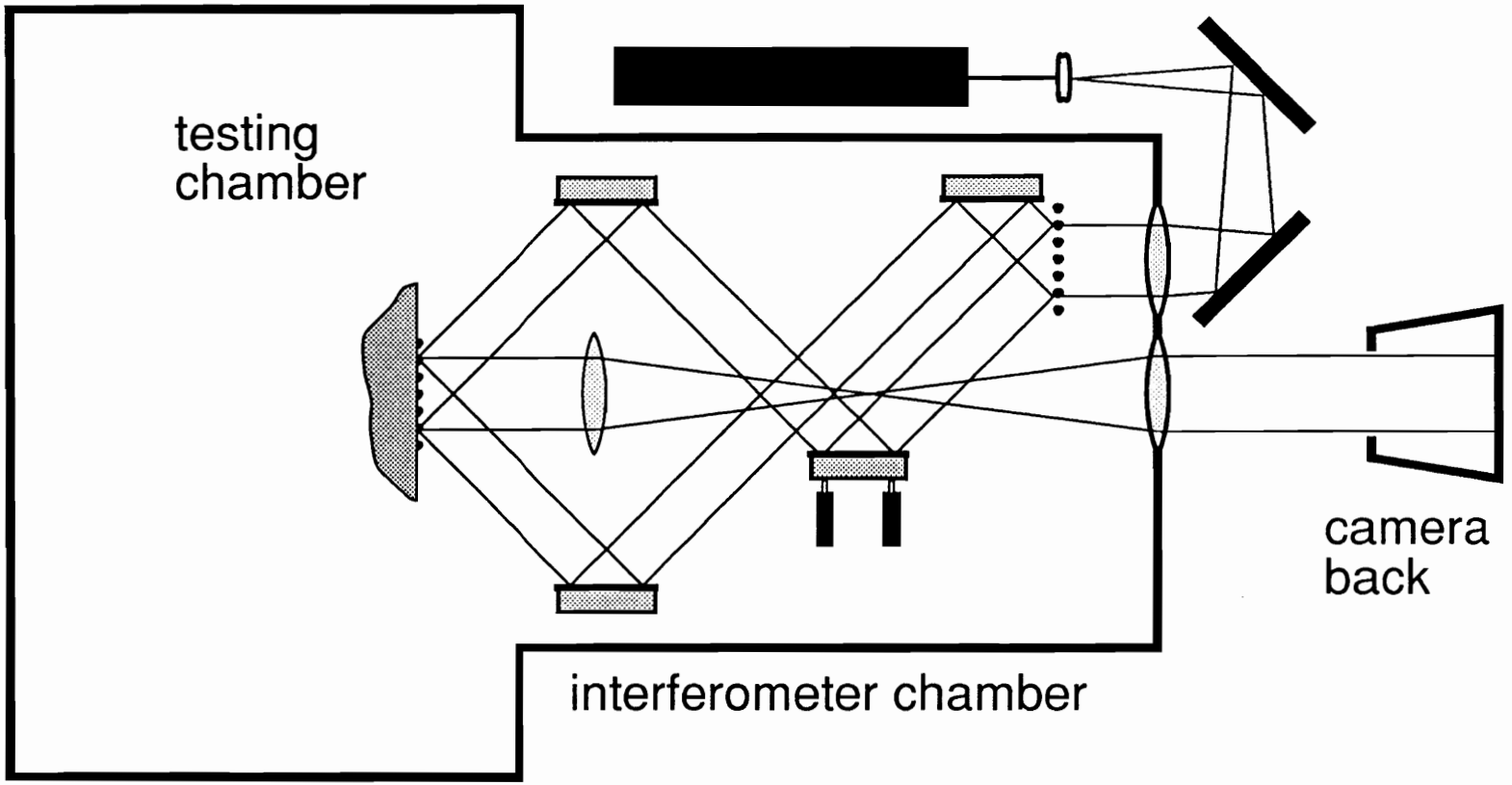

Figure 3.4 Schematic diagram of the vacuum oven for high-temperature moiré interferometry.

As mentioned in Section 2.4, a small angular movement of the illuminating beam will shift the location of the illuminated area without changing its size. Since the light source is outside the vacuum chamber, the illuminated region can be slightly moved by changing the illuminating beam with the outside mirrors. This feature makes tuning of the system easier.

The optical configuration consists of two windows, two linear diffraction gratings, and eight mirrors to illuminate the specimen. The windows are made of single lenses and are used as collimating elements. One is for U field measurement, and the other is for V field measurement. This arrangement not only allows easy selection of field but also minimizes the number of optical elements in the optical path, and therefore improves the efficiency of the system. The size of the illumination area is 25mm x 25mm, which is suitable for most applications.

The temperatures of the interferometer and the specimen are monitored by a number of thermocouples connected to a data acquisition system based on a Macintosh personal computer. The data acquisition board used also provides for control of the heaters, if such control is needed in some future application, such as a long-duration creep test.

In summary, the primary idea of this methodology is to provide a more stable testing environment than the other ones which provide the convection testing environment. Therefore, the vacuum is

provided for high-temperature measurements. The whole system setup is so compact that the loading due to the applied vacuum and the cost of the setup are reduced. In brief, the compactness is achieved by the separation of the illuminating source from the interferometer, and the use of the lens to obtain the collimation of the beam. The system is vibration-insensitive and provides many convenient features such as ease of control.

4 HIGH-TEMPERATURE SPECIMEN GRATING

The epoxy grating can withstand up to 220°C, and the silicone rubber grating starts to degrade around 350°C. To be specific, the temperature limit of the specimen grating depends on the testing time and the bonding adhesive used for transferring. Since the goal of this work was to provide the capability to test various materials at temperatures as high as 1000°C, a new method of specimen grating preparation was necessary.

Instead of using the grating replication procedure from the mold grating directly, the so-called plasma-etched grating for higher temperature use was chosen in this study. It is a procedure similar to the one widely used in the micro-chip industry and investigated as the specimen grating by some researchers [40,49]. For example, Sciammarella et al. [49] electroetched directly on the surface of the specimen without the additional step of evaporating a thin metallic layer on top. The etched grating had a frequency of 40 lines/mm. This sensitivity was too low to meet our objectives. A preliminary investigation of the plasma-etched technique to create a high-sensitivity specimen grating was studied in [40] by Morton and Czarnek, but no high-temperature measurements were reported. This study was, in part, an extension of that work. The interference fringes obtained were intended to demonstrate the feasibility of this method. The measurements performed and some difficulties encountered are discussed in the next chapter. Here, the choice of

metallic layer, the approach of plasma-etched gold grating, and the heating method are discussed in detail.

4.1 Metallic Layer

After the melting point, oxidization rate, and reflectance at high temperatures were considered, the metallic layer for the plasma-etched approach was selected. A list of the melting points of several materials is given in Table 4.1 [50]. In general, at lower temperatures, aluminum is preferred because of its low cost and high reflectance. The low melting point (only about 660°C) and the high oxidization rate at high temperature which accelerates the deterioration of the grating limit its application to high-temperature moiré.

Gold performs better than aluminum because it is inert to oxygen even in a high-temperature environment, and has a melting point as high as 1060°C. Another strength is that the reflectance of gold is high at high temperatures. Also, gold's softness makes it easy to etch. Since only a tiny amount of gold is necessary for vacuum deposition, cost was not a problem.

Tungsten has a very high melting point but also has a high oxidization rate, so a high vacuum environment is necessary. Also, it is more difficult to evaporate than aluminum and gold. For this reason, the cost of the setup for grating making will be raised if

Table 4.1 Melting points of several materials.

Material	Melting Point (°C)
Aluminum	660.37
Gold	1064.43
Iron	1535
Silver	961.93
Tungsten	3410

tungsten is used. Tungsten is a poor alternative unless very high temperature measurement is required. Therefore, with its many advantages, gold was chosen as the metallic layer in our high-temperature work.

It should be noted that, in principle, a grating can be etched directly into the specimen material. However, this procedure would require separate developmental work for each new material to be tested. Having a standardized coating makes grating preparation a more routine procedure.

4.2 Plasma-Etched Gold Grating

The high-temperature grating was produced by etching through a photoresist mask and into the metallic layer. The preparation procedure is illustrated in Figure 4.1. The first step was to polish the surface of the specimen to a surface roughness of about the same order as the wavelength of the light used, or better. Then the specimen was cleaned and degreased. To improve adhesion, the specimen was placed in a vacuum chamber equipped with a plasma-etching device to clean the surface with plasma beam. A thin layer of gold was vacuum-deposited on the prepared surface. The thickness of this layer was on the order of 100 Å (Angstrom).

After the specimen was removed from the vacuum chamber, the metallic layer was coated with photoresist by the spinning or

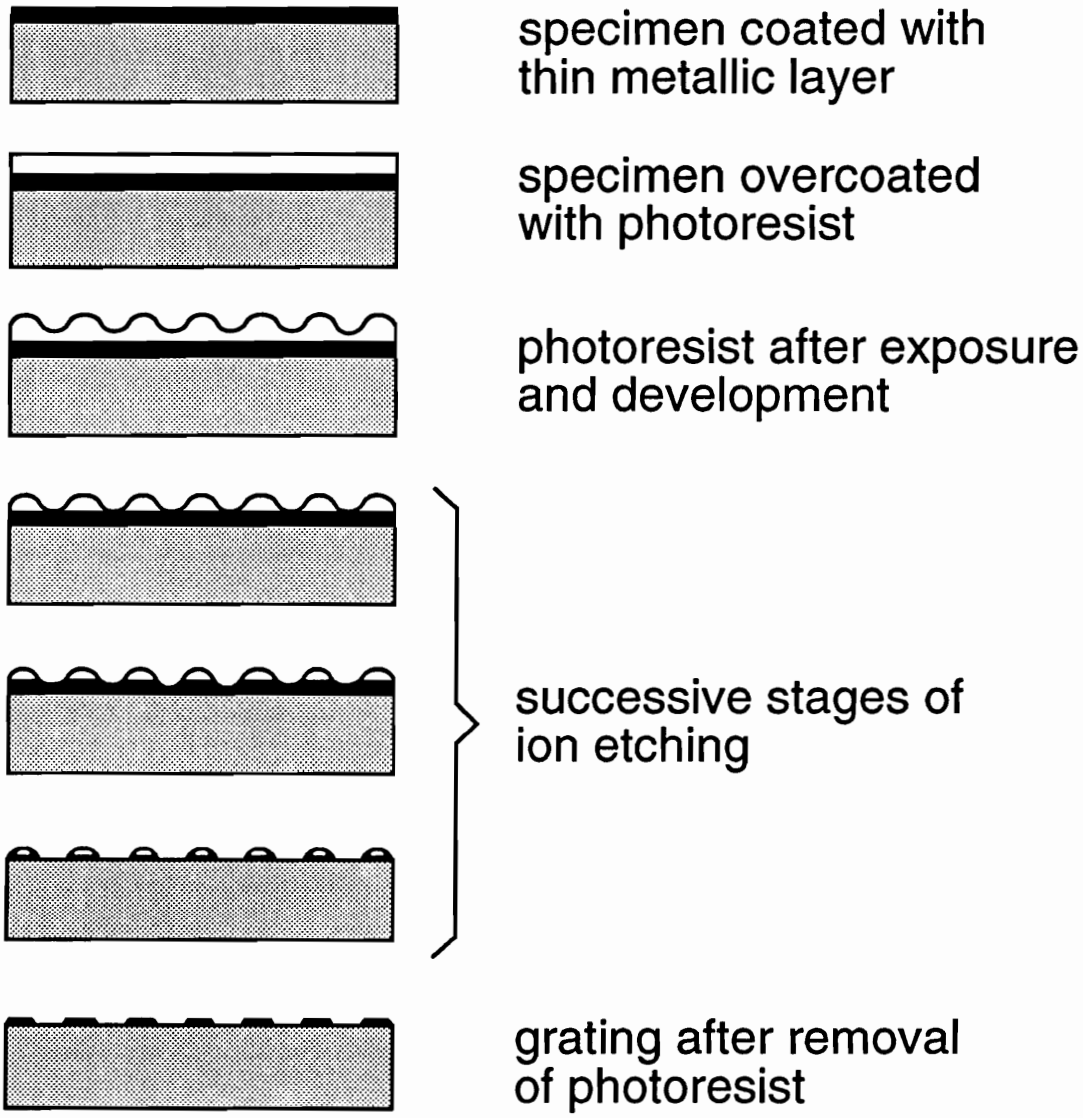

Figure 4.1 Preparation procedure of etched grating for high-temperature applications.

dragging method, depending on the geometry of the specimen. The spinning method is usually recommended for circular shapes, while the dragging method is for irregular shapes. Different spin rates ensure control over the thickness of the photoresist layer. Also, the ratio of photoresist to thinner is critical in controlling the layer thickness. Once coated with photoresist, the specimen was baked in an oven at 90°C for 30 minutes, or at 60°C for 1 hour. An environment with a yellow safety light is preferred for all work with the photoresist because the photoresist grating is insensitive to yellow light.

The specimen was then positioned in an interferometry system where the interference of two collimated beams produces uniformly spaced planes of constructive interference separated by planes of destructive interference. Because the photoresist is more sensitive to shorter wavelength light sources, a high-power Krypton laser with violet color and a wavelength of 413 nm was used as a source of light to shorten the exposure time. However, the exposure time was still around 60 seconds at the power intensity of 62 $\mu W/cm^2$ on the specimen. A HeCr laser at 430 nm can be an alternative source of light, but the necessary exposure time is much longer. The frequency of interference planes was chosen to be 600 lines per millimeter.

A positive photoresist was used. Therefore, after development, the exposed photoresist dissolved during the

developing process, and a photoresist grating mask with bar and space for a linear grating was created. Subsequently, the specimen was positioned in the vacuum chamber which was filled with oxygen at a pressure of the order of one millitorr. The plasma source was activated, and the specimen was etched for a few minutes. The quality of the grating was examined under a microscope, and the etching was continued if needed. Once a satisfactory result was obtained, the photoresist was dissolved away with acetone, and the remaining gold strips became a linear diffraction grating. In practice, a phase grating or amplitude grating can be obtained, depending on the etching time.

Similarly, a cross grating could be made by exposing in both horizontal and vertical directions. When measurement at extremely high temperature is expected, the specimen can be etched directly without using a metallic layer. Sometimes, if the specimen is too hard, it is difficult to etch into the specimen even though the photoresist has been etched out completely.

4.3 Heating Method

There are three modes of heat transfer: convection, radiation, and conduction. As mentioned earlier, vacuum is important and has been used in this study. For this reason, the convection heat transfer cannot be used; only contact and radiant heaters were

considered. In this study, conduction heat transfer was chosen by using a commercial resistance heater, resistance wire, or a so-called ceramic heater. The heater power was controlled by a transformer. Because the specimens were usually small, the temperature difference on the surface of the specimen was minimal and stable after a few minutes at constant power. Since the radiant heater is more expensive, and neither extremely high temperature nor temperature uniformity was required, the conduction heat transfer was the preferred method in this study.

As the testing temperatures are below 600°C, commercial resistance heaters such as kapton heater (approximately up to 200°C) and strip heater (approximately up to 600°C) are available. A thermally conductive silicone paste is used to increase the thermal conductivity between the specimen and the heater.

At higher temperatures, the available commercial heaters, mostly with their large sizes compared to the specimen, could emit much radiant heat to the optical system. For this reason, a ceramic heater which attached directly to the specimen was used to minimize the size of the heater. Figure 4.2 depicts the preparation of a ceramic heater. The first step was to wrap the resistance wire around a ceramic plate which was about the same size as the specimen. The wire used was a Nickel-Chromium alloy resistance wire (also known as Nichrome wire) able to withstand temperatures up to 1150°C. A thicker copper wire was used to connect the

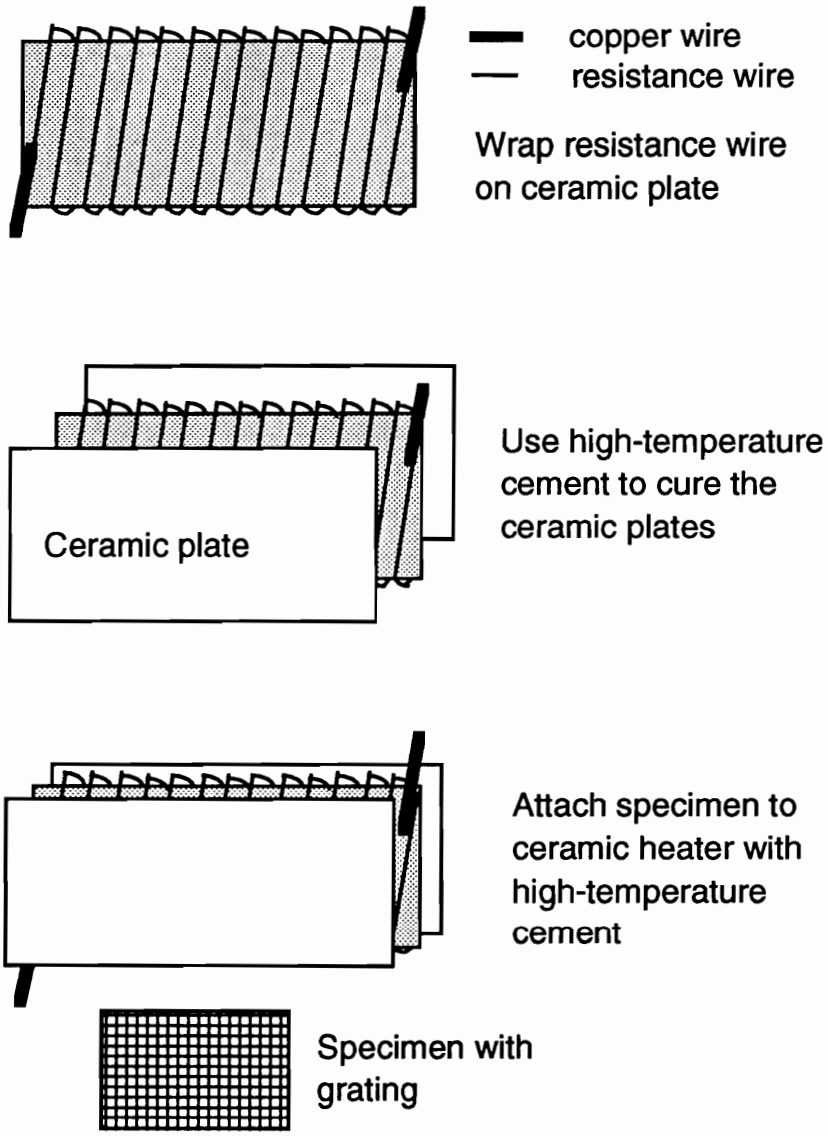

Figure 4.2 Preparation procedure of ceramic heater for high-temperature applications.

resistance wire to an electric outlet to avoid the exposure of the resistance wire outside of the heater. This precaution reduced the chance of premature failure at the connection point. Then this ceramic plate with resistance wires was sandwiched between two ceramic plates, and sealed by using a high-temperature air-set cement which has high thermal conductivity and excellent electrical insulation. After curing, the ceramic heater was connected to a power supply and was ready for high-temperature tests. Measurements at high temperatures are demonstrated in Chapter 5.

Tungsten wire, which has a very high melting point, was tried in place of the resistance wire in the ceramic heater. A test was performed up to 700°C, at which point the wires suddenly burned through. This phenomenon was attributed to the fast oxidation rate of tungsten at high temperatures. This would have been an alternative for a high temperature heating element if a better vacuum had been achieved.

5 MEASUREMENTS AT HIGH TEMPERATURES

A new method for high-temperature measurements using moiré interferometry is demonstrated in this chapter. After the high-temperature moiré system was set up, a number of experiments were performed to exploit the capability of moiré interferometry at high temperatures. The survivability of the grating played an important role. Thus, this part of the work was divided into two branches. One was the investigation of the use of a silicone rubber grating in which epoxy was replaced by silicone rubber as the transferring adhesive. This work was intended to extend the temperature limit of the specimen grating when the replication procedure was used. The other direction was the plasma-etched grating used to move moiré interferometry to a temperature close to 1000°C.

5.1 Silicone Rubber Grating

In order to have a specimen grating with higher temperature resistance, the early study was focused on the choice of high-temperature silicone rubber instead of epoxy. It was similar to the work of Kang et al. [30]. In our experimental study, gold was used as a metallic layer, while the silicone rubbers GE RTV 630 and GE RTV 31 were used as the adhesive.

Basically, the preparation procedure is similar to that for the epoxy grating. Figure 5.1 gives a detailed illustration of the procedure. In brief, after the specimen surface is cleaned, a primer is applied uniformly to the surface by means of the dragging method in order to get good adhesion between the rubber and the specimen. The silicone rubber is prepared by mixing the silicone rubber compounds and silicone curing agent thoroughly; the mixture is more viscous than PC10 epoxy. Since the curing time is around 48 hours, the mixture can be positioned in a vacuum chamber to get rid of the air inside the mixture. Then a weight is applied to control the thickness of the silicone rubber. After having been cured and separated, the specimen with the sinusoidal silicone rubber grating is vacuum-deposited with a metallic layer for better reflection. Note that in the epoxy grating, the metallic layer was coated before replication.

Silicone rubber was observed to turn black if aluminum was used for the coating. As mentioned in the previous chapter, gold has good characteristics at high temperatures. Therefore, the silicone rubber was also coated with gold in our study.

A test was performed on a steel block on which a grating of 1200 lines/mm frequency was replicated by the use of GE RTV 630 silicone rubber. Figure 5.2 shows the fringe patterns for both U and V fields at a temperature of 210°C. Stable fringe patterns were observed for at least an hour. When the temperature of the specimen

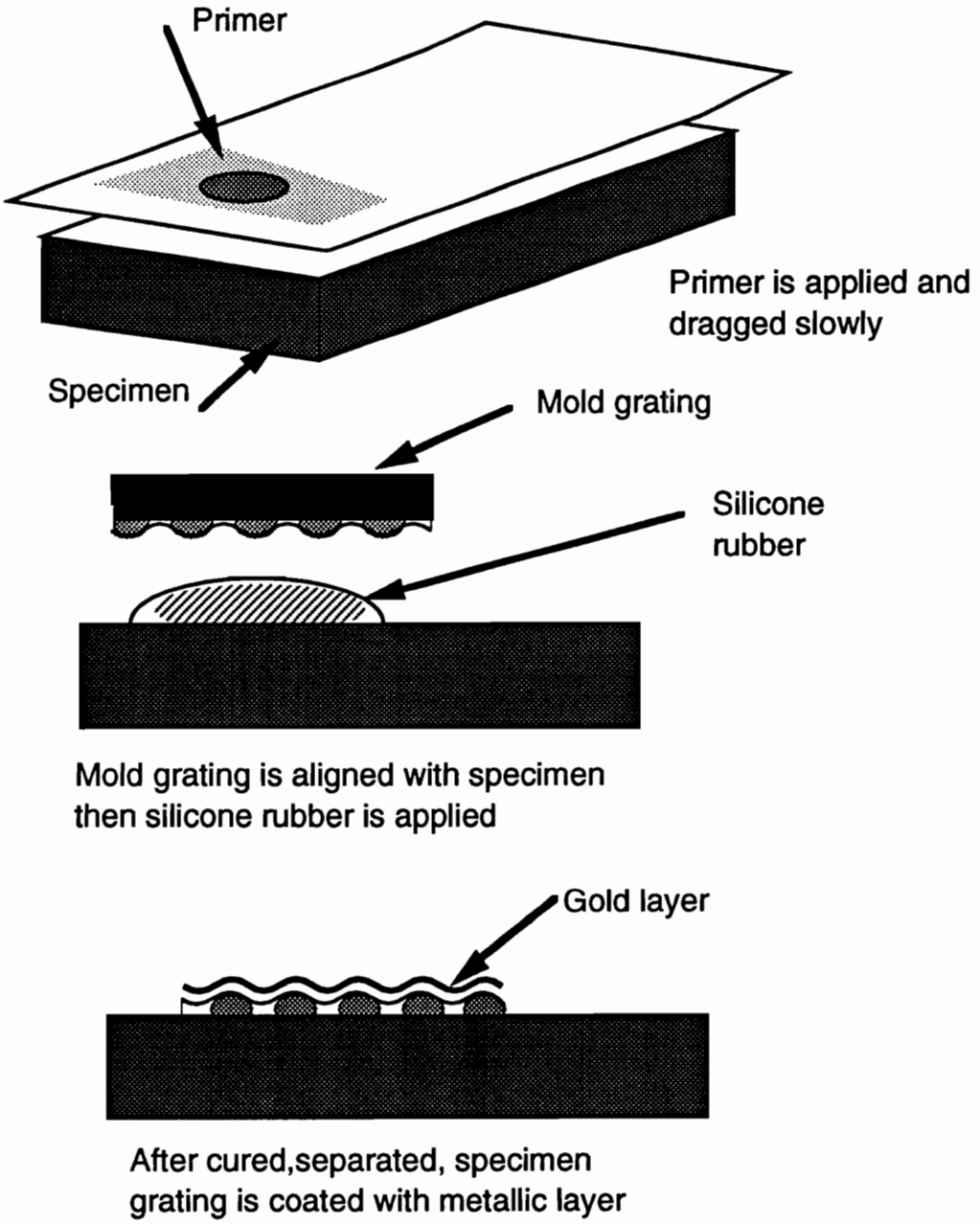

Figure 5.1 Preparation procedure of silicone rubber.

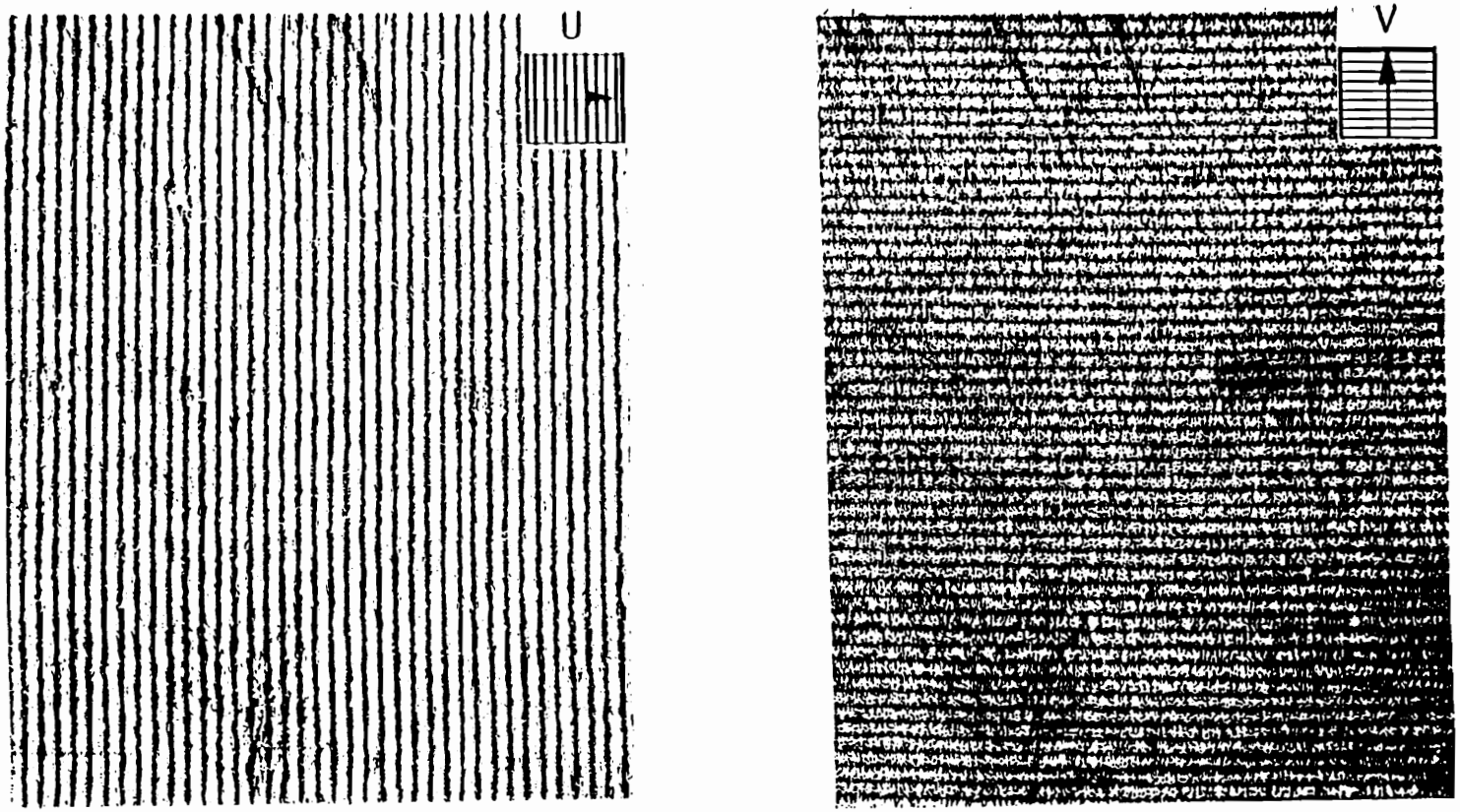

Figure 5.2 U and V displacement patterns representing the thermal deformation of a steel block with silicone rubber grating. Temperature was 210°C.

was above 350°C, the specimen grating began to degrade. Then the specimen grating deteriorated rapidly. The last recorded patterns were at the temperature of 357°C. As shown in Figure 5.3, the loss of contrast and deterioration of the grating could be observed in some regions. This result matches well with the manufacturer's data sheet, according to which the recommended working temperatures range up to 204°C.

RTV 31 silicone rubber for high-temperature applications was also tested; the highest temperature obtained was around 350°C. In summary, according to our experimental result and manufacturer's information, the silicone rubber grating could not survive above 400°C. It is comfortable to use below 350°C for a short term test.

The silicone rubber grating extends the application of the moiré technique up to around 350°C; however, this does not meet the temperature objective. The measurement using a plasma-etched grating is demonstrated in the following section.

5.2 Plasma-Etched Gold Grating

For the plasma-etched grating, gold is also used as the metallic layer in this study. Its preparation procedure was described in Chapter 4. To confirm that the approach selected for high-temperature grating preparation was feasible, an etched gold specimen grating was created on a block of silicon-carbide ceramic

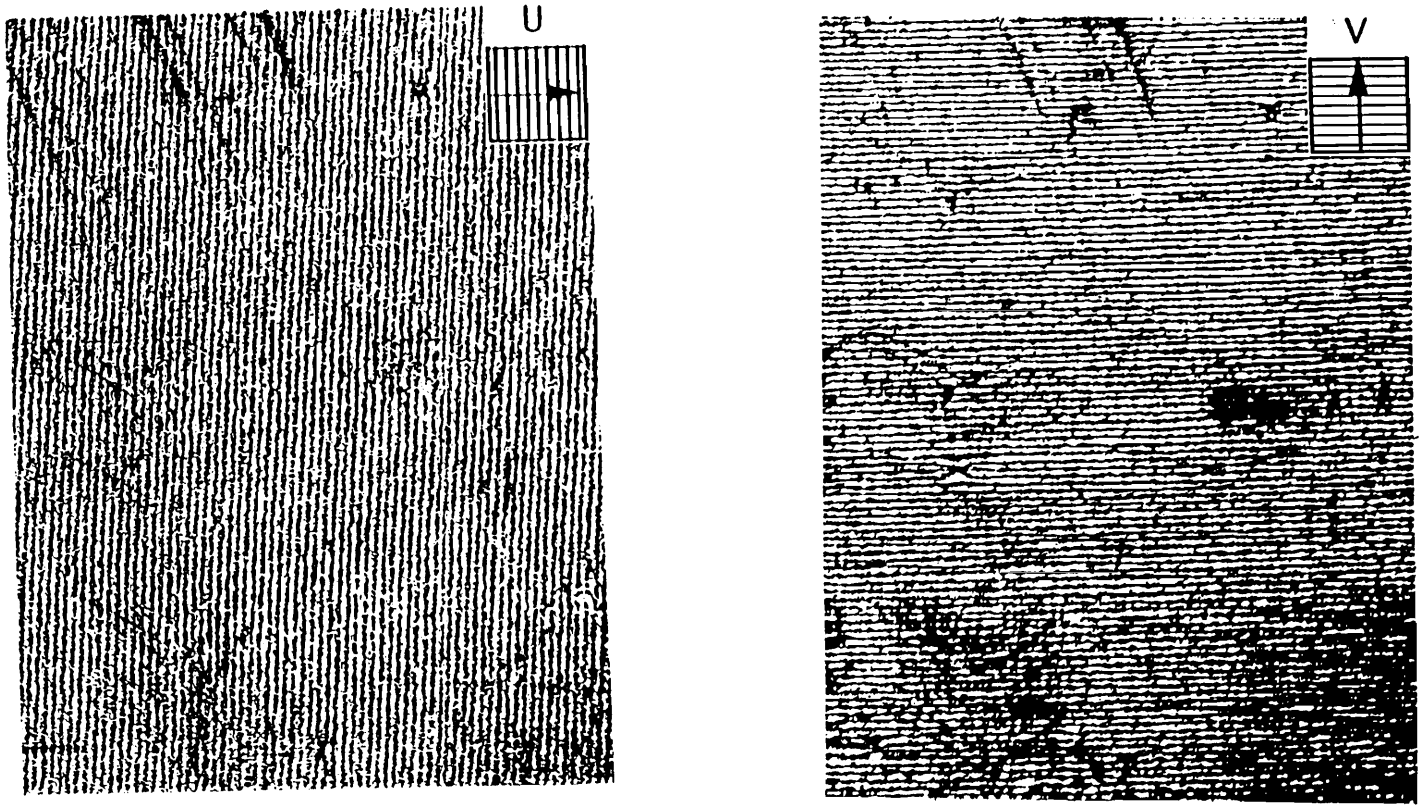

Figure 5.3 U and V displacement patterns representing the thermal deformation of a steel block with silicone rubber grating. Temperature was 357°C.

which has both a high melting temperature and a high thermal conductivity. The specimen was polished with diamond paste to reach a mirror-like surface finish. The high temperature diffraction grating was tested to examine its survivability and diffraction at elevated temperatures. Thus, the specimen was positioned in a furnace and heated in 100°C increments up to 1100°C. At each temperature step, the grating was illuminated with a laser beam and a diffracted beam was observed on a screen. No deterioration of the grating was noticed, and the diffraction was good at all temperature steps, indicating that moiré measurements can be performed at these temperatures by using this kind of grating, at least for short periods of time.

These results confirmed the feasibility of using the plasma-etched grating as a high-temperature specimen grating. However, in practice, instability in the moiré system, low intensity of the grating, or background noise could result in nonphotographable patterns. For this reason, obtaining stable and photographable interferometric fringe patterns at high temperatures was the final goal which would demonstrate that the proposed high-temperature moiré system and specimen grating were a workable experimental method. Silicon-carbide, metal-matrix composite and quartz, each having high working temperatures, were chosen as specimens. Only thermal loading was applied.

The specimen gratings were linear gratings etched with the frequency of 600 lines/mm. Therefore, the second diffraction order was used in our setup for the following tests with the sensitivity of 417 nm per fringe order. Equations (2.1), (2.10) and (2.11) can give the relationship between the diffraction order and the frequency of the specimen grating.

5.3 Silicon-Carbide Ceramic

The same specimen used for the previous test was then wrapped with the resistance wire (Nickrome wire) and positioned in the vacuum oven. The resistance wire was used as the heating element, and was able to withstand temperatures up to 1150°C. After the system was tuned to the null field, the specimen was heated slowly to above 500°C. The vacuum was kept at a pressure of 1.1 torrs. The highest temperature at which a pattern was recorded was 520°C. Soon afterwards, the resistance wire burned. The recorded pattern is illustrated in Figure 5.4.

5.4 Metal/Matrix Composite

The first test proved that high-temperature measurements can be performed on real structural materials, provided the surface can be polished to optical quality. The second test was on a

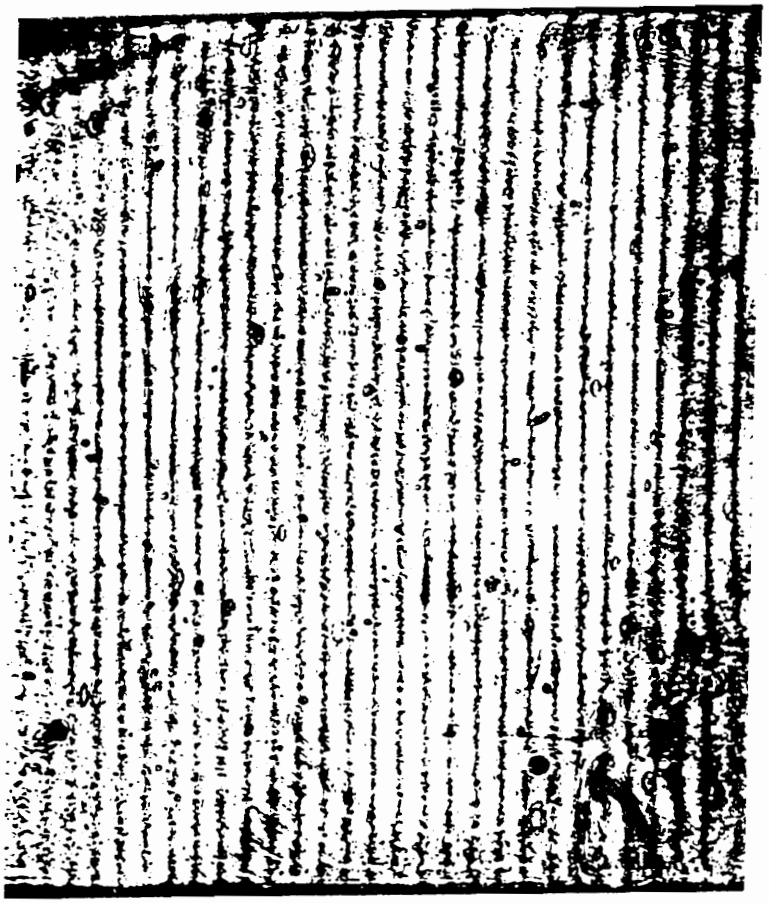

Figure 5.4 Moiré pattern representing the horizontal displacement field due to thermal deformation of a silicon carbide specimen at 520°C.

metal/matrix composite. The composition of the specimen was titanium as matrix and silicon-carbide as fiber. Similar polishing work as mentioned before was performed on this specimen. It appeared that the quality of the polish of this specimen was slightly lower than that of the silicon-carbide specimen. Even so, a high contrast fringe pattern was recorded at the temperature of 434°C, as shown in Figure 5.5.

A ceramic heater was also used in this test. As mentioned earlier, this design would minimize the size of the heater and reduce the emission of heat to the optical system. However, as the temperature rose to 650°C, the specimen surface started to glow, and the ceramic heater turned red and produced more radiation. This background noise became more intense as the temperatures got higher, and reduced the contrast of the fringe pattern and made the fringe pattern unphotographable. As mentioned in Section 2.3, an optical filter system based on a lens and an aperture was arranged to filter out spatially incoherent noise. The lens was used to converge the information beams, and the spatial filter was located at the focal point, as shown in Figure 5.6. The size of the aperture should be as small as possible so that more noise could be filtered, but it should not disturb the information beams. Figure 5.7 shows the pattern at 765°C with the filter arrangement; tiny carrier fringes of rotation were added. It can be observed that a small region of deterioration occurred.

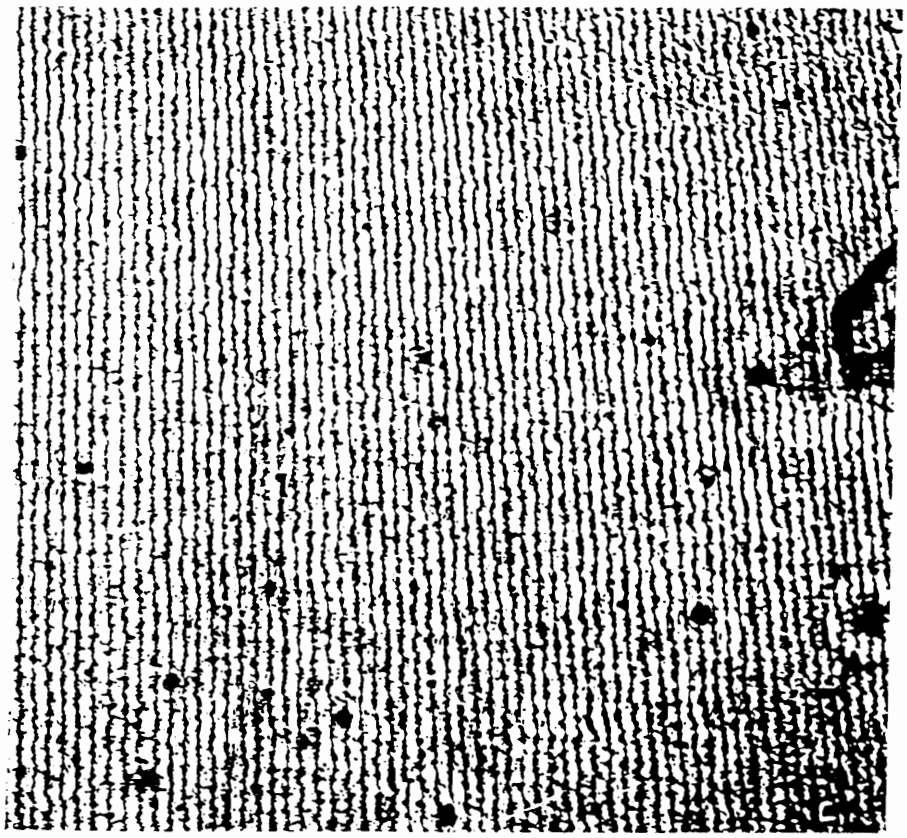

Figure 5.5 Moiré pattern representing the horizontal displacement field due to thermal deformation of a metal/matrix composite specimen at 434°C.

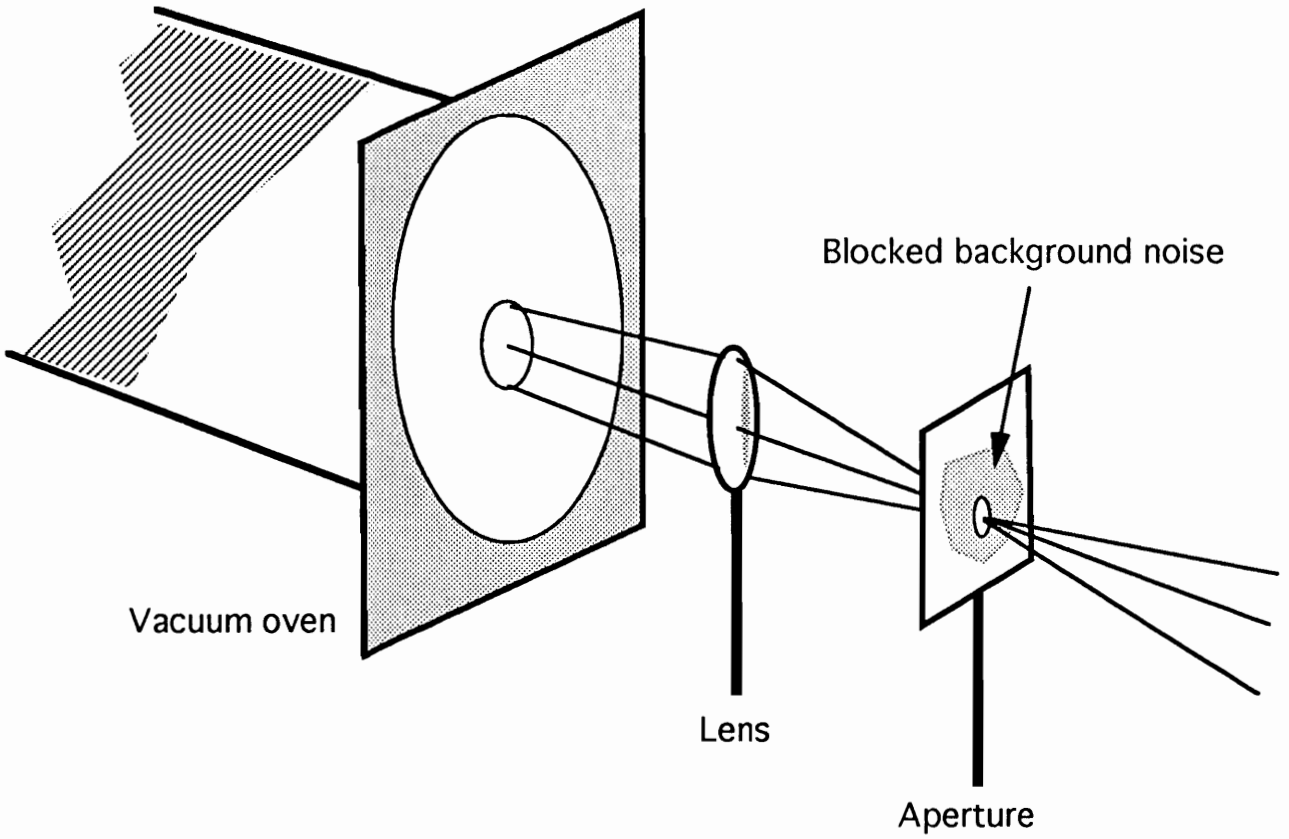

Figure 5.6 Optical filter arrangement. An aperture was used to block the background noise.

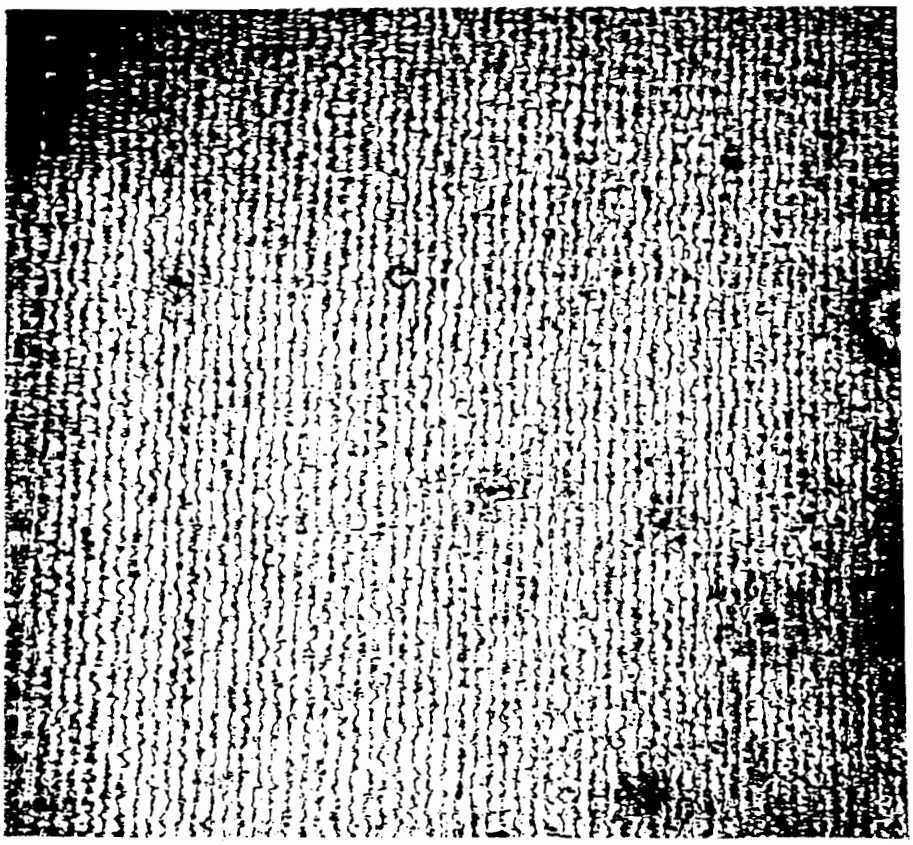

Figure 5.7 Moiré pattern representing the horizontal displacement field due to thermal deformation of a metal/matrix composite specimen at 765°C.

When the temperature went up to 800°C, the interference pattern's contrast gradually degraded and at around 830°C was unphotographable. This phenomenon is ascribed to the oxidation of the specimen which makes the specimen blacker as the temperature increases. This material typically begins to oxidize in air around 760°C. The vacuum testing environment retarded the oxidation rate.

5.5 Quartz Specimens

The above test demonstrated that one advantage of the plasma-etched grating is that the flatness of the specimen's surface is not very critical. Also, testing in vacuum eliminated thermal convection currents. In order to minimize the cost and time required for specimen preparation, further tests were conducted on polished quartz specimens that can be purchased commercially. Since the specimens were transparent, the back surfaces were ground to avoid double reflections which could produce thickness fringes (Fizeau fringes). In addition, black pencil was used to paint the back surface, in order to obscure the glow from the heater. Two types of thermocouples, K and E, were attached to the specimen. The maximum useful temperatures for types K and E range up to 1250°C and 900°C, respectively. So, the temperature reading can be monitored precisely from the room temperature to 1000°C.

The first test performed on the quartz utilized a circular disk which was wrapped with heating wire around its edge. Also high-temperature ceramic cement was applied on the edge to reduce the exposed area of wire. The circular shape of the disk made it easy to apply the photoresist to the specimen by spinning. A more uniform photoresist grating could be obtained, resulting in a more uniform efficiency of an etched grating. Figure 5.8 illustrates the fringe pattern at a temperature of 680°C. A small carrier fringe of rotation was added. No significant contrast loss was observed due to the glow from the specimen and heater.

Heater failure governed the peak test temperatures of several tests. To reach higher test temperatures, additional tests were performed, but on thinner quartz plates which were more readily heated. Also, several selections were tried to make the heater survive at higher temperatures, for instance different diameters and alloys of heating wires, and different arrangements for wire wrapping. Measurements above 800°C were demonstrated as follows.

Even though the above filter arrangement (Figure 5.6) worked at temperatures around 800°C, the optical noise emitted from the ceramic heater was too high above 850°C. The orange glow from the heater made for very low-contrast fringes. The effect of noise on the contrast of the interferogram was mentioned in Section 2.3. A narrow band interference filter with the central wavelength at 632

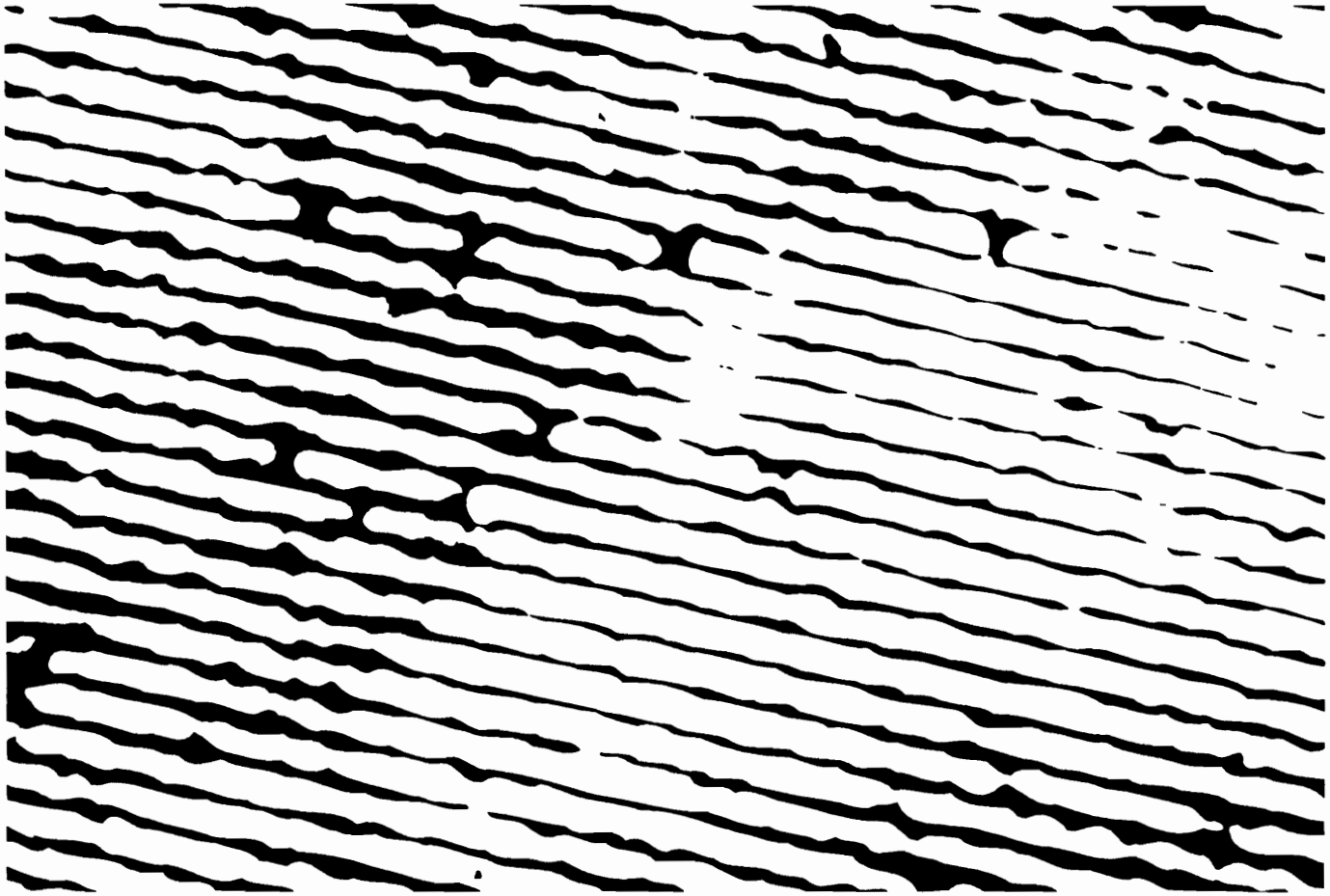

Figure 5.8 Moiré pattern representing the horizontal displacement field due to thermal deformation of a quartz specimen at 680°C. A small carrier pattern of rotation was added.

nm (the wavelength of the laser source) and half bandwidth of 10 nm was used to further minimize the background noise. Figure 5.9 depicts the setup for this purpose. This setup was based on Figure 5.6; here, the interference filter was placed in front of the vacuum oven. Apparently, the intensity of the information beam in this arrangement would be lower than it was in the original setup without the filter arrangement. Therefore, a slightly longer exposure was necessary. Figure 5.10a shows the pattern without the use of this filter at the temperature of 860°C. As can be seen in the central part of the specimen, the temperature was so high that only a bright picture and a low-contrast fringe are observed. Figure 5.10b shows the high quality pattern obtained by using the filter at a temperature of 880°C. As can be seen, the contrast is significantly enhanced and a larger region is observed.

This arrangement eliminated the background noise very effectively and resulted in a successful experiment at a temperature of 980°C after several attempts. The specimen was a quartz plate cemented to a ceramic heater. No mechanical load was applied, but the difference between the thermal coefficient expansion of quartz and that of the underlying ceramic material caused the development of stresses high enough to fracture the quartz plate. Figure 5.11 demonstrates a fragment of a fringe pattern recorded at this temperature. As can be seen, the contrast is very good and the fringes are stable and well defined. However, part of the grating deteriorated, and the pattern could not be recorded at that spot.

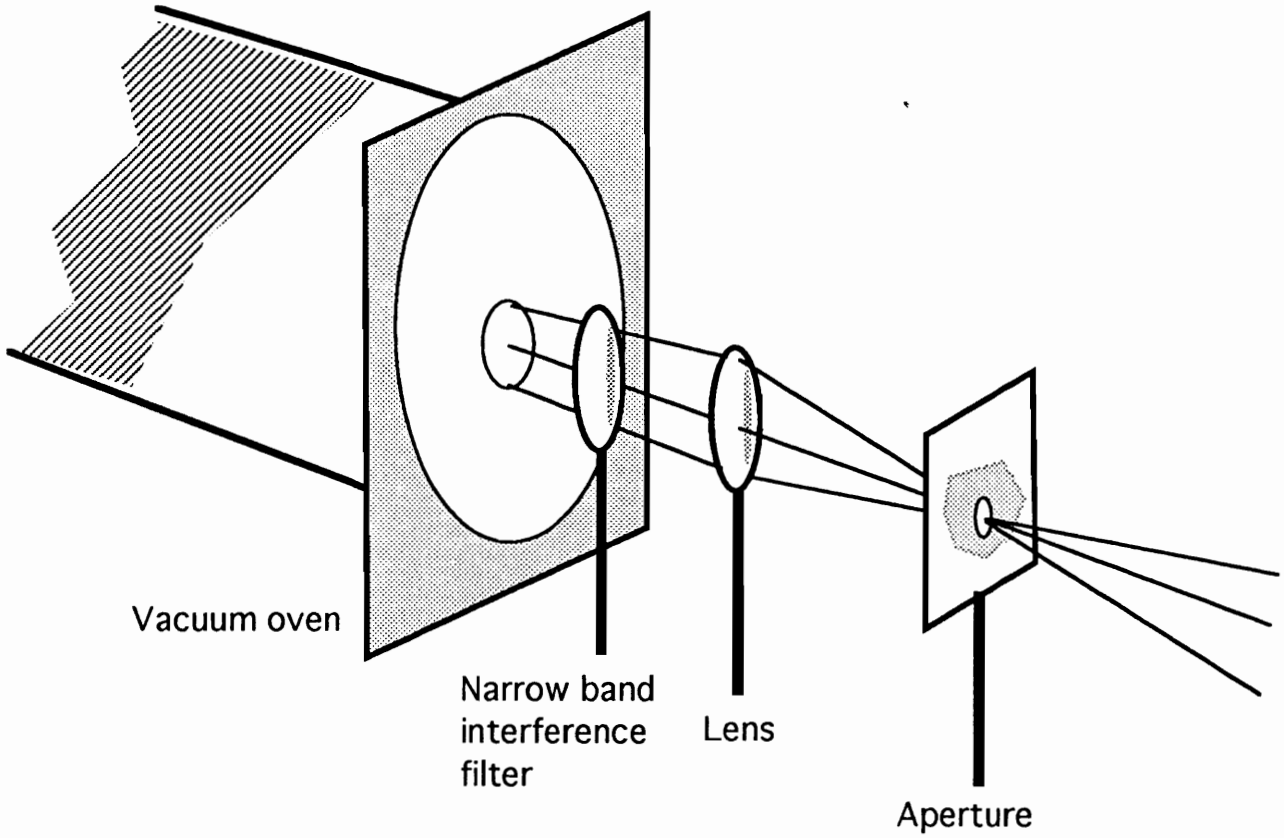

Figure 5.9 Optical filter arrangement. A narrow band interference filter was used together with an aperture to block the background noise.

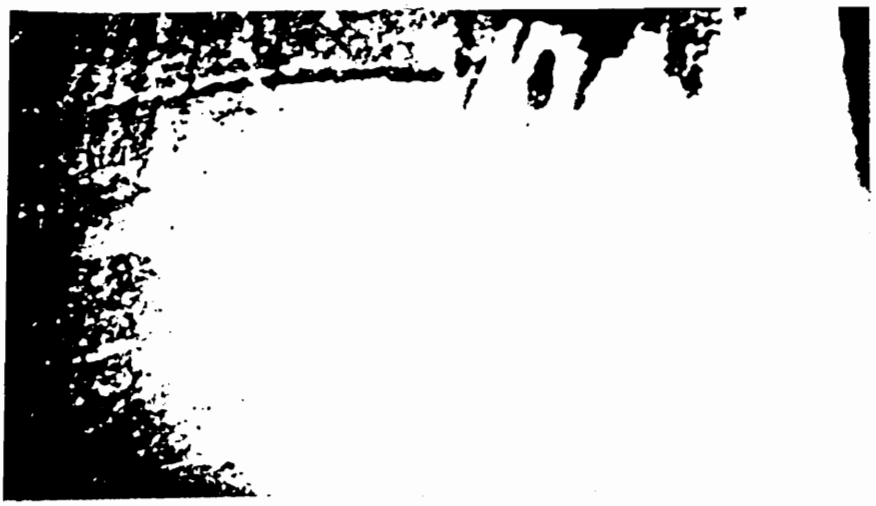

(a) 860°C

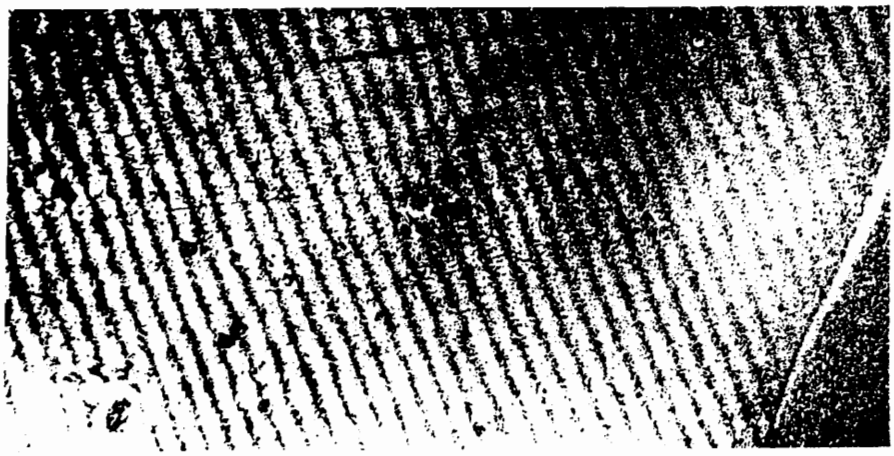

(b) 880°C

Figure 5.10 The effect of the filter system is demonstrated.
(a) The moiré pattern at 860°C without filter, and
(b) moiré pattern at 880°C with filter.

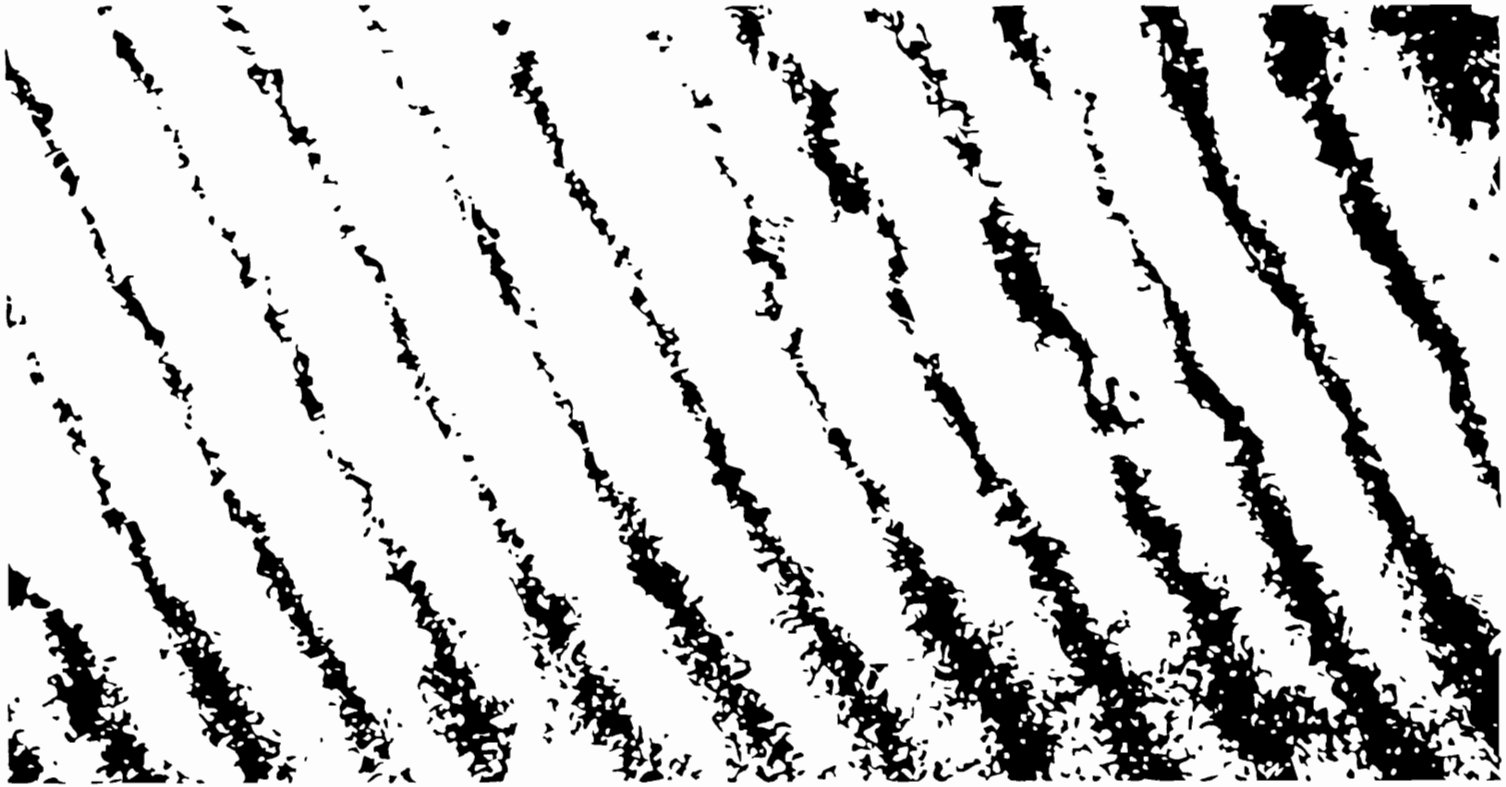

Figure 5.11 Moiré pattern representing the horizontal displacement field due to thermal deformation of a quartz specimen at 980°C.

This last experiment proves that measurements can be performed at these temperature levels as long as the specimen grating can survive. As mentioned before, a gold grating can survive a short exposure to temperatures as high as 1100°C at an atmospheric pressure. However, several experiments performed in vacuum, where the heating rate is much lower, showed that gratings etched into a very thin gold layer slowly evaporate from the surface of the substrate. In the experiment, the layer of gold was not uniform, and only its thickest part survived.

5.6 Summary

Silicone rubber used in the replication procedure extended the survivability of the replicated specimen grating up to a temperature of 350°C. By using the plasma-etched grating, the objective of extending the range of applications of moiré interferometry to temperatures close to 1000°C has been reached. The superiority of a high-temperature moiré system with vacuum testing environment has been confirmed. The system effectively isolated the vibration and minimized thermal convection currents which caused the instability of pattern. For test temperatures above 650°C, the background noise, which degraded the contrast of the interference pattern, was minimized effectively by the use of the above mentioned filter systems.

Several successful tests with a high-quality interference pattern were performed on some high-temperature high-performance materials at elevated temperatures. These tests indicate the feasibility of using a plasma-etched gold grating as a specimen grating for high-temperature measurements. Also, slower oxidation rate of specimen grating in vacuum environment than in atmospheric environment will allow longer testing time and higher temperature measurement.

6 APPLICATIONS

The methodology of using a vacuum interferometer and plasma-etched specimen grating for the deformation measurements at high temperatures was demonstrated in the previous chapter. Some practical applications of the newly developed system are demonstrated in this chapter. The measurements were performed within the temperature limit of the epoxy grating while thermal loading was applied. Furthermore, a high-resolution data-reduction technique was used for the analysis of the strain distribution of a cutting tool bit.

6.1 Thermal Expansion of Aluminum

The free thermal expansion of an aluminum block was investigated. This specimen was cut from a sheet of aluminum 7075 with a thickness of 6.7 mm. The specimen grating was replicated with a cross reflective grating with a frequency of 1200 lines/mm. The specimen was then positioned in the high-temperature vacuum oven and heated to around 220°C. The vacuum was kept at a pressure of 2 torrs. As mentioned previously, conduction heating transfer was achieved with a commercial strip heater. In order to get better heat transfer between the heater and the specimen, a highly conductive paste was applied to the specimen/heater interface. The

fringe pattern was photographed after a few minutes for stabilization of a certain temperature.

Aluminum is isotropic; thus, a one-dimensional measurement was sufficient to provide the information for the analysis of free thermal expansion. The horizontal U displacement patterns at different temperatures are illustrated in Figures 6.1a and 6.1b. Because fringes were dense enough to analyze, no carrier pattern was added.

The normal strain, ε_x, is easily calculated by using Equation (2.4a). Here, $\lambda/(2\ \sin\theta)$ is equal to 1/2400. Then Equation (2.4a) becomes Equation (6.1):

$$\varepsilon_x = \frac{1}{2400}\frac{\Delta N_x}{\Delta x} = \frac{1}{2400}\frac{\Delta N_p}{(\Delta x_p/M)}, \qquad (6.1)$$

where ΔN_x represents the difference of fringe order between two points with the distance Δx on the specimen. Alternatively, ΔN_p represents the difference of fringe order between two points with the distance Δx_p in the photo, and M represents the magnification factor, which is obtained by taking the ratio of the size in the photo to that on the real specimen.

The procedure described above gives an average strain which can provide precise information for isotropic materials. Figure 6.2

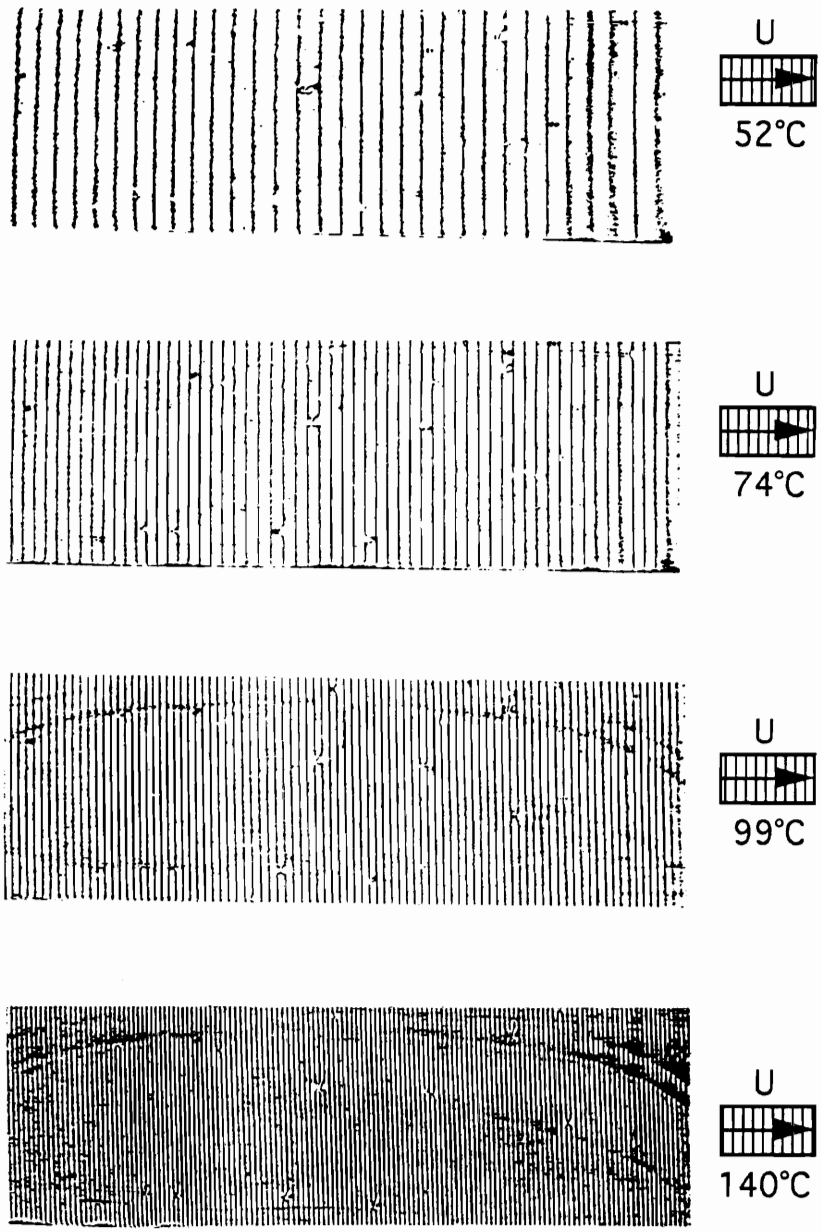

Figure 6.1a U displacement patterns representing the horizontal thermal deformation of an aluminum block at 52°C, 74°C, 99°C, and 140°C.

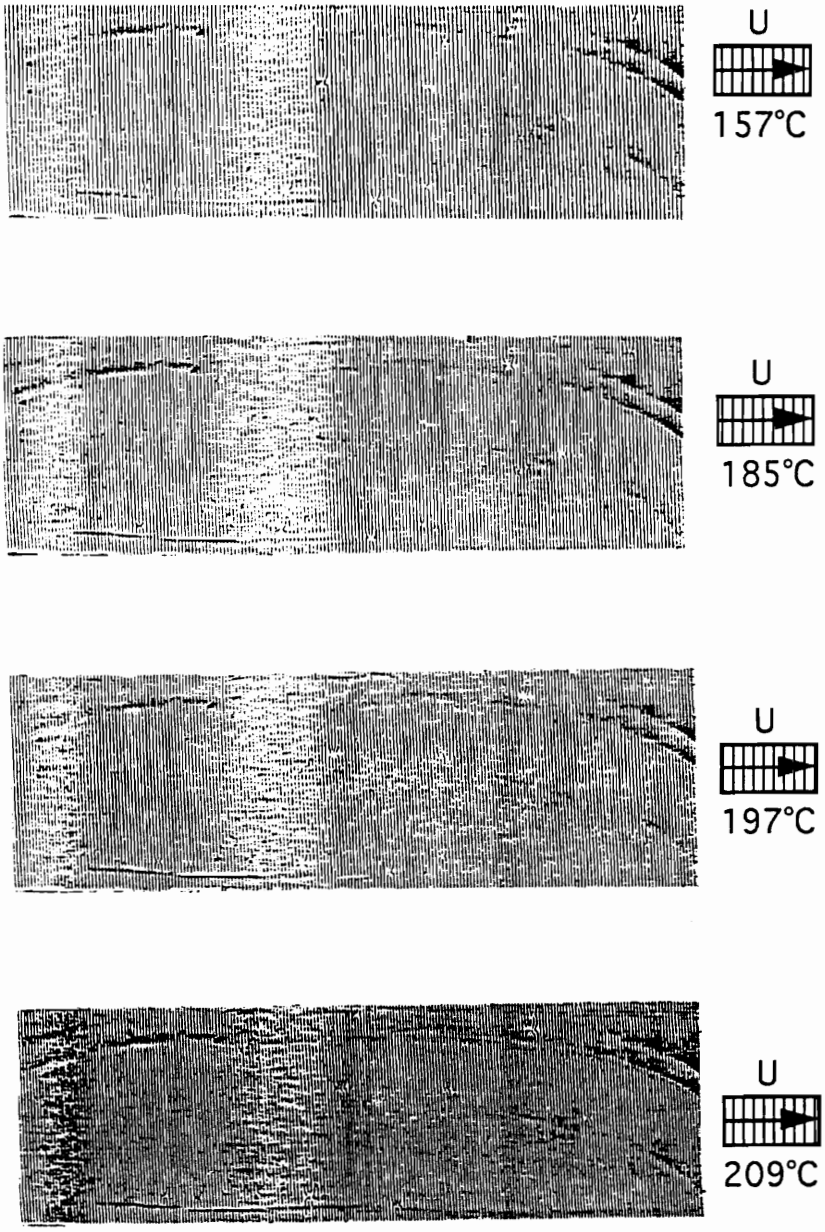

Figure 6.1b U displacement patterns representing the horizontal thermal deformation of an aluminum block at 157°C, 185°C, 197°C, and 209°C.

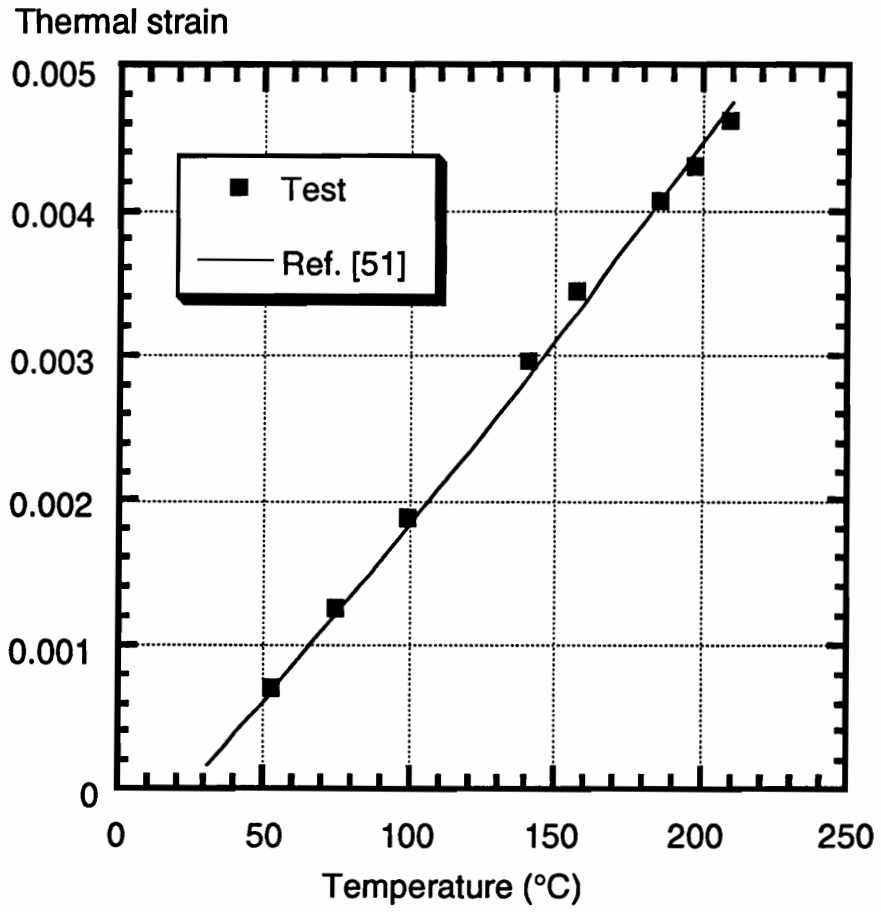

Figure 6.2 Comparison of thermal strains in aluminum: experimental results versus reference [51].

shows a good correlation between the test data and the values from the material properties book [51]. The test data are marked as square blocks. This is linear strain, indicating the strain relative to room temperature at 22°C. The discrepancy is within the error band of the instrumentation used in this experiment.

This test confirmed the validity of the optical system and the proposed approach.

6.2 Thermal Deformation of a Graphite/Epoxy Composite

A high-frequency diffraction grating was replicated on a graphite/epoxy composite coupon, with a stacking sequence of $[0_2/60_2/-60_2]_s$ and a thickness of 1.75 mm. The coupon was made of AS4 graphite fibers and 3502 epoxy system. Figure 6.3 illustrates the preparation of the specimen and the coordinate system used. In this work, measurement of thermal deformation of this specimen was demonstrated; the ply interface was the particular region of interest. The patterns were photographed every 40°C up to 180°C, beginning from room temperature, the temperature at which the null field was obtained.

Figure 6.4a illustrates the longitudinal or U displacement patterns at the temperatures of 60°C and 100°C. Illustrated in Figure 6.4b are the patterns at 140°C and 180°C. It can be seen that the strain gradient ($\partial U/\partial y$ or $\partial Nx/\partial y$) at the ply interface increases

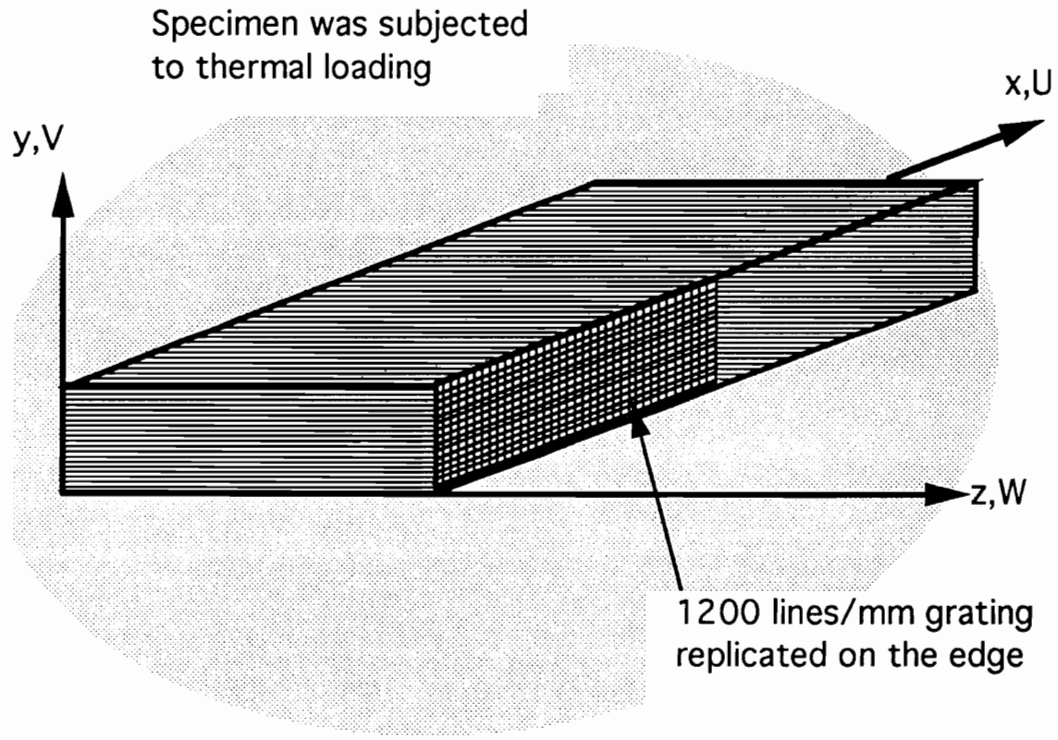

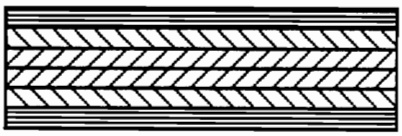

Stacking sequency:$[0_2/60_2/-60_2]_S$
Thickness:1.75mm

Figure 6.3 AS4-3502 graphite/epoxy composite specimen.

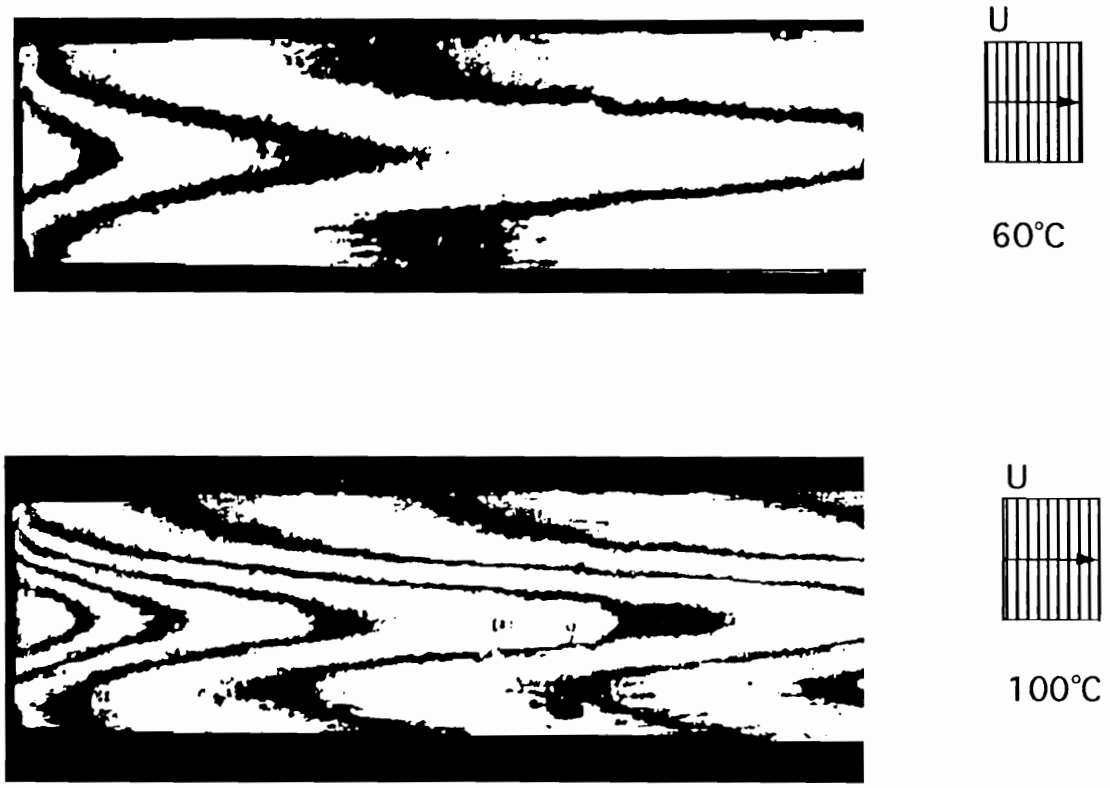

Figure 6.4a Horizontal (U) patterns representing the thermal deformation of the graphite/epoxy specimen at 60°C and 100°C.

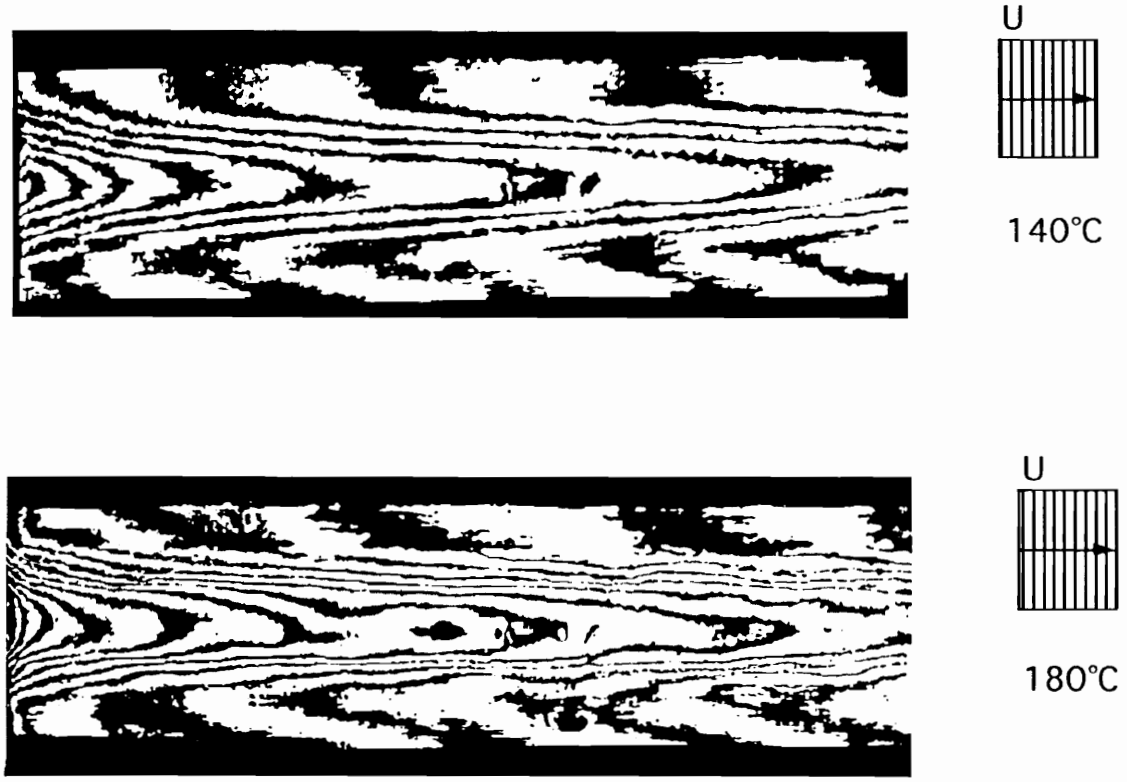

Figure 6.4b Horizontal (U) patterns representing the thermal deformation of the graphite/epoxy specimen at 140°C and 180°C.

with temperature, and occurs because of the thermal expansion mismatch between fibers and the matrix leading to edge effects. The shape of the fringes in these patterns is characteristic of the edge effect in this ply configuration. A large strain gradient, as evidenced in the pattern at 180°C, is ascribed to the fact that the material passed through the glass transition temperature and some residual stresses were released, causing a sudden increase in the deformation.

6.3 Metal/Matrix Composite with Optical Fiber

Optical fibers are commonly embedded in structural components as sensors. In this study, an optical fiber was bonded to the top of a metal/matrix composite, then coated with a ceramic layer. A high-frequency grating was replicated on the surface of the specimen which was cut from a sheet of plate. Figure 6.5 shows the configuration of this specimen. Thermal loading was applied to investigate the significance of the strain concentration around the optical fiber.

A representative thermal deformation in both U and V fields is shown in Figure 6.6. The temperature was 69°C. The location of the optical fiber could be seen easily. No drastic change of fringe was observed around the optical fiber, i.e., there was no significant thermal strain mismatch due to the presence of the optical fiber.

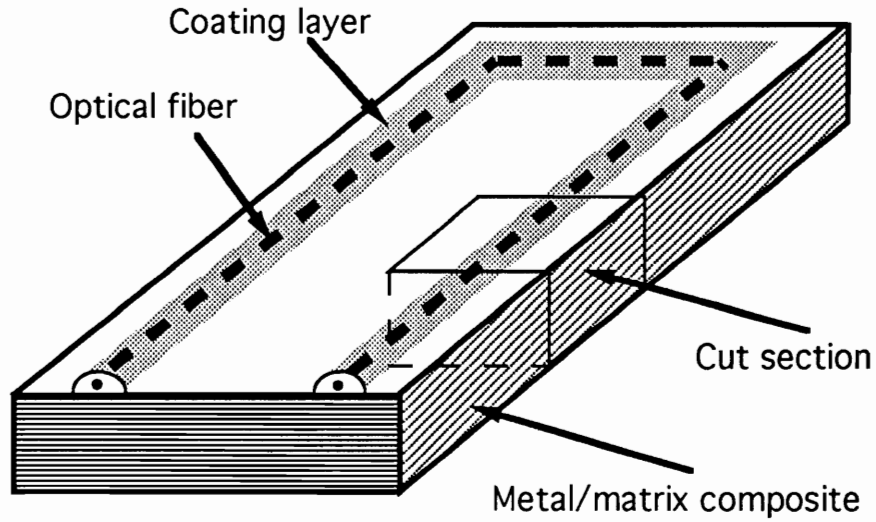

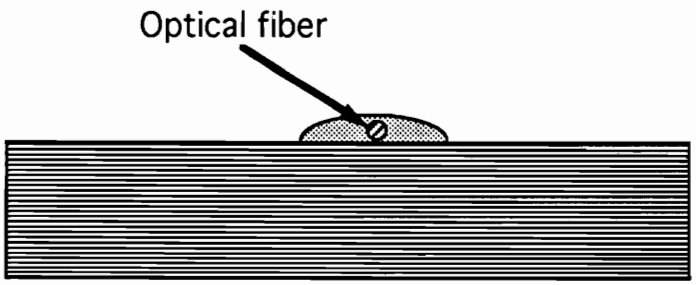

Enlarged view of cut section

Cross grating replicated on this surface

Figure 6.5 Metal/matrix composite with optical fiber.

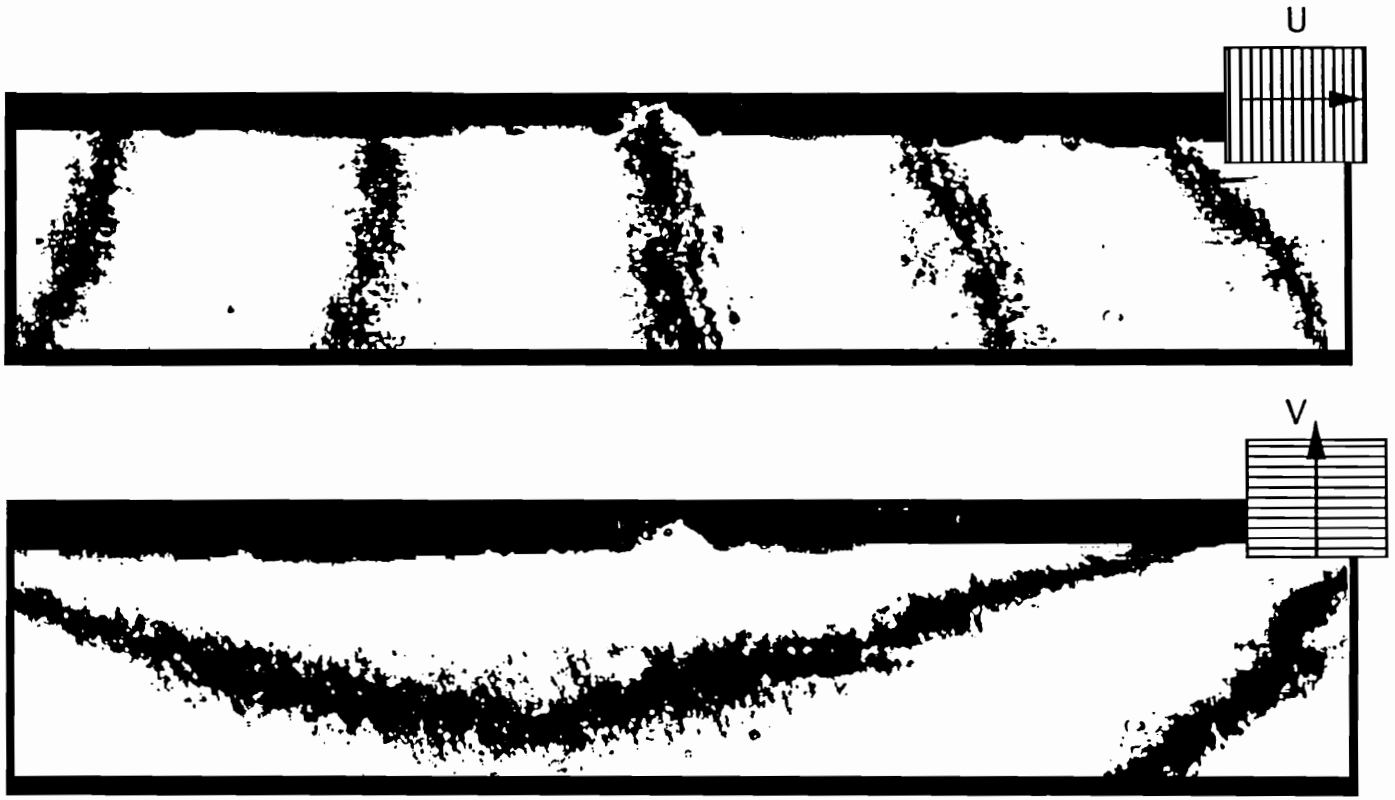

Figure 6.6 Thermal deformation in both U and V fields of a metal/matrix composite with an optical fiber at 69°C.

This test was performed in temperatures up to 185°C. Carrier fringes of rotation were introduced and recorded in Figure 6.7 with enlarged views of the region of the optical fiber. The patterns also show the insignificance of thermal strain mismatch because the strain gradient of the fringes does not change much compared to that in the far field. Several tests were performed on this type of specimen, and similar results were observed. These tests confirm that it is possible to position the optical fiber on the surface of the structure in order to avoid considering thermal strain concentration.

The same arrangement using a different ceramic coating was also tested. The specimen preparation was the same as the last one. No significant thermal mismatch was observed either. Besides, an interesting phenomenon was noticed in one test. Figure 6.8a demonstrates the fringe patterns at the temperature of 78°C. No evident phenomenon was observed, but after the carrier fringes of rotation were added, the significant strain concentration around the optical fiber was noticed in both U and V fields. Figure 6.8b demonstrates the fringe patterns. The carrier fringes of rotation could enhance the data resolution for local variation. This test provides a good demonstration of the capability of this system. However, this concentration may be ascribed to the defect embedded in the ceramic around the region of the optical fiber.

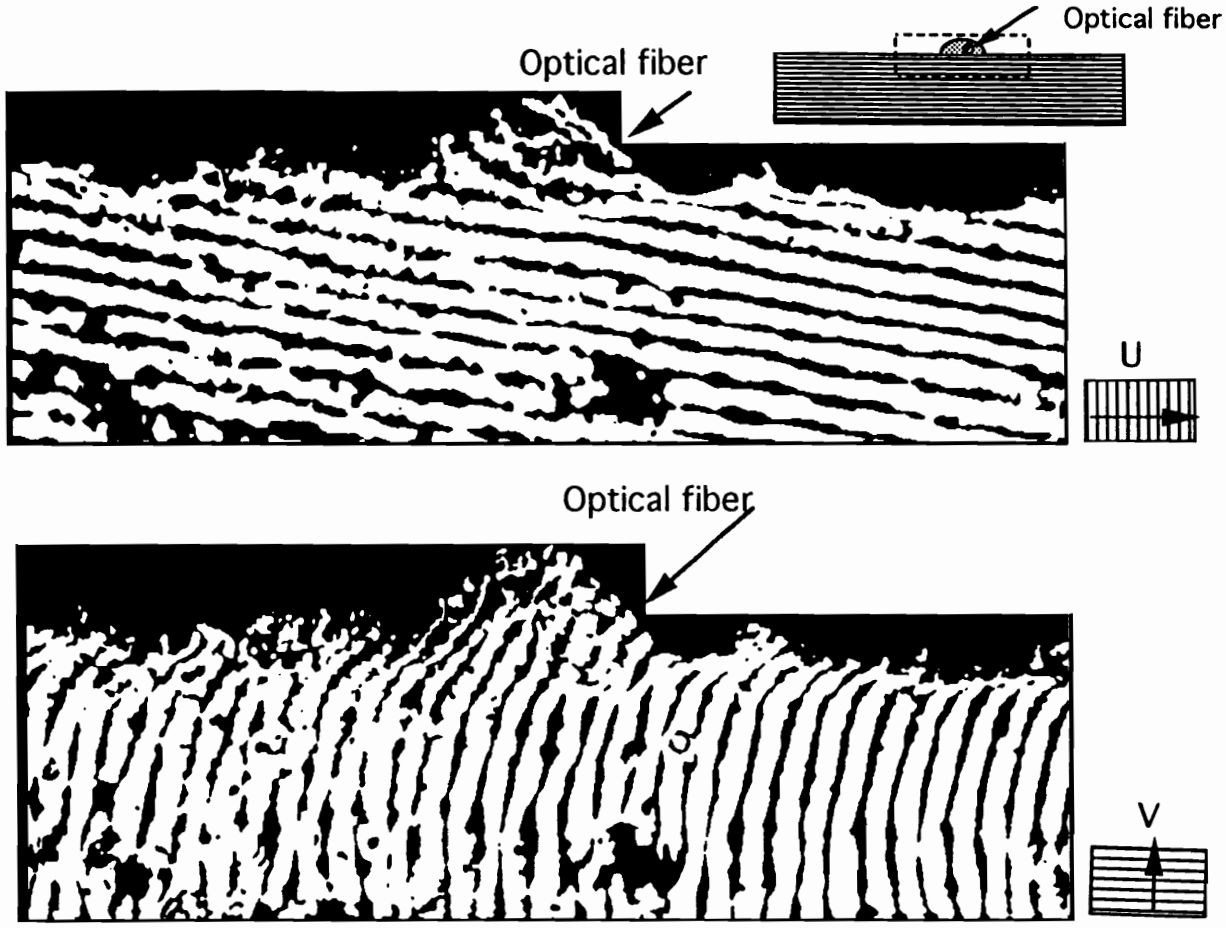

Figure 6.7 Thermal deformation in both U and V fields of a metal/matrix composite with an optical fiber at 185°C. Carrier fringes of rotation were added.

Figure 6.8a Thermal deformation in both U and V fields of a metal/matrix composite with an optical fiber at 78°C. A ceramic layer was coated.

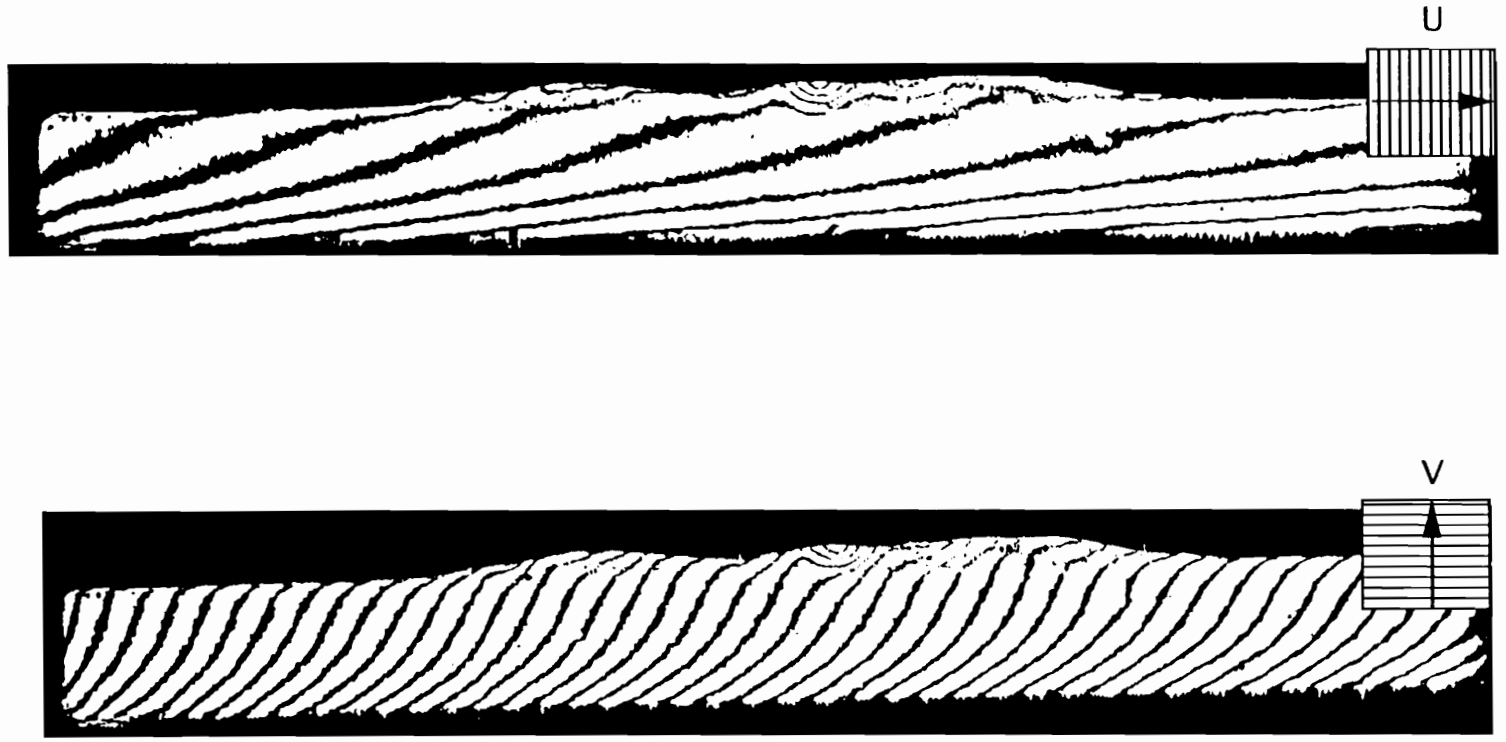

Figure 6.8b Thermal deformation in both U and V fields of a metal/matrix composite with an optical fiber at 78°C. A ceramic layer was coated. Tiny carrier fringes of rotation were added.

6.4 Cutting Tool Bit

6.4.1 Thermal Deformation Measurement

A cutting tool bit is an assembly of at least three different materials, which are steel, tungsten carbide, and an alloy of copper. Strain concentration is natural in the region of the material interfaces. In practice, during machining, the tool is subjected to a thermal loading. For this reason, thermal deformation mismatch between the different materials of the tool was observed to further the understanding of this practical situation. The strain distribution was measured. The interfaces were the areas of interest.

The specimen was cut from a commercial tool bit having an uneven side surface. After polishing, a grating with a frequency of 1200 lines/mm was replicated on the surface, as illustrated in Figure 6.9. The specimens were heated and fringe patterns were recorded at several temperature steps. Figures 6.10a and 6.10b show the representative patterns of U and V fields at the temperature of 219°C. A significant thermal deformation mismatch was observed around carbide/steel, carbide/alloy of copper, and alloy of copper/steel interfaces. In order to employ the high-resolution data-reduction technique, the original fringe patterns were photographed with slight overexposure and with carrier fringes of rotation, as shown in Figures 6.10c and 6.10d.

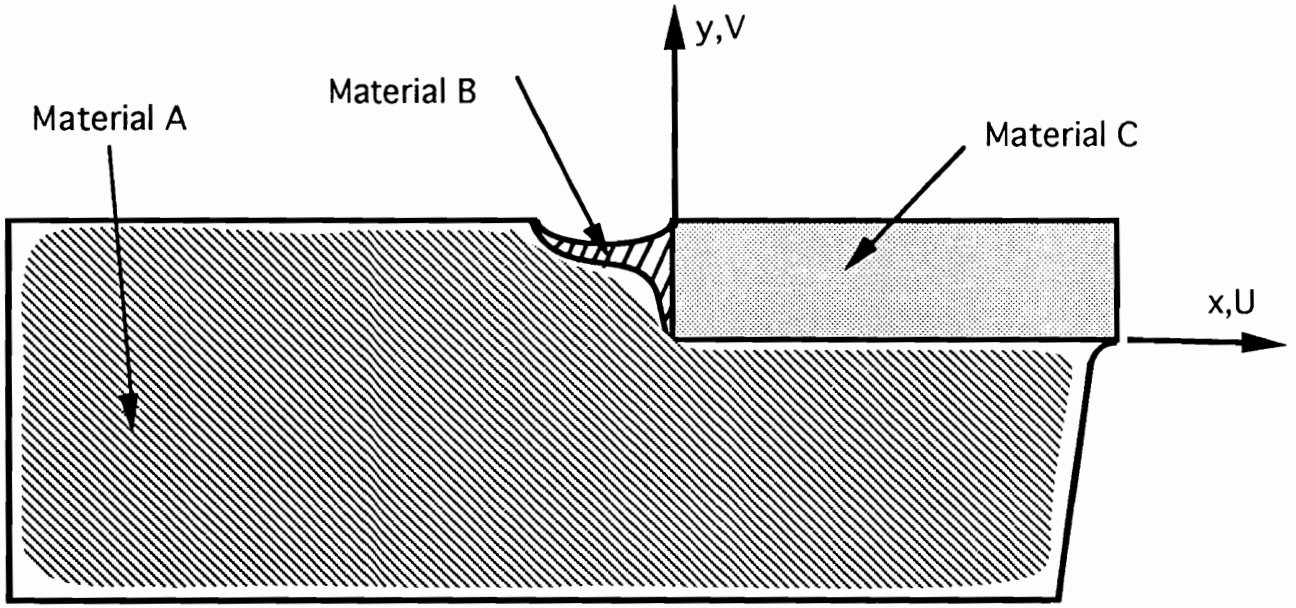

Material A: Steel
Material B: Alloy of copper
Material C: Tungsten carbide

Figure 6.9 The cutting tool bit specimen.

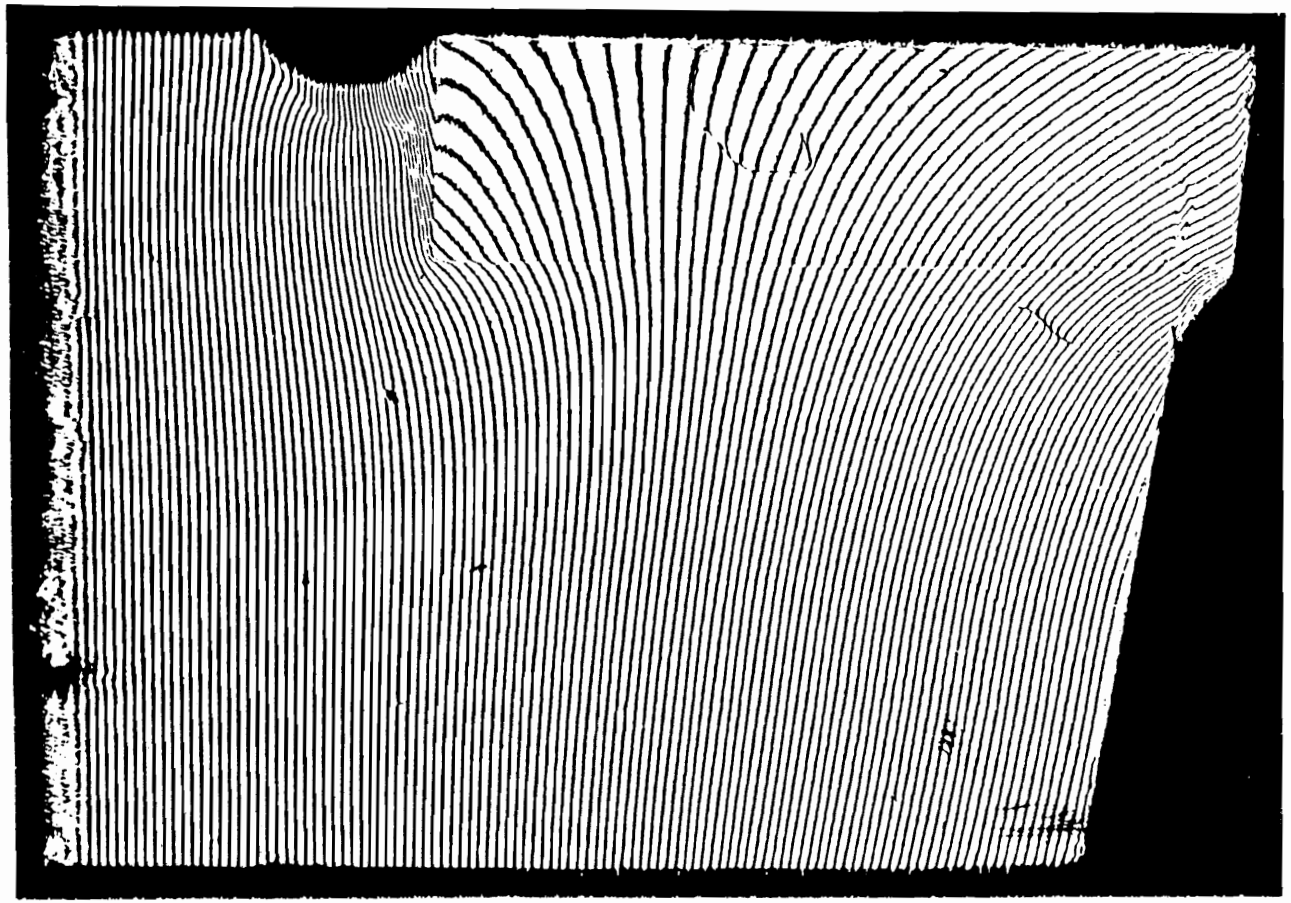

Figure 6.10a Horizontal (U) pattern representing thermal deformation of the cutting tool bit specimen at 219°C.

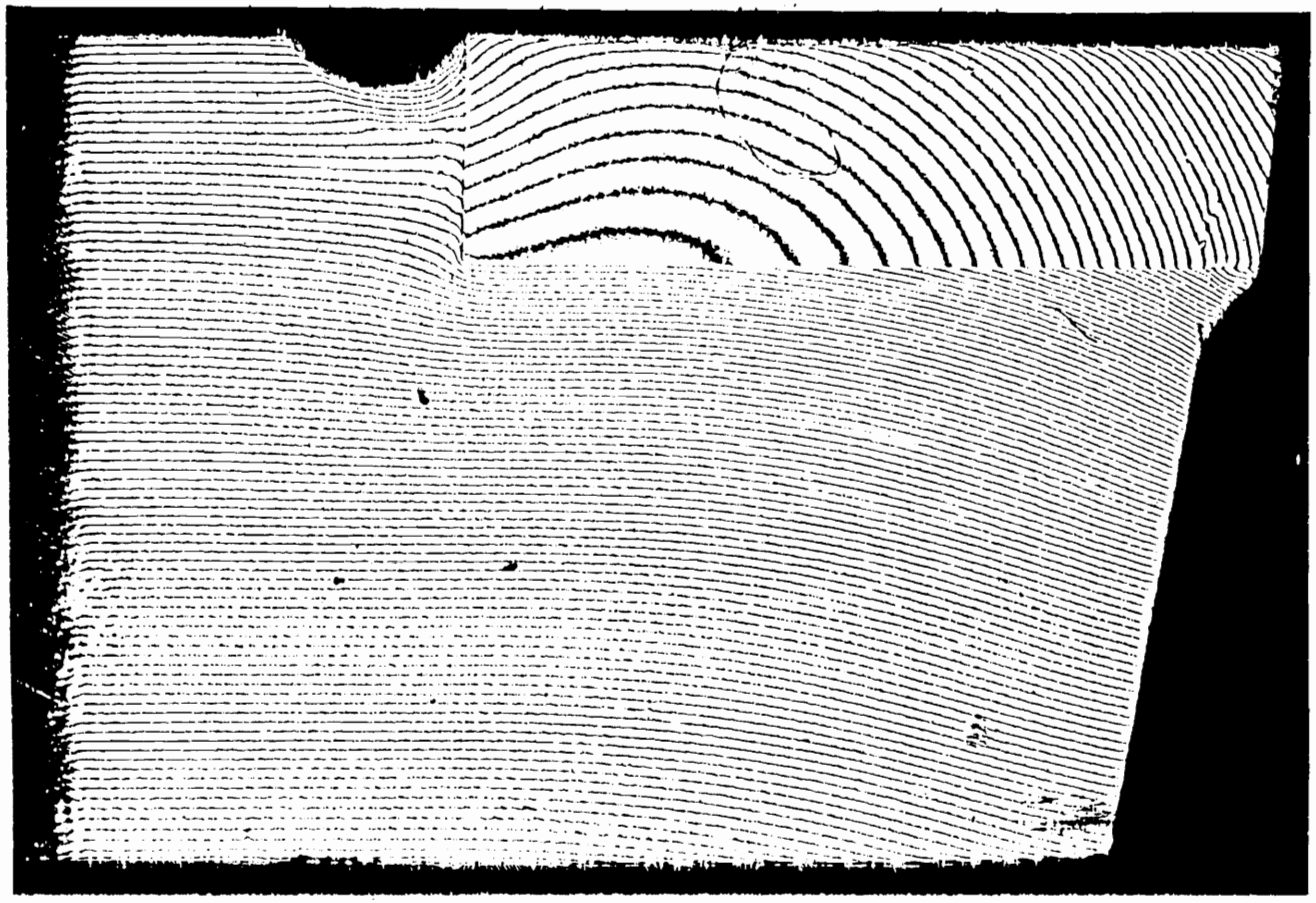

Figure 6.10b Vertical (V) pattern representing thermal deformation of the cutting tool bit specimen at 219°C.

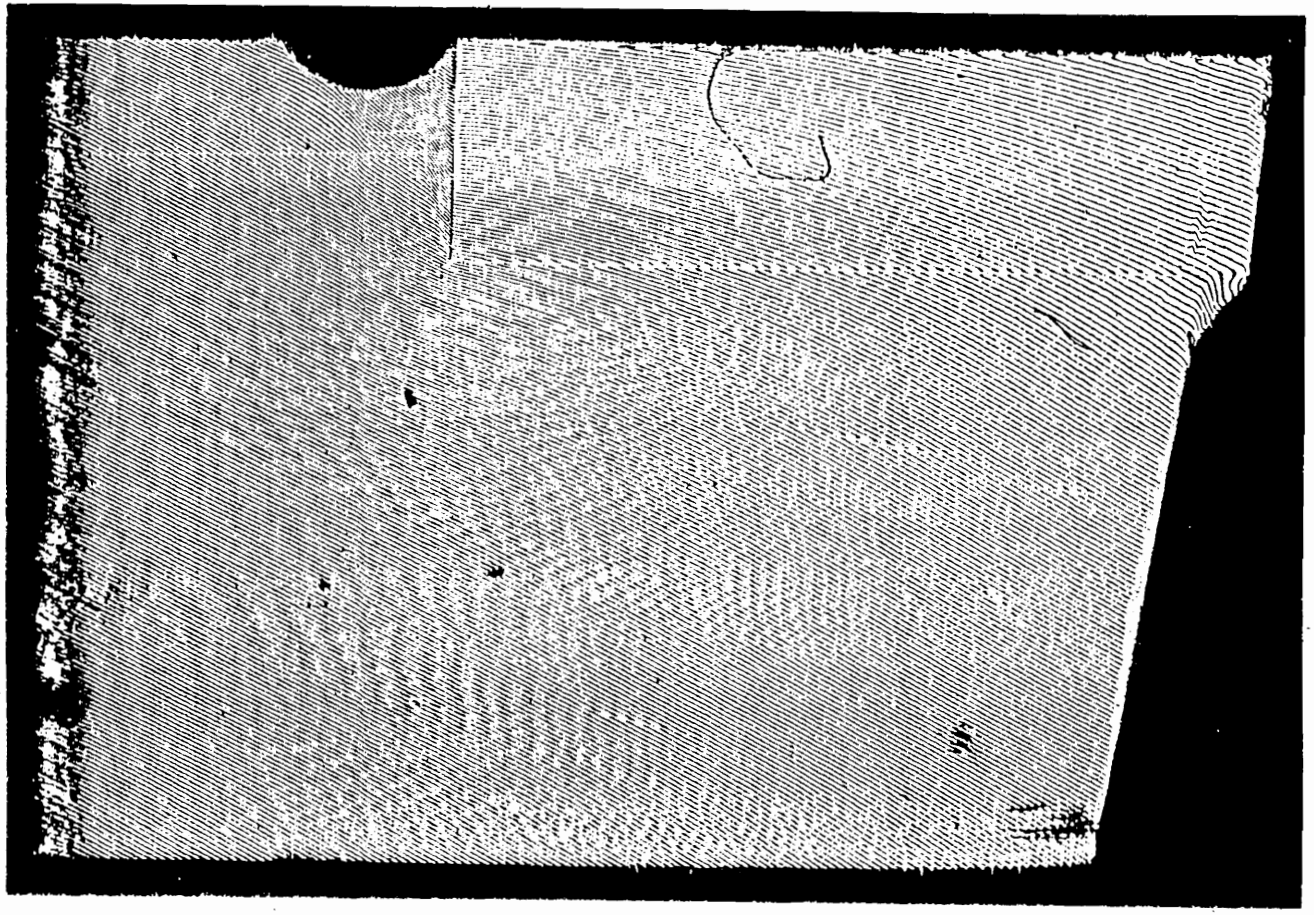

Figure 6.10c Horizontal (U) pattern representing thermal deformation of the cutting tool bit specimen at 219°C. Carrier fringes of rotation were added.

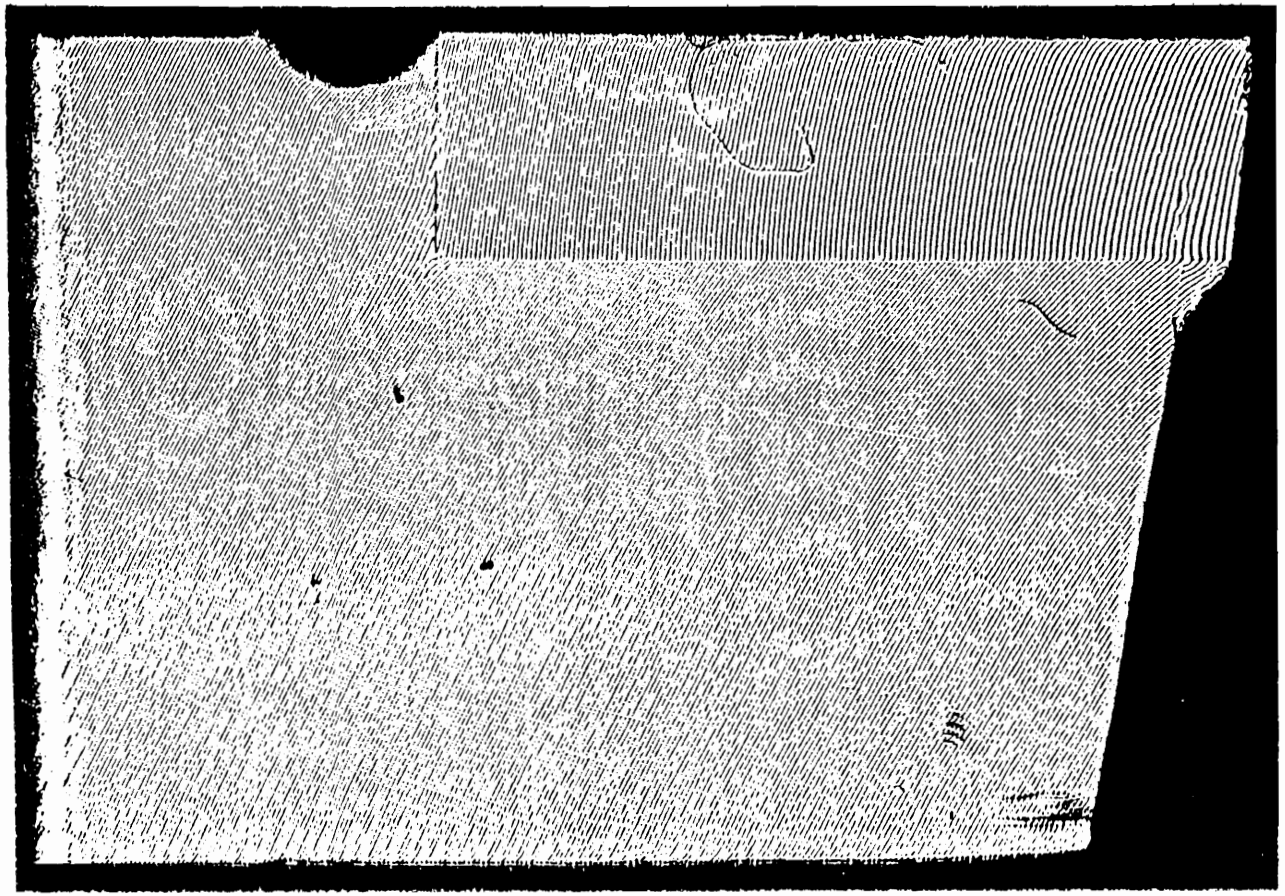

Figure 6.10d Vertical (V) pattern representing thermal deformation of the cutting tool bit specimen at 219°C. Carrier fringes of rotation were added.

6.4.2 Thermal Strain Analysis

The high-resolution data-reduction technique [45,46] provides a unique method of resolving the full-field strain contour based on the displacement patterns. Full integration of this technique was completed by Czarnek and Lin [47,48] by introducing the data-smoothing approach. Thermal strain of the specimen was demonstrated on the part of tungsten carbide by using this technique to resolve the thermal deformation. In brief, in order to apply this technique, the patterns were digitized on the slightly overexposed pictures with appropriate carrier fringes of rotation, and only on the center of a fringe which is the point of highest resolution. The digitized data included the coordinates and fringe numbers of each data point. Approximately 300 data points were collected from the patterns. They were digitized more densely near the interface of carbide and steel, and that of carbide and alloy of copper. Less dense digitization was performed in the region away from the interfaces, to expedite the analysis of the fringe patterns. A random mesh based on the triangular element, as shown in Figure 6.11, was then created by the auto-mesh generation program.

The program based on the Finite Element Method smoothed the digitized data, minimizing the scatter of the data due to digitizing error. The resolution of the nonhomogenity in the material was enhanced. The smoothed displacement patterns with a contour interval of 417 nm are illustrated in Figures 6.12a and 6.12b,

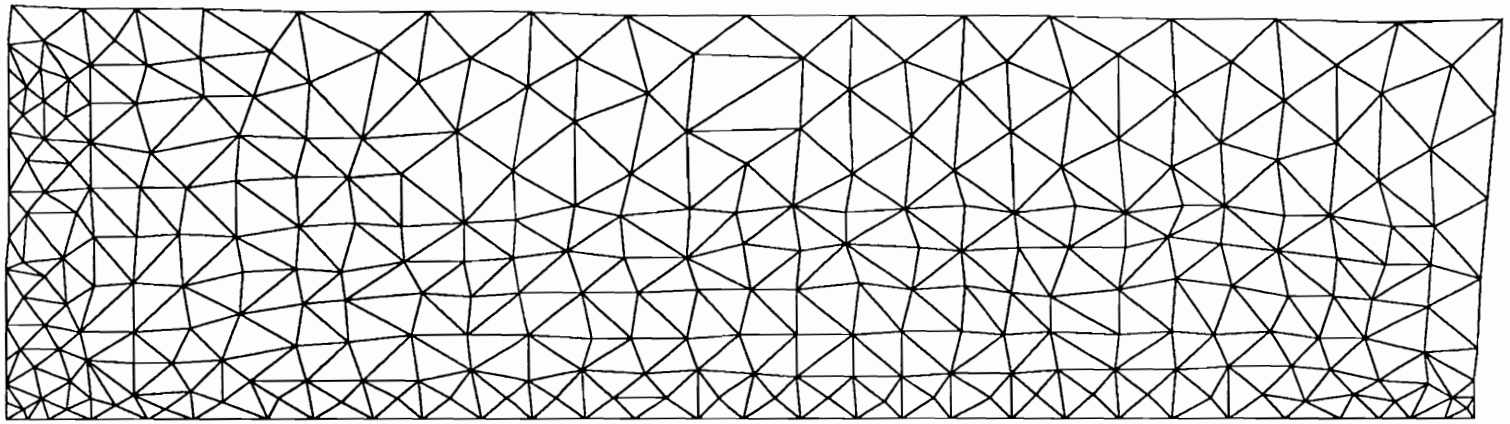

Figure 6.11 A random mesh generated on the carbide part of the specimen according to the digitized coordinates.

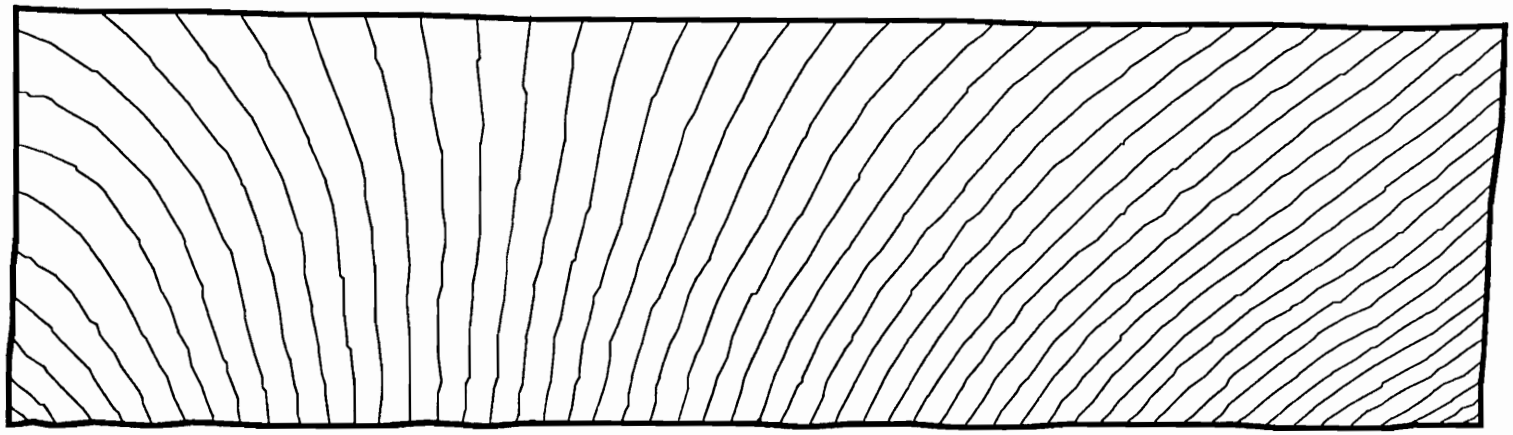

Figure 6.12a The smoothed U-displacement pattern demonstrating a good agreement with the original fringe pattern. Contour interval is 417 nm.

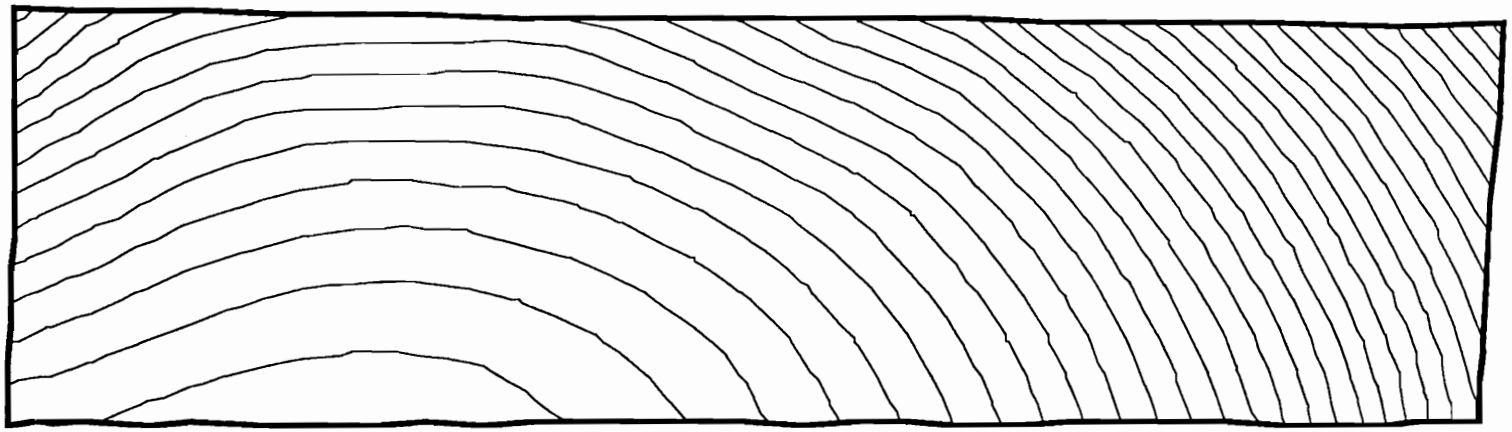

Figure 6.12b The smoothed V-displacement pattern demonstrating a good agreement with the original fringe pattern. Contour interval is 417 nm.

respectively. Good agreement was observed when the computer-generated patterns were compared with the original patterns, thus confirming that no mistake was made during the digitizing process.

The smoothed strain contours ε_x, ε_y, and γ_{xy} are shown in Figures 6.13a, 6.13b, and 6.13c. The absolute values of strain are also indicated. Note that the nonuniform distribution of strain contours, primarily from digitizing errors, was greatly reduced. The contour interval is set at 200 μm/m for normal strain and shear strain contours. The ranges of measured normal strains were from 140 μm/m to 2580 μm/m for ε_x, and 180 μm/m to 1980 μm/m for ε_y. The shear strain γ_{xy} varied from -2090 μm/m to 1980 μm/m. These results show that local strain concentrations occur on the front and rear edges near the interface, which are physically correct. The strain distribution along the section A-A', located in the region near the interface, could be determined and is plotted in Figure 6.14. The maximum shear strain was 2090 μm/m, and the maximum normal strain equalling 2580 μm/m existed near the front edge. This was due to the significant thermal deformation mismatch between the carbide and the steel. When this shear strain level was compared to that at the far field, a strain concentration factor of 4 was observed.

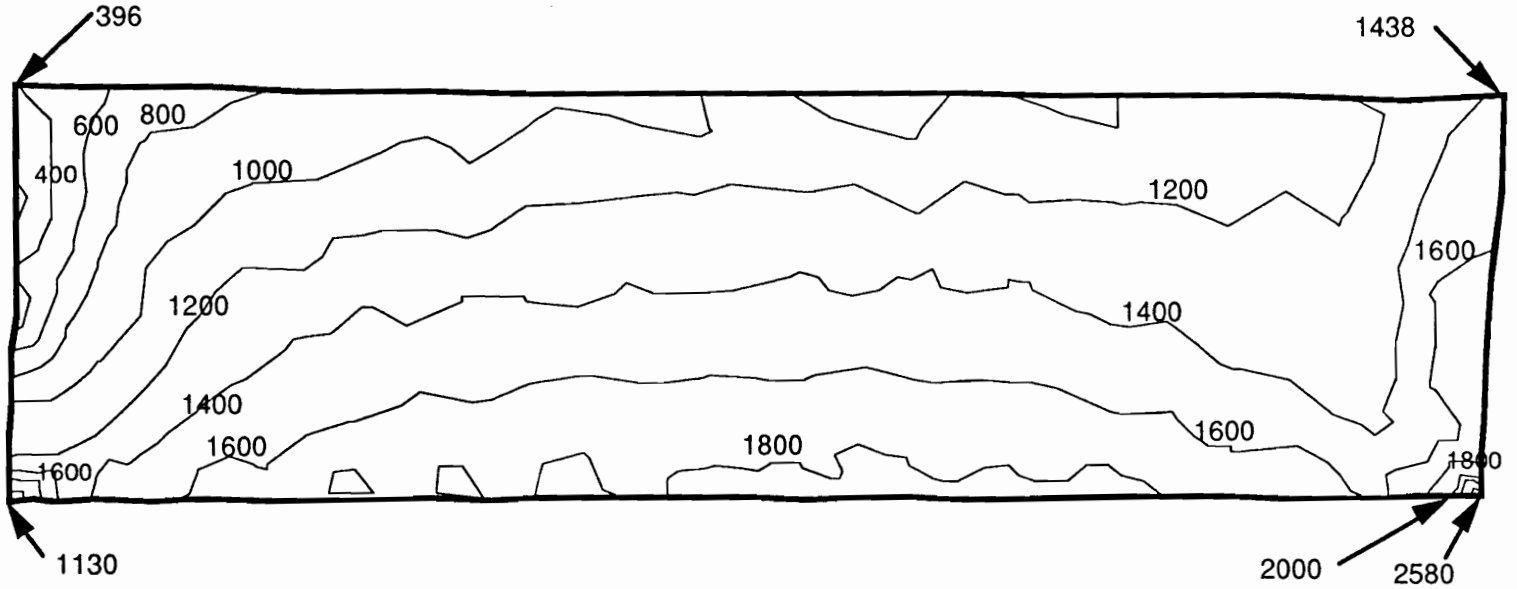

Figure 6.13a Contour map of the measured normal strain ε_x on the carbide part of the specimen. Contour interval is 200 μm/m.

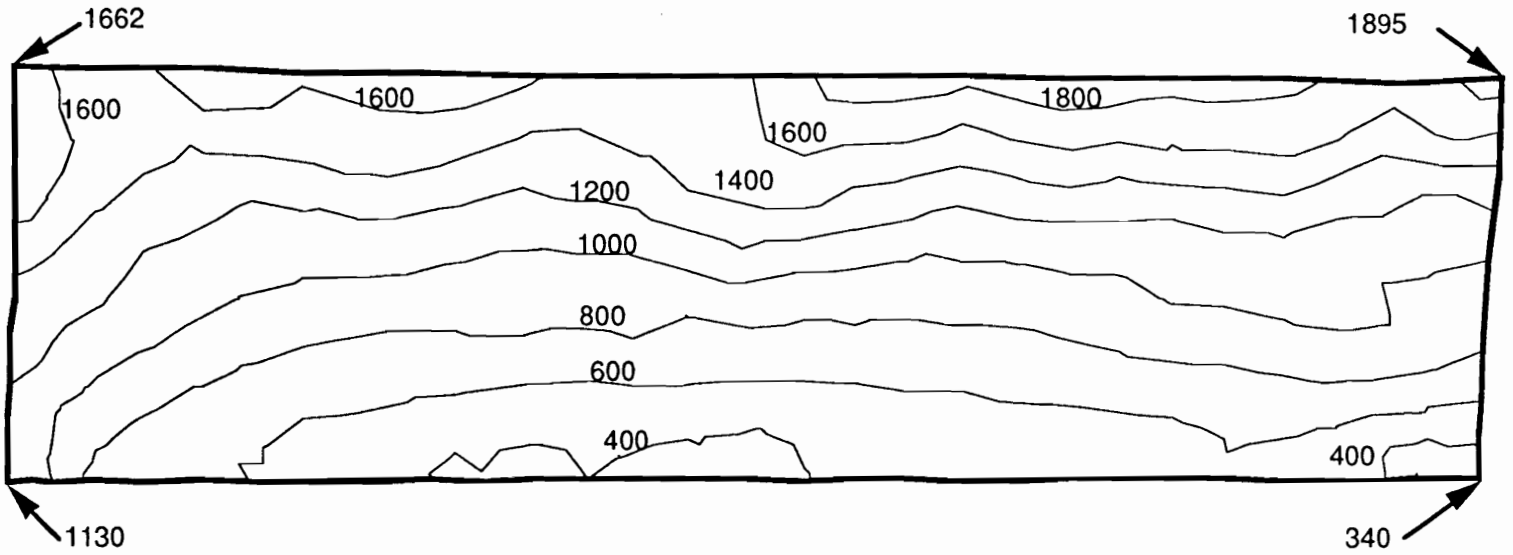

Figure 6.13b Contour map of the measured normal strain ε_y on the carbide part of the specimen. Contour interval is 200 μm/m.

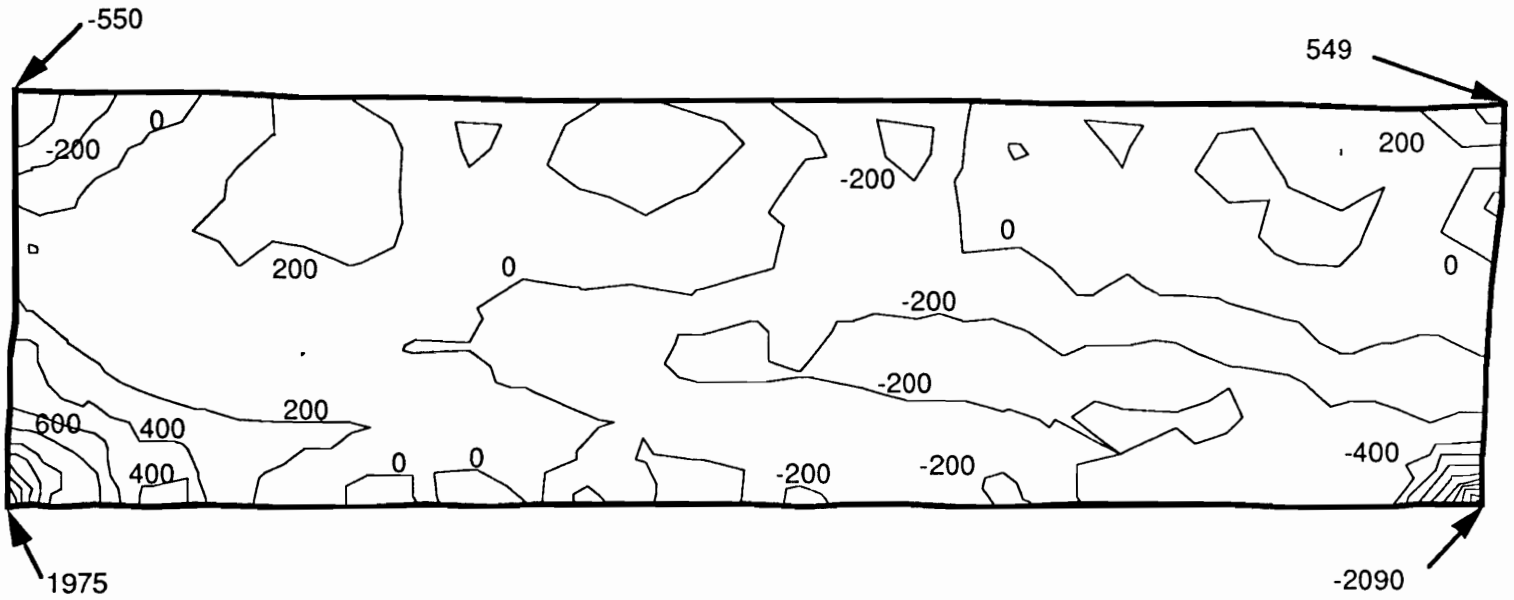

Figure 6.13c Contour map of the measured normal strain γ_{xy} on the carbide part of the specimen. Contour interval is 200 μm/m.

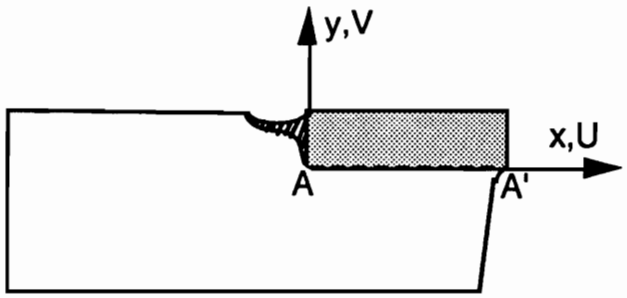

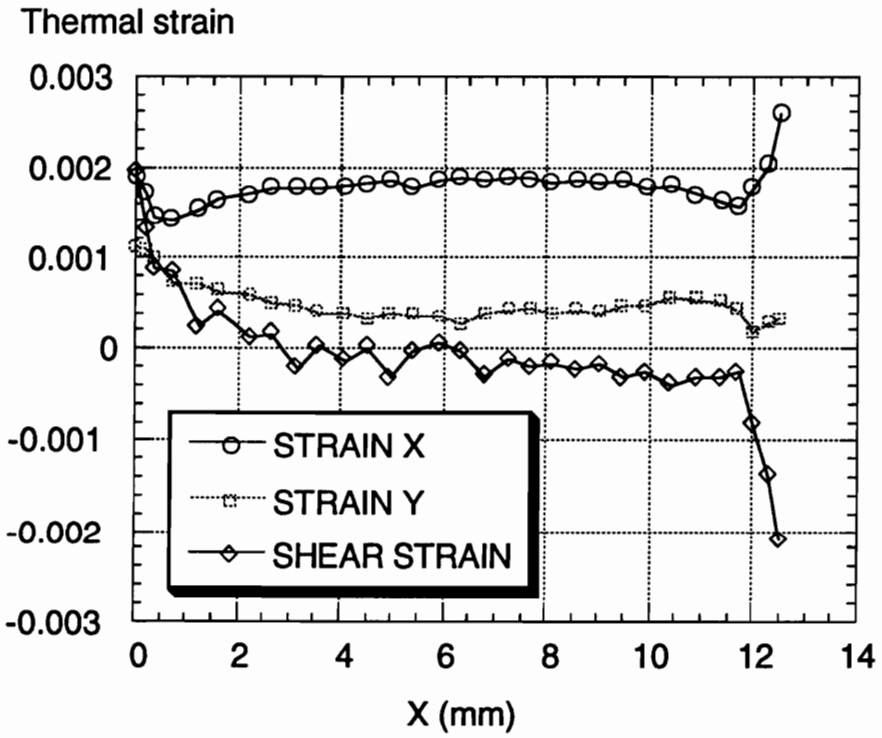

Figure 6.14 The distribution of strains in the carbide near the interface (along line A-A').

6.5 Summary

The applications of the high-temperature moiré system have been demonstrated with several practical cases. The system has been developed to the point where measurements of deformation can be performed routinely at temperatures ranging from 22°C to 220°C. In this range, replicated gratings can still be used and heating is relatively easy. This range can be extended to about 350°C if silicone rubber is used instead of epoxy resins.

The system was verified by the test of free thermal expansion of an aluminum block. Then two additional tests were performed. One was based on the thermal deformation mismatch due to the release of residual stress of a graphite/epoxy composite, and the other one involved the presence of an optical fiber on top of a metal/matrix composite.

The study of the thermal deformation of a cutting tool bit demonstrated the advantages of the full-field hybrid method for the strain analysis, such as the fact that no material property is required in its analysis and the resolution can be as high as 20 nm.

7 DISCUSSION AND FUTURE WORK

This study concentrated on the development of a high-sensitivity moiré interferometric technique for measuring in-plane deformation of specimens at high temperatures. In order to prove the feasibility of the moiré technique at a high temperature, the existence of photographable interference fringes at that temperature is essential. For this reason, the emphasis of the study was on the thermal loading rather than on the quantitative or mechanical tests. Several successful tests were demonstrated in Chapters 5 and 6. Some obstacles encountered and suggestions for future work on improving the method are addressed in the following sections.

7.1 Heating Method

The major obstacle in measurements at higher temperatures is the difficulty of heating in a vacuum. In this work, conduction heat transfer was chosen by using the strip heater and ceramic heater for the test temperatures below and above 600°C, respectively. When test temperature was low and the size of the specimen was small, temperature uniformity on the surface of the specimen could be maximized by keeping the power the same for a few minutes.

For the tests above a temperature of 600°C, the specimens were significantly constrained by the ceramic heater when the two were bonded together. In this case, a free thermal expansion test could not be performed up to 980°C in this setup. Also, due to the temperature limit (1150°C) of the heating wire (Nichrome wire), the durability of the ceramic heater was near its temperature limit.

To achieve higher temperatures, a radiant heater such as a high-power CO_2 laser seems to be an expensive but promising choice as a source of infrared radiation. In industry, this laser has been demonstrated to be practical and used as a cutting tool. It is a source of light producing a small but intense heating zone. Therefore, the thermal deformation on the optical components caused by this heating source will be greatly minimized. In addition to having higher temperatures, the constraint problem will be overcome due to no contact between the specimen and the heater.

7.2 Background Noise

Another problem that occurs at temperatures around 700°C and above is the glow from the specimen and the heater. In this study, this problem was overcome by the use of a spatial filter and a narrow band interference filter which eliminated the coherent noise and noncoherent noise, respectively. Thus, the contrast loss due to background noise was greatly minimized.

For future higher-temperature measurements, stronger power of lasers than that of a helium-neon laser used in the current system can further overcome the contrast loss due to the background noise. It can also shorten the exposure time, thus making the measurements less sensitive to vibration. The design of the vacuum interferometer preserved the possibility of using an argon laser, with a wavelength of 514 nm, allowing an increase in power by two orders of magnitude.

7.3 High-Temperature Specimen Grating

A plasma-etched grating was used as a high-temperature specimen grating in this study. For a test temperature of around 1000°C, the gratings survived at least about three to four hours—long enough for most tests. However, long-term durability of the specimen grating is necessary for some tests such as a creep test. This durability could be further increased by etching the grooves directly on the specimen. In this case, the specimen grating would survive as long as the material.

Another factor relating to the quality of the etched grating is the thickness uniformity of the photoresist. The thickness of the photoresist was controlled by the spinning rate of the spinner in this study. This thickness could not be controlled uniformly over the whole area of the specimen surface, causing the varied intensity of

the photoresist grating. Therefore, the intensity of the etched grating, which was obtained from etching through the photoresist to the gold layer, varied. If the techniques used in the electronics industry were available in a laboratory, the thickness uniformity of the photoresist would be greatly enhanced.

Besides, the specimen grating replication procedure has its own advantages, such as easy preparation; therefore, the development of a higher-temperature adhesive would be beneficial to routine measurements.

7.4 The Whole System

High-power lasers, windows, and convection ovens are often seen in the design of high-temperature work. High-power lasers are used to reduce the exposure time and freeze the motion of fringe patterns, thus minimizing the effect of thermal convection currents. However, unless necessary, they are not preferred for the safety of operators and optics. The use of windows in convection ovens could cause uncertain error in the measurement due to the thermal deformation of windows. Probably, if the test temperature is not very high, the effect is not very significant. However, it is a risky choice for higher-temperature measurements. This study introduced a vacuum testing environment. No window was used between the specimen and interferometer. The thermal expansion of the windows

and the thermal convection currents were greatly minimized. In short, the core idea of this methodology provides a more reliable testing environment for measurements at temperatures even higher than the reported temperature at 980°C [52].

The thermocouples were also attached to the interferometer. It was observed that the temperature increase on the interferometer was insignificant. This fact indicates that the thermal deformation on the instrument is negligible.

The design of a loading system is expected. Then, the behavior of a component subjected to mechanical as well as thermal loading at high temperatures can be investigated in this system.

8 CONCLUSIONS

The capability of high-sensitivity moiré interferometry was enhanced to allow performing the in-plane deformation measurements at high temperatures. Successful tests extended the temperature limit of the technique to 980°C. The stable and well-defined interference patterns at high temperatures confirmed the feasibility of the developments including the high-temperature moiré system and high-temperature specimen grating. The features of this new approach and difficulties overcome are listed as follows:

- A testing environment with vacuum was provided to minimize the convection thermal current at high temperatures. This environment provided an approach for even higher temperature measurements.
- Plasma-etched gold grating was used as the high-temperature specimen grating and successfully applied to some structural materials.
- Vibration was effectively isolated by the design of an air-suspension system and an achromatic interferometer.
- The contrast of interference fringes at high temperatures was enhanced by the use of a spatial filter and a narrow band interference filter to minimize the background noise from the glow of the specimen and heater.

— The goals of stability, compactness, flexibility, and ease of control for the system were reached.

For routine tests, the newly developed optical system was demonstrated for several practical measurements subjected to thermal loading. Free thermal expansion or thermal deformation mismatch was observed. If combined with the high-resolution data-reduction technique, this experimental technique can provide extremely powerful full-field, high-sensitivity, and high-resolution measurements of deformation and strain in the high-temperature regime.

REFERENCES

1. Guild, J., "The Interference Systems of Crossed Diffraction Grating; Theory of Moiré Fringes," Clardendon Press, Oxford, 1956.

2. Sciammarella, C. A., "The Moiré Method-A Review," Experimental Mechanics, Vol. 22, No. 11, pp. 418-433, 1982.

3. Durelli, A. J., "Discussion of The Moiré Method-A Review," Experimental Mechanics, Vol. 23, No. 4, pp. 446-449, 1983.

4. Czarnek, R., "Structural Testing, A Monograph for the Society for Experimental Mechanics-Moiré Interferometry", Editors: R.T. Reese and W.A. Kawahara (In press).

5. Patorski, K., "Moiré Methods in Interferometry," Optics and Lasers in Engineering, Vol. 8, pp. 147-170, 1988.

6. SEM Proceedings: 4th Annual Hostile Environments and High Temperature Measurements Conference Proceedings, Mar. 24-25, 1987, Windsor Locks, Connecticut.

7. SEM Proceedings: 5th Annual Hostile Environments and High Temperature Measurements Conference Proceedings, Mar. 22-23, 1988, Costa Mesa, California.

8. SEM Proceedings: 6th Annual Hostile Environments and High Temperature Measurements Conference Proceedings, Nov. 6-8, 1989, Kansas City, Missouri.

9. Ma, L.-C., Wu, T.-T. and Zhao, L.-B., "Development of Temperature-Compensated Resistance Strain Gages for Use to 800°C," Experimental Mechanics, Vol. 30, No. 1, pp. 17-19, Mar. 1990.

10. Meyer, R., " Axial-Torsional Extensometer For Use To 1200°C," 4th Annual Hostile Environments and High Temperature Measurements Conference Proceedings, Mar. 24-25, 1987, Windsor Lock, Connecticut, pp. 82-93.

11. Sciammarella, C. A., " Strain Measurement at High Temperatures by Optical Techniques," 4th Annual Hostile Environments and High Temperature Measurements Conference Proceedings, Mar. 24-25, 1987, Windsor Lock, Connecticut, pp. 44-52.

12. Hunter, A. R. and Martinson, R. H., "Strain Measurements at High Temperatures by Optical Methods," SEM Proceedings: 5th Annual Hostile Environments and High Temperature Measurements Conference Proceedings, Mar. 22-23, 1988, Costa Mesa, California, pp. 68-69.

13. Pryor, T. R. and North, W. P. T., "The Diffractographic Strain Gage," Experimental Mechanics, Vol. 11, pp. 565-568, 1971.

14. Sharpe, W. N., Jr., "The Interference Strain Gage," Experimental Mechanics, Vol. 8, pp. 164-170, 1968.

15. Sharpe, W. N., Jr., "Applications of the Interferometric Strain/Displacement Gage," Optical Engineering, Vol. 21, No. 3, pp. 483-488, May/June 1982.

16. Sharpe, W. N., Jr. and Wang, K. C., "Small Attachable Interferometric Strain Gages," Proceedings of the 1987 SEM Spring Conference, Houston, Texax, pp. 509-513.

17. Pih, H. and Liu, K. C., "Laser Diffraction Methods for High-temperature Strain Measurements," Experimental Mechanics, Vol. 31, No.1, pp. 60-64, 1991.

18. Marion, R. H., "A New Method of High-temperature Strain Measurement," Experimental Mechanics, Vol. 18, No. 4, pp. 134-140, 1978.

19. Tompkins, S. S., Bowles, D. E. and Kennedy, W. R., "A Laser-Interferometric Dilatometer for Thermal-Expansion Measurements of Composites," Experimental Mechanics, Vol. 26, No. 1, pp. 1-6, Mar. 1986.

20. Chiang, F. P., Anastasi, R., Beatty, J. and Adachi, J., "Thermal Strain Measurement by One-beam Laser Speckle Interferometry," Applied Optics, Vol. 19, No. 16, pp. 2701-2704, 15 Aug 1980.

21. Yamaguchi, I., "Simplified Laser-Speckle Strain Gauge," Optical Engineering, Vol. 21, pp. 214-218, May/June 1982.

22. Yamaguchi, I., "Advances in the Laser Speckle Strain Gauge," Optical Engineering, Vol. 27, No. 3, pp. 214-218, Mar. 1988.

23. Chiang, F. P., Zhao, Y. Y. and Chen, D. J., "High Temperature Strain Measurement Using Laser Speckles," Proceedings of the 1988 SEM 5th Annual Hostile Environments and High Temperature Measurements Conference, pp. 49-52.

24. Lant, C. T. and Barranger, J. P., " Progress In High Temperature Speckle-Shift Strain Measurement System," SEM Proceedings, Hologram Interferometry and Speckle Metrology, Nov. 5-8, 1990, Baltimore, Maryland, pp. 203-209.

25. Løkberg, O. J., Malmo, J. T. and Slettemoen, G. A., "Interferometric Measurements of High Temperature Objects by Electronic Speckle Pattern Interferometry," Applied Optics, Vol. 24, No. 19, pp. 3167-3172, 1985.

26. Malmo, J. T., Løkberg, O. J. and Slettemoen, G. A.,"Interferometric Testing at Very High Temperatures by TV Holography (ESPI)," Experimental Mechanics, Vol. 28, No. 3, pp. 315-321, Sep. 1988.

27. Joenathan, C., "Recent Developments in Electronic Speckle Pattern Interferometry," Proceedings of the 1991 SEM Spring Conference, Milwaukee, pp. 198-204.

28. Hofling, R., Aswendt, P. and Totzauer, W., "Digital Speckle Interferometry and Speckle Photography Applied to Thermal Strain Measurements of Advanced Materials," SEM Proceedings, Hologram Interferometry and Speckle Metrology, Nov. 5-8, 1990, Baltimore, Maryland, pp. 465-472.

29. Bowles, D. E., Post, D., Herakovich, C. T. and Tenney, D. R., "Moiré Interferometry for Thermal Expansion of Composites," Experimental Mechanics, Vol. 21, pp. 441-447, 1981.

30. Kang, B. S.-J., Wang, F. X. and Liu, Q. K., "High Temperature Moiré Interferometry for Use to 550 C," Proceedings of the 1990 SEM Fall Conference, 25th Anniversary Edition, Baltimore, Maryland, pp. 457-464, 1990.

31. Sciammarella, C. A., Bhat, G. and Vaitekunas, J., "Measurement of Strains at High Temperatures by Means of Electro-Optics Holography," Proceedings of the 1991 SEM Spring Conference, Milwaukee, Wisconsin, pp. 205-214.

32. Czarnek, R., "Three-Mirror, Four-Beam Moiré Interferometer and its Capabilities," Optics and Lasers in Engineering, Vol. 15, pp. 93-101, 1991.

33. Czarnek, R., "New Methods in Moiré Interferometry," Ph.D. Dissertation, Engineering Science & Mechanics Department, Virginia Polytechnic Institute & State University, Dec. 1984.

34. Czarnek, R., "High Sensitivity Moiré Interferometry with Compact Achromatic Interferometer," Optics and Lasers in Engineering, Vol. 13, No. 2, pp. 99-115, 1990.
35. Czarnek, R., Lee, J. and Lin, S.-Y., "Testing of Composite Materials at Elevated Temperatures Using Moiré Interferometry," Proceedings of the International Conference on Composite Materials (ICCM/8), Paper number 36-O, Honolulu, Hawaii, July 1991.

36. Jarrell, R. F. and Stroke, G. W., "Some New Advances in Grating Ruling, Replication, and Testing," Applied Optics, Vol. 3, No. 11, pp. 1251-1262, Nov. 1964.

37. Horsfield, W. R., "Ruling Engine with Hydraulic Drive," Applied Optics, Vol. 4, No. 2, pp. 189-193, Feb. 1965.

38. White, J. W. and Fraser, W. A., "Making Optical Elements," U.S. Patent 2,464,738, Mar. 15, 1949.

39. Sadat, A. B. and Reddy, M. Y., "Plastic Strain Analysis of the Machined Surface Region Using Fine Grid Etched by Photoresist Technique," Experimental Mechanics, Vol. 29, No. 3, pp. 346-349, 1989.

40. Morton, J. and Czarnek, R., "Dynamic Response of Advanced Material Systems: A Photomechanics Approach," Quarterly Report, DARPA/ONR project number N0014-88-K-0741, June 1989.

41. Forno, C., "Welds at High Temperatures Studied by Moiré photography,' Welding and Metal Fabrication, Vol. 46, No. 10, pp. 661-667, Dec. 1978.

42. Cloud, G. L., Radke, R. and Periffer, J., "Moiré Gratings for High Temperatures and Long Times," Experimental Mechanics, Vol. 19, No. 4, pp. 19N-21N, 1979.

43. Cloud, G. L., and Bayer, M., "Moiré to 1370°C," Experimental Techniques, Vol. 12, No. 4, pp. 24-27, 1988.

44. Czarnek, R., "Super High Sensitivity Moiré Interferometry with Optical Multiplication," Optics and Lasers in Engineering, Vol. 13, pp. 87-98, 1990.

45. Czarnek, R., Lee, J. and Rantis, T., "Moiré Interferometry with Enhanced Resolution," Experimental Techniques, Vol. 14, No. 4, pp. 24-28, 1990.

46. Lee, J., "High Resolution Interferometric Measurements of Residual Strains in Composites", Ph.D. Dissertation, Engineering Science & Mechanics Department, Virginia Polytechnic Institute & State University, December 1990.

47. Lin, S.-Y., Czarnek, R. and Lee, J., "Integration and Processing of High-resolution Moiré-interferometry Data," Proceedings of the 1991 SEM Spring Conference, Milwaukee, Wisconsin, pp. 513-518, 1991.

48. Lin, S.-Y., "Integration and Processing of High-Resolution Moiré-Interferometry Data," Ph.D. Dissertation, Engineering Science & Mechanics Department, Virginia Polytechnic Institute & State University, May 1992.

49. Sciammarella, C. A. and Rao, M. P. K., "Failure Analysis of Stainless Steel at Elevated Temperatures," Experimental Mechanics, Vol. 19, No. 1, pp. 389-398, Nov. 1979.

50. The 1992-1993 Catalog, AEASR/Johnson Matthey Company.

51. Thermo Physical Research Center Handbook of Thermophysical Properties (Purdue University), The TPRC Data Series, Vol. 12.

52. Czarnek, R., Wu, J.-J., Lin, S.-Y. and Lee, J., "High-Temperature, High-Sensitivity Moiré Interferometry," Experimental Techniques, (in press).

VITA

Jau-Je Wu

Jau-Je Wu was born on October 2, 1963 in Taipei County, Taiwan, Republic of China to Tsung-Bo and Ju Lein Wu. His college education began in 1981 when he was admitted to the Naval Architecture Department of National Taiwan College of Marine and Technology in Keelung, Taiwan. In 1985, he received his B.S. degree and continued his graduate study in the Naval Architecture Department of National Taiwan University, Taipei, Taiwan. His research was concentrated on the experimental study on the behavior of the crack propagation. In 1987, he received his M.S. degree and then joined the Navy as a teaching officer in a training base. Upon completion of two years of military service, he furthered his graduate study at Virginia Polytechnic Institute and State University in 1989. His interest in experimental mechanics led him to study under Dr. Czarnek's guidance in the Engineering Science and Mechanics Department. Since then, he has conducted his research work on the moiré interferometry applied to measurements at high temperatures. His current research interest includes developments of experimental methods, emphasized on moiré interferometry, and their applications to solid mechanics.